

RESOLUTION OF DIGITAL ELEVATION MODELS AND TERRAIN ATTRIBUTES,
APPARENT ELECTRICAL CONDUCTIVITY, AND PREDICTION OF PALOUSE
SOILSCAPE B_t HORIZONS

By

DAVID UBERUAGA

A thesis submitted in partial fulfillment of
the requirements for the degree of

MASTERS OF SCIENCE

MAY 2004

WASHINGTON STATE UNIVERSITY
Department of Environmental Science
and Regional Planning

To the Faculty of Washington State University:

The members of the Committee appointed to examine the dissertation/thesis of
DAVID UBERUAGA find it satisfactory and recommend that it be accepted.

Chair

ACKNOWLEDGEMENTS

The process I started approximately four years ago, to obtain a masters degree in environmental science, required both knowledge and support from others. There are a number of individuals that I relied on for this, David Huggins, Richard Rossi, Bruce Frazier, Shawn Wetterau, Ryan Davis, and Shelley Ann Jones (the misses). David Huggins not only allowed me to fulfill the requirements of a masters degree while being his employee, he also guided me through much of the process. His ability to polish the roughest of writing styles has not only created a better end product, but also created a learning environment. Rick Rossi, with an amazing ability to explain complex problems, was essential in the understanding and implementation of geostatistics throughout this project. Rick was always willing to offer guidance and a new perspective when things got tough. Bruce Frazier not only supplied a practical approach for the project, he also provided insight to the end use. Shawn Wetterau, with a willingness to help me with all the work responsibilities that I neglected during this process, created a guilt free environment where I could focus on the task at hand. Shawn always strives for perfection and I never feared for the quality of projects he undertook in my place. Ryan Davis bought me a milkshake on a night when my sanity was in jeopardy. That milkshake was a small oasis reminding me that life did not always have to be work, and there were simple pleasures to be had.

Shelley Ann Jones was the foundation from which this project began. Her ability to calm me when I was angry, encourage me when I was frustrated, and help me when I was overwhelmed not only saved my sanity, but also gave me the motivation to attack the project and finish it. She was always there when I needed her. Thank you Shelley Ann.

RESOLUTION OF DIGITAL ELEVATION MODELS AND TERRAIN ATTRIBUTES,
APPARENT ELECTRICAL CONDUCTIVITY, AND PREDICTION OF PALOUSE
SOILSCAPE B_t HORIZONS

ABSTRACT

By David Uberuaga, M.S.
Washington State University
May 2004

Chair: David R. Huggins

Rapid, field-scale data collection using global positioning systems (GPS) and electromagnetic induction are increasingly used for precision farming applications including prediction of terrain attributes and soil properties. Research objectives were to: (1) create a digital elevation model (DEM) using real time, kinematic GPS; (2) use terrain attributes, interpolation techniques and resolution selection to evaluate DEMs and reduce error; (3) assess abilities to predict soil Bt horizon presence with terrain attributes and apparent soil electrical conductivity (EC_a) using classification and regression tree (CART) analyses; and (4) validate Bt horizon prediction using indicator kriging (IK) and an independent core set of Bt horizon data.

Elevation data was collected over a 61 ha field with a survey grade GPS at the Cunningham Agronomy Farm (CAF) and interpolated using multiple techniques to create DEMs. Plan and profile curvature, derived from the DEMs, were found to be useful for assessing DEM error and evaluating interpolation and resolution scales for final DEM selection. To predict soil Bt horizon presence, terrain attributes of slope, aspect, curvature, global solar insolation, flow accumulation, flow direction, specific catchment area, and wetness index were calculated using the selected DEM at 1-m to 30-m resolutions. Field-scale EC_a data was collected and

interpolated using ordinary kriging at the same resolutions. Terrain attribute and EC_a data for all resolutions, were analyzed using CART for Bt horizon prediction and creation of field zones.

Zones created using the CART analysis with EC_a and terrain attribute data predicted Bt horizon presence with 58% and 62% accuracy for the soil core and IK mapped data, respectively. Bt horizon presence was correlated to greater EC_a. When EC_a data was omitted, 30-m profile curvature was the primary predictor for Bt horizon presence. Prediction rates of 69% and 53% were achieved for the soil core and IK mapped data, respectively, using terrain attributes. The low validation using the IK map indicates that using terrain attributes alone may not be readily extrapolated to predict Bt horizon presence in other fields. The CART analysis also indicated that terrain attributes calculated at multiple resolutions were useful for Bt horizon prediction.

TABLE OF CONTENTS

ACKNOWLEDGEMENTS	iii
ABSTRACT.....	iv
TABLE OF CONTENTS	vi
LIST OF TABLES	ix
LIST OF FIGURES	xii
CHAPTER I: RESOLUTION OF DIGITAL ELEVATION MODEL AND EVALUATION FROM CURVATURE ATTRIBUTES	1
1.1 Introduction.....	1
1.2 Materials and Methods.....	2
1.2.1 Site Background.....	2
1.2.2 Global Positioning System Setup.....	2
1.2.3 Data Processing.....	4
1.3 Results and Discussion	5
1.3.1 Survey	5
1.3.2 Data Interpolation	6
1.3.3 Curvature Rasters.....	8
1.3.4 Digital Elevation Model Error Assessment, Choosing a Final Interpolation Scheme... ..	9
1.3.5 Minimizing Digital Elevation Model Error by Increasing Raster Cell Size.....	11

1.4 Conclusion	12
1.5 Tables.....	13
1.6 Figures.....	26
1.7 References.....	65

**CHAPTER II: PREDICTING SOIL B_t HORIZONS FROM APPARENT SOIL
ELECTRICAL CONDUCTIVITY AND TERRAIN ATTRIBUTES 67**

2.1 Introduction.....	67
2.2 Materials and Methods.....	69
2.2.1 Horizon Information	69
2.2.2 Terrain Attributes.....	69
2.2.3 Apparent Electrical Conductivity	70
2.2.4 Indicator Kriging of Bt Horizon Presence or Absence	72
2.2.5 Classification and Regression Tree (CART) Analysis	72
2.3 Results and Discussion	75
2.3.1 Indicator Kriging of Bt Horizon	75
2.3.2 Terrain Attributes.....	75
2.3.3 Apparent Electrical Conductivity	78
2.3.4 Classification and Regression Tree.....	79
2.3.5 Validation of Classification and Regression Tree	82
2.4 Conclusion	83
2.5 Tables.....	85
2.6 Figures.....	94

2.7 References.....	127
---------------------	-----

LIST OF TABLES

Table 1.1. Results of real time, kinematic, global positioning system survey based on 30440 data points for the Cunningham Agronomy Farm.....	13
Table 1.2. Cross-validation of elevation results for local polynomial interpolation and ordinary kriging when used as exact interpolators.....	14
Table 1.3. Cross-validation results for digital elevation models created from local polynomial interpolation with increasing global polynomial influence.	15
Table 1.4. Plan curvature raster results for 2-m digital elevation models created from local polynomial interpolation with increasing global polynomial influence.	16
Table 1.5. Profile curvature raster results for 2-m digital elevation models created from local polynomial interpolation with increasing global polynomial influence.	17
Table 1.6. Realistic (>-1 and <1 radians per 100 m) and outlier cells (<-1 and >1 radians per 100 m) of plan curvature rasters for 2-m digital elevation models created from local polynomial interpolation with increasing global polynomial influence.	18
Table 1.7 Realistic (>-1 and <1 radians per 100 m) and outlier cells (<-1 and >1 radians per 100 m) of profile curvature rasters for 2-m digital elevation models created from local polynomial interpolation with increasing global polynomial influence.	19
Table 1.8. Cross-validation results for digital elevation models created using a local polynomial interpolation with increasing global influence.....	20
Table 1.9. Elevation statistics for digital elevation models created using local polynomial interpolation with 30% global and 70% local polynomial influence for increased raster cell size.	
.....	21

Table 1.10. Plan curvature raster results for increasing resolution from digital elevation models created using local polynomial interpolation with 30% global and 70% local polynomial influence.....	22
Table 1.11. Profile curvature raster results for increasing resolution from digital elevation models created using local polynomial interpolation with 30% global and 70% local polynomial influence.....	23
Table 1.12. Realistic (>-1 and <1 radians per 100 m) and outlier (<-1 and >1 radians per 100 m) cells of plan curvature rasters with increasing resolution from digital elevation models created using local polynomial interpolation with 30% global and 70% local polynomial influence.....	24
Table 1.13. Realistic (>-1 and <1 radians per 100 m) and outlier (<-1 and >1 radians per 100 m) cells of profile curvature rasters with increasing resolution from digital elevation models created using local polynomial interpolation with 30% global and 70% local polynomial influence.....	25
Table 2.1. Terrain attributes, their units, and importance calculated from digital elevation models for classification and regression tree analysis.....	85
Table 2.2. Elevation values for decreasing resolution of digital elevation models.	86
Table 2.3. Slope values for decreasing resolution of digital elevation models.....	86
Table 2.4. Aspect values for decreasing resolution of digital elevation models.....	87
Table 2.5. Plan curvature values for decreasing resolution of digital elevation models.	87
Table 2.6. Profile curvature values for decreasing resolution of digital elevation models.....	88
Table 2.7. Tangential curvature values for decreasing resolution of digital elevation models. ...	88
Table 2.8. Global solar insolation values for decreasing resolution of digital elevation models.	89
Table 2.9. Flow direction values for decreasing resolution of digital elevation models.	89
Table 2.10. Flow accumulation values for decreasing resolution of digital elevation models....	90

Table 2.11. Specific catchment area values for decreasing resolution of digital elevation models.	90
.....
Table 2.12. Wetness index values for decreasing resolution of Digital elevation models.	91
Table 2.13. Apparent soil electrical conductivity values for spring 2000 for decreasing resolution.....	92
Table 2.14. Apparent soil electrical conductivity values for fall 2000 for decreasing resolution.	92
Table 2.15. Classification and regression tree validation results from core set.....	93

LIST OF FIGURES

Figure 1.1. A 1996 aerial photograph of Cunningham Agronomy Farm.	26
Figure 1.2. Post plot of global positioning system data points collected during kinematic survey of the Cunningham Agronomy Farm in fall of 1999.	27
Figure 1.3. Post plot of global positioning system data points collected during kinematic survey of the Cunningham Agronomy Farm with position dilution of precision (PDOP) greater or less than 4.0.....	28
Figure 1.4. Cross-validation of ordinary kriging interpolation of 30440 global positioning system survey elevation points on the Cunningham Agronomy Farm.	29
Figure 1.5. Cross validation of exact local polynomial interpolation of 30440 global positioning system survey elevation points on the Cunningham Agronomy Farm.	30
Figure 1.6. A 2-m digital elevation model created from 100% local and 0% global polynomial interpolation.	31
Figure 1.7. A 2-m digital elevation model created from 90% local and 10% global polynomial interpolation.	32
Figure 1.8. A 2-m digital elevation model created from 80% local and 20% global polynomial interpolation.	33
Figure 1.9. A 2-m digital elevation model created from 60% local and 40% global polynomial interpolation.	34
Figure 1.10. A 2-m digital elevation model created from 40% local and 60% global polynomial interpolation.	35
Figure 1.11. A 2-m digital elevation model created from 20% local and 80% global polynomial	

interpolation.....	36
Figure 1.12. A 2-m digital elevation model created from 10% local and 90% global polynomial interpolation.....	37
Figure 1.13. A plan curvature raster created from 100% local and 0% global polynomial interpolation of a 2-m digital elevation model.....	38
Figure 1.14. A plan curvature raster created from 90% local and 10% global polynomial interpolation of a 2-m digital elevation model.....	39
Figure 1.15. A plan curvature raster created from 80% local and 20% global polynomial interpolation of a 2-m digital elevation model.....	40
Figure 1.16. A plan curvature raster created from 60% local and 40% global polynomial interpolation of a 2-m digital elevation model.....	41
Figure 1.17. A plan curvature raster created from 40% local and 60% global polynomial interpolation of a 2-m digital elevation model.....	42
Figure 1.18. A plan curvature raster created from 20% local and 80% global polynomial interpolation of a 2-m digital elevation model.....	43
Figure 1.19. A plan curvature raster created from 10% local and 90% global polynomial interpolation of a 2-m digital elevation model.....	44
Figure 1.20. A profile curvature raster created from 100% local and 0% global polynomial interpolation of a 2-m digital elevation model.....	45
Figure 1.21. A profile curvature raster created from 90% local and 10% global polynomial interpolation of a 2-m digital elevation model.....	46
Figure 1.22. A profile curvature raster created from 80% local and 20% global polynomial interpolation of a 2-m digital elevation model.....	47

Figure 1.23. A profile curvature raster created from 60% local and 40% global polynomial interpolation of a 2-m digital elevation model.....	48
Figure 1.24. A profile curvature raster created from 40% local and 60% global polynomial interpolation of a 2-m digital elevation model.....	49
Figure 1.25. A profile curvature raster created from 20% local and 80% global polynomial interpolation of a 2-m digital elevation model.....	50
Figure 1.26. A profile curvature raster created from 10% local and 90% global polynomial interpolation of a 2-m digital elevation model.....	51
Figure 1.27. Close up of 2-m plan curvature raster created from 60% local and 40% global polynomial interpolation showing streaking created from collection method with survey points overlain.	52
Figure 1.28. Diagram of antenna height differences due to sway of pickup truck on slopes when traveling in opposite direction	53
Figure 1.29. Frequency histogram of 2-m plan curvature raster created from 100% local polynomial interpolation.....	54
Figure 1.30. A 1-m digital elevation model created from 30% global and 70% local polynomial interpolation.	55
Figure 1.31. A 2-m digital elevation model created from 30% global and 70% local polynomial interpolation.	56
Figure 1.32. A 5-m digital elevation model created from 30% global and 70% local polynomial interpolation.	57
Figure 1.33. A 10-m digital elevation model created from 30% global and 70% local polynomial interpolation.	58

Figure 1.34. A 15-m digital elevation model created from 30% global and 70% local polynomial interpolation.....	59
Figure 1.35. A 20-m digital elevation model created from 30% global and 70% local polynomial interpolation.....	60
Figure 1.36. A 25-m digital elevation model created from 30% global and 70% local polynomial interpolation.....	61
Figure 1.37. A 30-m digital elevation model created from 30% global and 70% local polynomial interpolation.....	62
Figure 1.38. A plan curvature raster created from 70% local and 30% global polynomial interpolation of a 2-m digital elevation model.....	63
Figure 1.39. A profile curvature raster created from 10% local and 90% global polynomial interpolation of a 2-m digital elevation model.....	64
Figure 2.1. The 369 random points created from a 30.48-m grid superimposed on the Cunningham Agronomy Farm with indication of Bt horizon presence or absence.....	94
Figure 2.2. Indicator kriging of the probability of Bt horizon presence and elevation contours from 2-m digital elevation model.	95
Figure 2.3. Slope map created from 2-m digital elevation model for 36.4 ha Cunningham Agronomy Farm.....	96
Figure 2.4. Aspect map created from 2-m digital elevation model for 36.4 ha Cunningham Agronomy Farm.....	97
Figure 2.5. Plan curvature map created from 2-m digital elevation model for 36.4 ha Cunningham Agronomy Farm.	98
Figure 2.6. Profile curvature map created from 2-m digital elevation model for 36.4 ha	

Cunningham Agronomy Farm.....	99
Figure 2.7. Tangential curvature map created from 2-m digital elevation model for 36.4 ha	
Cunningham Agronomy Farm.....	100
Figure 2.8. Global solar insolation map created from 2-m digital elevation model for 36.4 ha	
Cunningham Agronomy Farm.....	101
Figure 2.9. Flow direction map created from 2-m digital elevation model for 36.4 ha	
Cunningham Agronomy Farm.....	102
Figure 2.10. Flow accumulation map created from 2-m digital elevation model for 36.4 ha	
Cunningham Agronomy Farm.....	103
Figure 2.11. Specific catchment area (A_s) map created from 2-m digital elevation model for 36.4 ha Cunningham Agronomy Farm.....	104
Figure 2.12. Wetness index map created from 2-m digital elevation model for 36.4 ha	
Cunningham Agronomy Farm.....	105
Figure 2.13. Graph of 1-m digital elevation model elevation data for 184 core locations <i>versus</i> increasing raster cell sizes.....	106
Figure 2.14. Graph of 1-m digital elevation model slope data for 184 core locations <i>versus</i> increasing raster cell sizes.....	107
Figure 2.15. Graph of 1-m digital elevation model aspect data for 184 core locations <i>versus</i> increasing raster cell sizes.....	108
Figure 2.16. Graph of 1-m digital elevation model plan curvature data for 184 core locations <i>versus</i> increasing raster cell sizes.....	109
Figure 2.17. Graph of 1-m digital elevation model profile curvature data for 184 core locations <i>versus</i> increasing raster cell sizes.....	110

Figure 2.18. Graph of 1-m digital elevation model tangential curvature data for 184 core locations <i>versus</i> increasing raster cell sizes.....	111
Figure 2.19. Graph of 1-m digital elevation model global solar insolation data for 184 core locations <i>versus</i> increasing raster cell sizes.....	112
Figure 2.20. Graph of 1-m digital elevation model flow direction data for 184 core locations <i>versus</i> increasing raster cell sizes.	113
Figure 2.21. Graph of 1-m digital elevation model flow accumulation data for 184 core locations <i>versus</i> increasing raster cell sizes.	114
Figure 2.22. Graph of 1-m digital elevation model specific catchment area data for 184 core locations <i>versus</i> increasing raster cell sizes.	115
Figure 2.23. Graph of 1-m digital elevation model wetness index data for 184 core locations <i>versus</i> increasing raster cell sizes.	116
Figure 2.24. Raster of 2-m apparent electrical conductivity (EC_a) for spring of 2000.....	117
Figure 2.25. Raster of 2-m apparent electrical conductivity (EC_a) for fall of 2000.	118
Figure 2.26. Graph of 1-m raster apparent electrical conductivity data for 184 core locations <i>versus</i> increasing raster cell sizes for spring of 2000.	119
Figure 2.27. Graph of 1-m raster apparent electrical conductivity data for 184 core locations <i>versus</i> increasing raster cell sizes for fall of 2000.	120
Figure 2.28. Classification and Regression Tree analysis output for Bt horizon presence using terrain attributes and EC_a data.	121
Figure 2.29. Map of zones five, six, and 13 from Classification and Regression Tree analysis using terrain attributes and apparent electrical conductivity data (EC_a).	122
Figure 2.30. Classification and Regression Tree analysis output for Bt horizon presence predicted	

with terrain attributes.....	123
Figure 2.31. Map of zones four, seven, 14, 20 created from Classification and Regression Tree analysis using terrain attributes.....	124
Figure 2.32. Histogram of indicator kriged values for zones five, six, and 13 from classification and regression tree analysis using terrain attributes and apparent electric conductivity (EC _a) data.	
.....	125
Figure 2.33. Histogram of indicator kriged values for zones four, seven, 14, and 20 from classification and regression tree analysis using terrain attributes.	126

CHAPTER I: RESOLUTION OF DIGITAL ELEVATION MODEL AND EVALUATION FROM CURVATURE ATTRIBUTES

1.1 Introduction

Terrain attributes are currently being used to predict a variety of natural phenomena, such as water flow, soil erosion (Wilson and Gallant, 2000), and soil properties (Moore et al., 1993). Terrain attributes are, however, a function of the quality and resolution of the digital elevation model (DEM) from which they are derived. It has been found that DEMs with resolutions of 10-m or finer, improve prediction of erosion and sediment catchment (Schoorl, et al., 2000). In addition, as the spatial resolution of the DEM becomes coarser, the variance of derived attributes decreases, and attribute values approach the population mean (Thompson et al., 2001). The United States Geological Survey (USGS) currently offers 10-m DEMs for most counties in the United States created from topographic maps with known error (Russell et al., 1995). Although a 10-m DEM is considered fine resolution, global positioning system (GPS) technology exists that allows for the creation of even finer resolution DEMs. Real time kinematic (RTK) GPS technology can create highly accurate position data, with horizontal and vertical error of less than 2 cm, every second (Trimble Navigation, 2001). The use of RTK GPS, however, can be complicated and time consuming when covering large areas using typical foot survey protocol. The objectives of this experiment are to utilize RTK GPS in a rapid data collection to: (1) create DEMs with various interpolation methodology and resolution; (2) evaluate DEM accuracy through the usage of curvature; and (3) utilize interpolation method and spatial resolution to evaluate error and aid in DEM selection.

1.2 Materials and Methods

1.2.1 Site Background

The GPS survey was conducted on the Washington State University (WSU) Cunningham Agronomy Farm (CAF), a research site located approximately 8 km north of Pullman, Washington (Latitude -117.0892203 Longitude 46.77855434) (Figure 1.1). The CAF encompasses 61 hectares of irregularly oriented hills and ridges separated by U-shaped draws. The soils are well-drained, moderately permeable, silt loams consisting of complex associations of Palouse (fine-silty, mixed, mesic Pachic Ultic Haploxerolls), Naff (fine-silty, mixed mesic Ultic Argixerolls), Thatuna (fine-silty, mixed, mesic Xeric Argialbolls), and Staley (fine-silty, mixed, mesic Calcic Haploxerolls) soils. The mean precipitation between 1951 and 1980 was 54.15 cm (PCFS, 2004).

1.2.2 Global Positioning System Setup

A Trimble RTK 4400 was used to collect the elevation data with corresponding Easting and Northing values in the fall of 1999. The projection used was Universal Transverse Mercator (UTM) with World Geodetic System (WGS) 1984 zone 11N datum. When operating with at least 4 satellites, the Trimble unit is capable of gathering measurements in the vertical and horizontal plane with an accuracy of 0.02 m every second (Trimble Navigation, 2001). The GPS is comprised of two major pieces of equipment, a base station and a rover unit. A central location was chosen for the placement of the base unit, which allowed for continuous communication to the rover unit and the base unit did not need to be moved throughout the survey. Although a geographical benchmark is desired for the placement of the base unit, if given adequate time, the base unit can accurately calculate its own position within 2 cm (Trimble

Navigation, 2001). In this instance, the base unit remained stationary for two hours to calculate its position.

With the base unit in place, the rover unit antenna was attached to the passenger side of a half-ton pickup. The rover unit's antenna height from the ground was measured at the outset of the survey and input into the unit with the pickup located on flat ground. With the rover unit in place, the pickup was driven around the field in a north-south, east-west grid pattern while collecting position information from satellites and correction information from the base unit. During the survey, the same areas were passed over multiple times from different directions. Care was taken during the collection process to drive along ridge tops and valleys in order to have adequate data for the interpolation in areas where the terrain changed rapidly. The GPS data was logged every second using a Trimble TCS1 logging device. The Position Dilution of Precision (PDOP) mask was set at 6.0 during the majority of the survey. The mask filters GPS readings with a PDOP value greater than the mask. The PDOP is a unitless figure of merit expressing the relationship between the error in user position and the error in satellite position (Montana State University, 2004). When the relationship between the satellites and the GPS unit is inconsistent or poor, the calculated PDOP value will increase. A low PDOP value, 2.0, is better than a high one, 8.0. In instances of rough terrain where the GPS rover unit is being jarred about rapidly, the PDOP value can increase. The PDOP mask was increased at times during the survey to allow for more data collection in rough terrain. Once the rough terrain was passed over, the mask was again decreased. This adjustment of the PDOP mask was infrequent, and in general, it was not a problem during the survey.

1.2.3 Data Processing

Trimble software was used to export the data as a text file including easting, northing, elevation, horizontal error, vertical error, and PDOP. Easting, northing, and elevation are the positional value for the logged point. Easting and northing are UTM and each whole unit is a meter in distance. Elevation data were exported in feet and converted to meters. Horizontal and vertical error estimations based on satellite coverage and the calculated PDOP, were logged for each point in meters. The text file containing survey data was converted into a Dbase file and imported into ArcGIS 8.2 (ESRI). Geostatistical Analyst was utilized for interpolation of the DEM and Spatial Analyst for the calculation of terrain attributes. A number of different interpolation methods were tried in order to create a DEM including inverse distance weighted, spline, ordinary kriging, and local polynomial interpolation. Cross-validation results are created by Geostatistical Analyst (ESRI, 2002) containing measured value, predicted value, and error for each point used in the interpolation. Cross-validation files were imported into a spreadsheet for graphing of measured *versus* predicted data. After selection of an interpolation method, DEMs were made for raster cell sizes of 1-m, 2-m, 5-m, 10-m, 15-m, 20-m, 25-m, and 30-m.

Plan and profile curvature values were calculated from DEMs of varying cell size using the D8 method in ArcGIS 8.2 (ESRI 2002). The D8 method uses the eight cells surrounding a cell and calculates attributes based on elevation differences between the center cell and the surrounding eight cells (Wilson and Gallant, 2000). The calculation of curvature values are based on the second derivative of polynomials fit to the surface using the D8 method. Plan curvature is the rate of slope change along the contour, while profile curvature is the rate of slope change in the direction of the slope. Curvature rasters were calculated for each DEM raster size:

1-m, 2-m, 5-m, 10-m, 15-m, 20-m, 25-m, and 30-m. A histogram of the plan curvature raster was created to assess data distribution. Realistic curvature ranges were selected using reported values (ESRI, 2002) and data distribution, and used to calculate the amount of error area and to evaluate DEM interpolation and resolution.

1.3 Results and Discussion

1.3.1 Survey

The GPS survey resulted in 30440 Easting and Northing values with corresponding elevation data. On average, this gave one point for every 19.88 m². The data collection time was approximately 9 hours with two hours required for instrument set-up. The spatial distribution of the collected data is shown in Figure 1.2. Due to the turning of the vehicle, a higher density of data points was collected at the edge of the field. Elevation ranged from 773.13 m to 817.78 m (Table 1.1). Although the PDOP mask was primarily set to 6.0, the mean PDOP was 3.22, a value of 4.0 is considered acceptable (Trimble Navigation, 2001). The number of values greater than 4.0 was 4041 of the 30440 points, 13.28% (Figure 1.3). The maximum predicted horizontal error was 2.74 cm with a mean of 1.09 cm. The maximum predicted vertical error was 4.56 cm with a mean of 1.74 cm (Table 1.1). Of the PDOP values greater than 4.0, the mean predicted horizontal error was 0.82 cm and vertical error was 1.94 cm (Table 1.1).

Problems encountered during the survey were: (1) greater PDOP values on rough terrain; and (2) the base station signal being shadowed by hills. The first problem was addressed by adjusting the PDOP mask to a higher value until readings were again logged. This is not a preferred technique for operation of the GPS since the higher PDOP values will potentially lead to greater error in the data. Although adjustment of the PDOP mask was not performed often

during the survey, it could be a larger problem for GPS surveys conducted on rougher fields or terrain. Communication losses between the base station and rover unit were also encountered during the survey. The rolling hills of the Palouse can create a shadow affect limiting the effective range of the base unit. Communication losses were limited by utilizing a central location that reduced the maximum distance between the rover and the base unit and minimized obstructions. Placement necessities of the base unit could limit the amount of survey area that is possible to cover from a single location and require relocating the base unit to maintain communication.

1.3.2 Data Interpolation

Cross-validations for ordinary kriging (OK) and a local polynomial interpolation (LPI) had a correlation coefficient of 1.0 (Figures 1.4 and 1.5, Table 1.2). Even with high correlation coefficients, exact interpolation of the data creates error in the DEM (Figure 1.6). There are areas in the DEM where elevation changes quickly over a small distance due to relatively large changes in the GPS readings. The GPS survey results did not indicate these measurement problems, as the maximum vertical error estimation was 4.56 cm. These errors indicate problems with the raw GPS data, and that smoothing of the DEM (not using an exact interpolation) may be necessary to achieve an accurate representation of the landscape. The interpolation method chosen for further analysis was the LPI due to its ease and ability to be used as a data smoother based on the ratio of global to local influence on the interpolation. A drawback to LPI is that it does not utilize spatial trends in the data like kriging; it simply relies on polynomial fitting through the points for interpolation. In instances with sparse data, the LPI could result in poor landscape representation; however, rapid data collection and the density of

points from the RTK GPS makes the LPI very adequate for DEM creation in this instance.

The LPI method fits a polynomial to the surrounding points to create a prediction value at an unmeasured point (ESRI, 2000). In ArcGIS, the percentage of global and local polynomial fitting is specified for point prediction. A local polynomial utilizes a number of local points to create the model used to predict the value. A global polynomial utilizes all of the data points to create a model to fit to the prediction point. When the influence of the global polynomial is increased it tends to smooth the data while inducing cross-validation error. When the local polynomial is predominant, the interpolation is more exact and smoothing is minimized. Since the DEM is the model used for the calculation of terrain attributes, any errors in the DEM will be accentuated in derived terrain attributes. Although the cross-validation of exact interpolators of the DEM had a correlation coefficient of 1.0, error in the DEM can still exist and can be revealed once terrain attributes are calculated.

The ability to smooth the DEM via interpolation method becomes important when creating the final DEM in order to reduce error in the derived terrain attributes. The LPI interpolation method provides the flexibility of being an exact interpolator or a data smoother. When functioning as an exact interpolator, LPI can return prediction values very similar to the original data when cross validating. When functioning as a smoother, LPI can smooth over local variations in the DEM created by the raw data; however, cross-validation error increases. Digital elevation models were created from the LPI with increasing global polynomial influence that increased data smoothing (Figures 1.6 – 1.12). Cross-validations were calculated for each interpolation scheme in order to assess how well the interpolation method performed. The greater the local influence, the smaller the cross-validation error (Table 1.3).

The cross-validation error increased as the influence of the global polynomial increased,

but visual errors in the DEM decreased as the DEM was smoothed (Figure 1.12). Smoothing can be beneficial for removal of visual data error, but it can also create a poor representation of the landscape (Figure 1.12). A compromise between exact interpolation and a smoothed interpolation must be found in order to create the best DEM from these data. Since calculation of curvature is sensitive to the DEM, curvature values were used to assess interpolation schemes.

1.3.3 Curvature Rasters

Curvature rasters were calculated for DEMs with varying amounts of interpolation smoothing (Figures 1.13 – 1.26). The 100% local LPI for the 2-m DEM resulted in plan curvature values of -752.09 to 626.92 radians per 100 m and profile curvature values of -776.28 to 862.1 radians per 100 m (Tables 1.5, 1.6). As the global influence increased, however, the range of curvature values decreased, with a substantial change between 20% global and 40% global for both plan and profile curvature rasters. The minimum plan curvature value changed from -1133.13 to -9.36 radians per 100 m, and the maximum value changed from 823.26 to 9.27 radians per 100 m for an increase in global influence from 20% to 40%, respectively. The minimum profile curvature value changed from -650.97 to -14.35 radians per 100 m, and the maximum value changed from 779.98 to 9.47 radians per 100 m as global influence increased from 20% to 40%, respectively. Although the range of curvature values at the 40% global influence are closer to reported values than the 100% local influence (Wilson and Gallant, 2000), they are still unrealistic. The unrealistic range in curvature value is an indication of DEM error.

The source of error in DEMs created from GPS data can be either inaccuracy in the GPS data and/or in the data collection method. Even though cross-validation of the exact LPI method had a correlation coefficient of 1.0; the resulting DEM still had sufficient error to create

unrealistic curvature ranges (Tables 1.4 and 1.5). Without any known benchmarks in the field, it is difficult to assess GPS accuracy. The output from the GPS suggests that the GPS was very consistent and accurate. Typically, if the GPS was producing inaccurate data, it is unlikely that it would do it consistently. Rather the readings would create erratic areas in the DEM due to poor satellite coverage and correction (Trimble Navigation, 2001). The DEMs created with the LPI of 70% or more local polynomial influence have this erratic error (Figures 1.6-1.8). The curvature rasters calculated from the DEMs with 70% or more local polynomial influence have very extreme ranges (Table 1.6). When the global influence approaches 40%, erratic DEM errors disappear (Figures 1.8-1.12), and calculated curvature ranges are reduced (Table 1.6). The curvature values for these smoother DEMs, however, have a range greater than what the literature suggests (Wilson and Gallant, 2000), which indicates that the collection method may also have introduced error.

Erratic errors in the DEM were smoothed by an LPI of 40% global 60% local; however, a streaking pattern appeared (Figure 1.27). It was found that when on a 35% slope, the height of the pickup bed on the uphill side was 15 cm higher than the downhill side (Figure 1.28). When the rover unit was driven back and forth on a slope, the antenna changed from the uphill side to the downhill side in adjacent passes, causing the relative height of the GPS antenna in reference to the surface to change by as much as 15 cm. The deviation in the height of the antenna from the ground during the survey cannot be accounted for by the GPS. Deviations in rover antenna elevation affected the data recorded, resulting in inaccurate elevation values.

1.3.4 Digital Elevation Model Error Assessment, Choosing a Final Interpolation Scheme

Plan and profile curvature rasters were used to assess DEM error. In order to utilize

curvature ranges as a tool, a realistic range for curvature was established from a histogram of the 2-m 100% local plan curvature raster. The frequency histogram showed that 80% of the plan curvature raster cells fell between -1 and 1 radian per 100 m (Figure 1.29). This range is consistent with reported values (ESRI, 2002) and is the assumed range for curvature values for our field. Establishing this realistic range allows the quantification of area error in the DEM that affects curvature values.

Error in the curvature rasters was used to assess DEM error based on the realistic range for curvature established by the histogram. Curvature rasters created from the DEMs of different local and global polynomial influence were classified as to whether or not a cell fell into the -1 to 1 radians per 100 m range. The number of cells outside of the realistic range were converted to an area and compared to the area of cells in the assumed range (Table 1.6). Plan curvature values outside of the -1 to 1 radians per 100 m ranged from 0 to 23%. Profile curvature rasters for the DEMs varied from 0 to 25% of the area outside of the realistic range (Table 1.7). The raster that had the most area outside the range was the 100% local LPI for both the plan and profile curvature. Rasters that had the least amount of area outside the realistic range were the 90% global LPI for both the plan and profile curvature rasters. In the percentage change from 20 to 40% global influence, the amount of outlier area for the plan curvature rasters decreased from 14 to 2% while profile rasters decreased from 16 to 3%, respectively.

Curvature surface area error and curvature range decreased, going from a maximum of 0.49 to 1.15 m and a minimum of -0.71 to -1.4 m, respectively (Table 1.7) with increasing global influence. The cross-validation error increased to over 4.0 m, as global influence exceeded 40% (Table 1.8). Taking into account both of these findings, an LPI of 30% global and 70% local was chosen as the final interpolation scheme used for the DEMs. It was chosen as a

compromise between curvature error and interpolation error. Cross-validation of the 30% global and 70% local interpolation had a maximum, minimum, and mean error of 0.60 m, -0.88 m, and 0.01m, respectively. A series of DEMs were created using the LPI method with 30% global and 70% local influence with increasing cell sizes: 1-m, 2-m, 5-m, 10-m, 15-m, 20-m, 25-m, and 30-m (Figures 1.30-1.37).

1.3.5 Minimizing Digital Elevation Model Error by Increasing Raster Cell Size

The second approach used to reduce error in the DEM was based on varying spatial resolution. The maximum and minimum plan curvature values changed from 203.16 to 0.81 radians per 100 m and -154.49 to -0.71 radians per 100 m, respectively as resolution increased from 1 to 30-m. The maximum and minimum profile curvature values changed from 207.88 to 0.82 radians per 100 m and -277.11 to -1.25 radians per 100 m, respectively as resolution increased from 1 to 30-m. The largest change in plan and profile curvature ranges occurred from the 1 to 2-m resolutions (Tables 1.10, 1.11). When the resolution changed from 1 to 2-m, plan curvature maximum values decreased from 203.16 to 52.17 radians per 100 m and the minimum values increased from -154.49 to -31.87 radians per 100 m. Similarly, profile curvature maximum values decreased from 207.88 to 50.33 radians per 100 m and the minimum values increased from -277.11 to -61.59 radians per 100 m when resolution increased from 1 to 2-m. The amount of error area also had the greatest reduction between the 1-m raster and 2-m raster (Table 1.12, 1.13). Here, the error area for plan curvature decreased from 7% to 2%, while profile curvature error decreased from 9% to 4% for the 1 and 2-m rasters, respectfully.

The improvement in curvature range and area error was not as substantial for any other raster cell size. At the 2-m level, both plan and profile curvature error areas were under 5%.

Coupled with the fact that there were only small improvements when increasing cell size beyond 2-m, the 2-m raster was identified as the finest resolution that could be created with an acceptable amount of error from this GPS data.

1.4 Conclusion

Real time kinematic GPS technology allows for rapid and accurate data collection of elevation data. In this survey, the data proved dense enough, 1 every 20 m², and accurate enough, within 2 cm, for the use of a variety of interpolation methods to create a DEM. Although interpolation had a cross-validation correlation coefficient of 1.0, there was error in the DEM from inaccurate GPS data and the collection technique. The calculations of plan and profile curvatures on all DEMs allowed for critiquing the interpolation scheme and raster cell size for each DEM. Once the amount of plan and profile curvature error was quantified based on calculated rasters, the DEMs could be compared for amounts of error. When error and cross-validation for the DEMs was coupled, a compromise was formed for choosing the best DEM that this survey could provide. A 2-m DEM created from a 30% global and 70% local LPI provided acceptable amounts of curvature error with minimal amounts of error from cross-validation.

1.5 Tables

Table 1.1. Results of real time, kinematic, global positioning system survey based on 30440 data points for the Cunningham Agronomy Farm.

Measurement	Maximum	Minimum	Mean
Elevation (m)	817.78	773.13	793.36
Horizontal Error (m)	0.027	0.003	0.01
Vertical Error (m)	0.046	0.006	0.02
PDOP* Value	17.64	0.10	3.22
Horizontal Error of PDOP Values > 4 (m)	0.027	0.001	0.010
Vertical Error of PDOP Values > 4 (m)	0.046	0.069	0.019

* Position Dilution of Precision (PDOP)

Table 1.2. Cross-validation of elevation results for local polynomial interpolation and ordinary kriging when used as exact interpolators.

<u>Cross Validation Result</u>	<u>Local Polynomial Interpolation</u>	<u>Ordinary Kriging</u>
----- m -----		
Maximum Predicted Elevation	817.66	817.77
Minimum Predicted Elevation	773.15	773.14
Mean Predicted Elevation	793.37	793.37
Maximum Prediction Error	1.00	0.28
Minimum Prediction Error	-0.40	-0.32
Mean Prediction Error	0.00	0.00

Table 1.3. Cross-validation results for digital elevation models created from local polynomial interpolation with increasing global polynomial influence.

<u>Global Polynomial Influence</u>	<u>Local Polynomial Influence</u>	<u>Maximum Predicted Value</u>	<u>Minimum Predicted Value</u>	<u>Mean Predicted Value</u>	<u>Maximum Prediction Error</u>	<u>Minimum Prediction Error</u>	<u>Mean Prediction Error</u>
----- % -----		----- m -----					
0	100	817.66	773.15	793.37	1.00	-0.40	0.00
10	90	817.65	773.15	793.36	0.99	-0.5	0.00
20	80	817.59	773.15	793.37	0.49	-0.71	0.00
40	60	816.81	773.14	793.38	1.15	-1.40	0.02
60	40	813.20	772.14	793.29	4.40	-5.74	-0.07
80	20	807.39	776.41	793.25	10.09	-14.51	-0.11
90	10	806.56	778.25	793.30	12.03	-16.65	-0.06

Table 1.4. Plan curvature raster results for 2-m digital elevation models created from local polynomial interpolation with increasing global polynomial influence.

<u>Global Polynomial Influence</u>	<u>Local Polynomial Influence</u>	<u>Maximum</u>	<u>Minimum</u>	<u>Mean</u>
----- % -----		----- radians/100 m -----		
0	100	626.92	-752.09	0.04
10	90	647.23	-742.65	0.05
20	80	823.26	-1133.13	0.02
40	60	9.27	-9.38	0.03
60	40	5.38	-6.65	0.02
80	20	1.08	-1.16	0.00
90	10	0.94	-0.60	0.00

Table 1.5. Profile curvature raster results for 2-m digital elevation models created from local polynomial interpolation with increasing global polynomial influence.

<u>Global Polynomial Influence</u>	<u>Local Polynomial Influence</u>	<u>Maximum</u>	<u>Minimum</u>	<u>Mean</u>
----- % -----		----- radians/100 m -----		
0	100	862.10	-776.28	0.04
10	90	762.71	-786.23	0.05
20	80	779.98	-650.97	0.02
40	60	9.47	-14.35	0.03
60	40	9.63	-9.27	0.02
80	20	2.50	-2.28	0.00
90	10	1.83	-2.02	0.00

Table 1.6. Realistic (>-1 and <1 radians per 100 m) and outlier cells (<-1 and >1 radians per 100 m) of plan curvature rasters for 2-m digital elevation models created from local polynomial interpolation with increasing global polynomial influence.

<u>Global Polynomial Influence</u>	<u>Local Polynomial Influence</u>	<u>Outlier Cells</u>	<u>Realistic Cells</u>	<u>Area of Outlier Cells</u>	<u>Area of Realistic Cell</u>	<u>Outlier Percentage of Total Area</u>
----- % -----	----- no. -----			----- m ² -----		- % -
0	100	35920	123036	143680	492144	23
10	90	32275	126681	129100	506724	20
20	80	21806	137150	87229	548600	14
40	60	3553	155403	14212	621612	2
60	40	814	158142	3256	632568	1
80	20	3	158953	12	635812	0
90	10	0	158956	0	635824	0

Table 1.7 Realistic (>-1 and <1 radians per 100 m) and outlier cells (<-1 and >1 radians per 100 m) of profile curvature rasters for 2-m digital elevation models created from local polynomial interpolation with increasing global polynomial influence.

<u>Global Polynomial Influence</u>	<u>Local Polynomial Influence</u>	<u>Outlier Cells</u>	<u>Realistic Cells</u>	<u>Area of Outlier Cells</u>	<u>Area of Realistic Cell</u>	<u>Outlier Percentage of Total Area</u>
----- % -----	----- no. -----			----- m ² -----		- % -
0	100	39274	119682	157096	478728	25
10	90	35851	123105	143404	492420	23
20	80	25285	133671	101140	534684	16
40	60	5110	153846	20440	615384	3
60	40	1424	157532	5696	630128	1
80	20	598	158358	2392	633432	0
90	10	612	1583441	2448	633376	0

Table 1.8. Cross-validation results for digital elevation models created using a local polynomial interpolation with increasing global influence.

<u>Global Polynomial Influence</u>	<u>Local Polynomial Influence</u>	<u>Maximum Error</u>	<u>Minimum Error</u>	<u>Mean Error</u>
----- % -----		-----	----- m ² -----	
0	100	1.00	-0.40	0.00
10	90	0.99	-0.49	0.00
20	80	0.49	-0.71	0.00
40	60	1.15	-1.40	0.02
60	40	4.40	-5.74	-0.07
80	20	10.09	-14.51	-0.12
90	10	12.03	-16.65	-0.06

Table 1.9. Elevation statistics for digital elevation models created using local polynomial interpolation with 30% global and 70% local polynomial influence for increased raster cell size.

<u>Raster Resolution</u>	<u>Maximum</u>	<u>Minimum</u>	<u>Mean</u>
----- m -----			
1	818.26	771.92	793.51
2	818.18	771.80	793.49
5	817.87	772.03	793.52
10	817.58	772.06	793.98
15	817.18	773.09	793.47
20	817.15	773.09	793.44
25	817.21	773.13	793.44
30	815.76	773.21	793.45

Table 1.10. Plan curvature raster results for increasing resolution from digital elevation models created using local polynomial interpolation with 30% global and 70% local polynomial influence.

<u>Raster Resolution</u>	<u>Maximum</u>	<u>Minimum</u>	<u>Mean</u>
-- m --	----- radians/100 m -----		
1	203.16	-154.49	0.03
2	52.71	-31.87	0.03
5	3.58	-6.35	0.03
10	1.98	-1.74	0.03
15	1.16	-0.91	0.03
20	1.31	-1.00	0.03
25	1.57	-0.92	0.03
30	0.81	-0.71	0.03

Table 1.11. Profile curvature raster results for increasing resolution from digital elevation models created using local polynomial interpolation with 30% global and 70% local polynomial influence.

<u>Raster Resolution</u>	<u>Maximum</u>	<u>Minimum</u>	<u>Mean</u>
-- m --	----- radians/100 m -----		
1	207.88	-277.11	0.03
2	50.33	-61.59	0.03
5	6.25	-7.22	0.03
10	2.39	-2.48	0.03
15	1.24	-1.93	0.03
20	0.99	-1.60	0.03
25	0.98	-1.61	0.03
30	0.82	-1.25	0.03

Table 1.12. Realistic (>-1 and <1 radians per 100 m) and outlier (<-1 and >1 radians per 100 m) cells of plan curvature rasters with increasing resolution from digital elevation models created using local polynomial interpolation with 30% global and 70% local polynomial influence.

<u>Raster Resolution</u>	<u>Outlier Cells</u>	<u>Realistic Cells</u>	<u>Area of Outlier Cells</u>	<u>Area of Realistic Cell</u>	<u>Outlier Percentage of Total Area</u>
-- m --	----- no. -----		----- m ² -----		-- % --
1	42007	593883	42007	593883	7
2	3470	155486	13880	621944	2
5	253	25227	6325	630675	1
10	23	6346	2300	634600	0
15	4	2828	900	636300	0
20	3	1581	1200	632400	0
25	1	1016	625	635000	0
30	0	709	0	638100	0

Table 1.13. Realistic (>-1 and <1 radians per 100 m) and outlier (<-1 and >1 radians per 100 m) cells of profile curvature rasters with increasing resolution from digital elevation models created using local polynomial interpolation with 30% global and 70% local polynomial influence.

<u>Raster Resolution</u>	<u>Outlier Cells</u>	<u>Realistic Cells</u>	<u>Area of Outlier Cells</u>	<u>Area of Realistic Cell</u>	<u>Outlier Percentage of Total Area</u>
-- m --	----- no. -----		----- m ² -----		-- % --
1	59256	576634	59256	576634	9
2	6327	152629	25308	610516	4
5	702	24778	17550	619450	3
10	122	6247	12200	624700	2
15	31	2801	6975	630225	1
20	8	1576	3200	630400	1
25	2	1015	1250	634375	0
30	2	707	1800	636300	0

1.6 Figures



Figure 1.1. A 1996 aerial photograph of Cunningham Agronomy Farm.

Surveyed Points

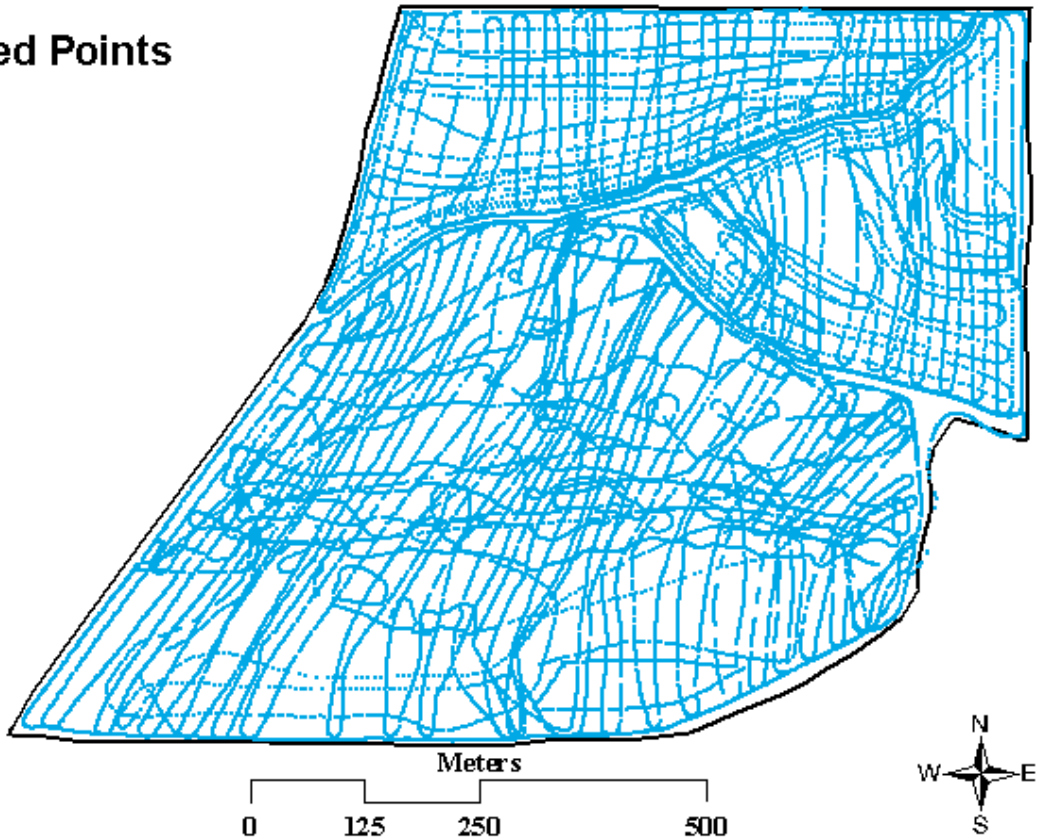


Figure 1.2. Post plot of global positioning system data points collected during kinematic survey of the Cunningham Agronomy Farm in fall of 1999.

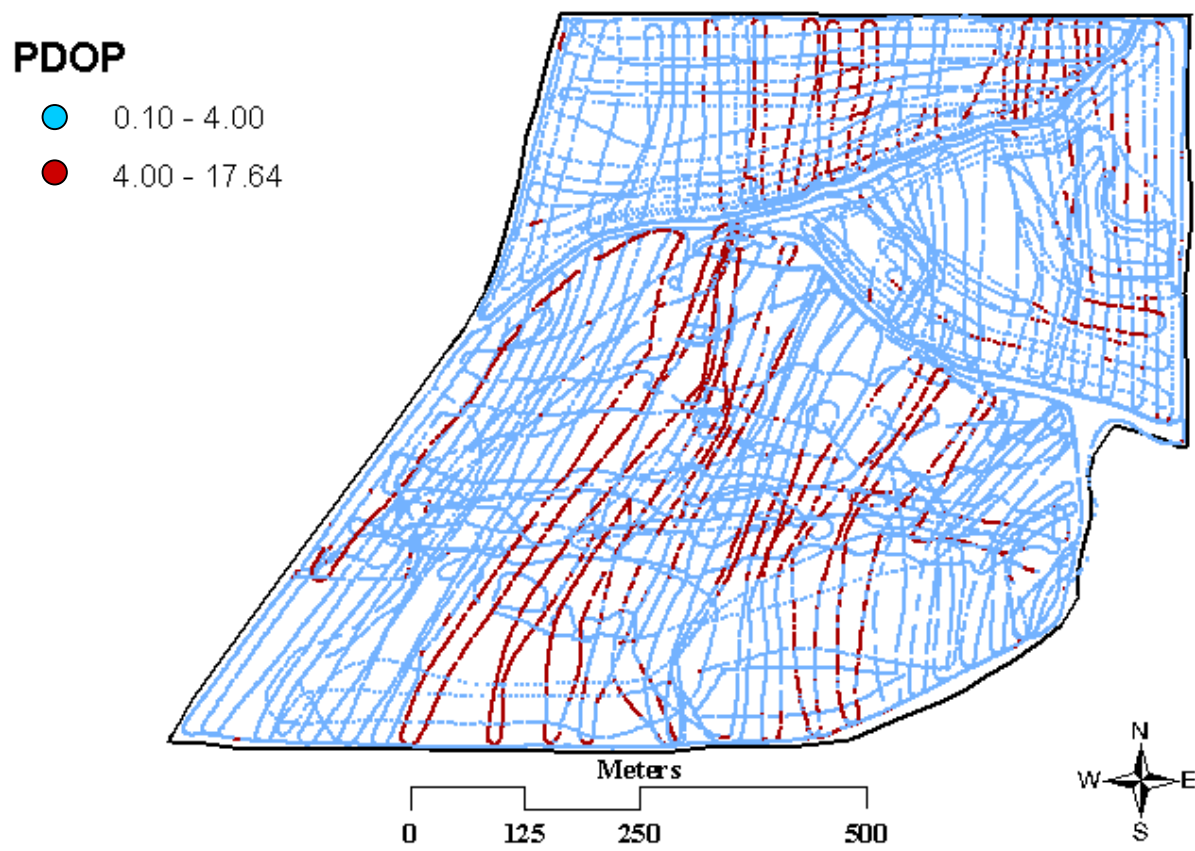


Figure 1.3. Post plot of global positioning system data points collected during kinematic survey of the Cunningham Agronomy Farm with position dilution of precision (PDOP) greater or less than 4.0.

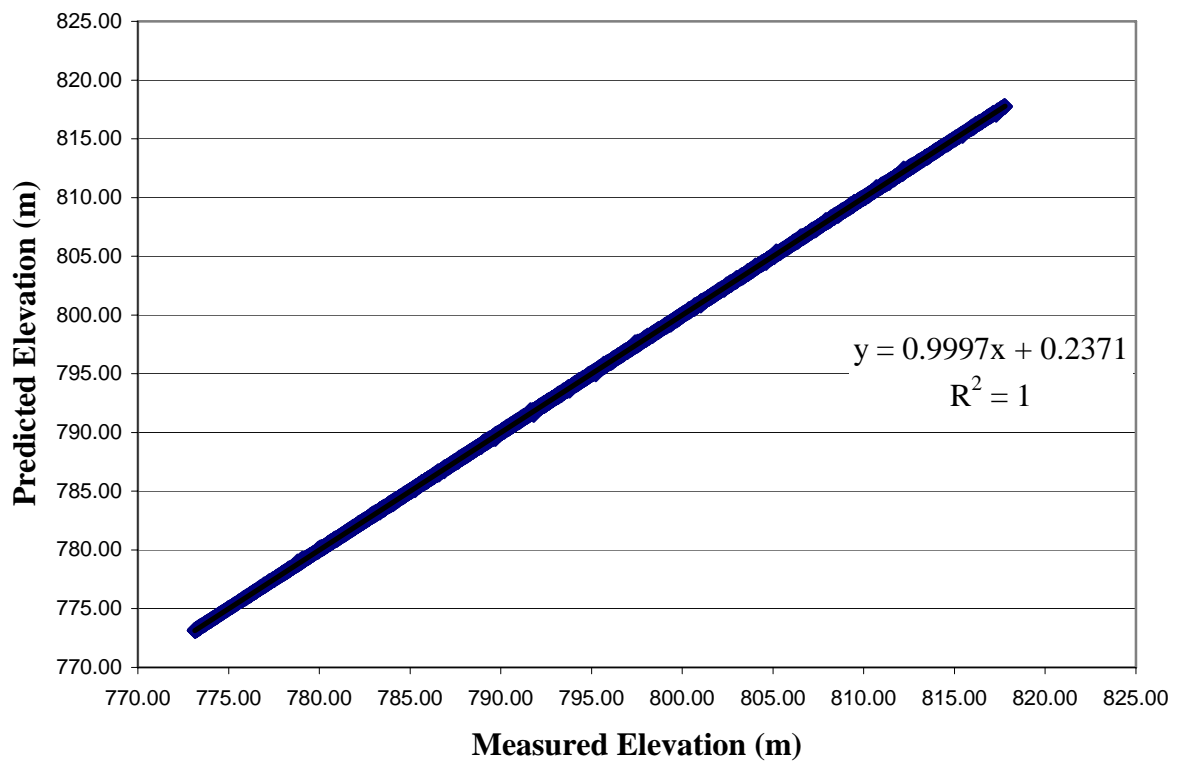


Figure 1.4. Cross-validation of ordinary kriging interpolation of 30440 global positioning system survey elevation points on the Cunningham Agronomy Farm.

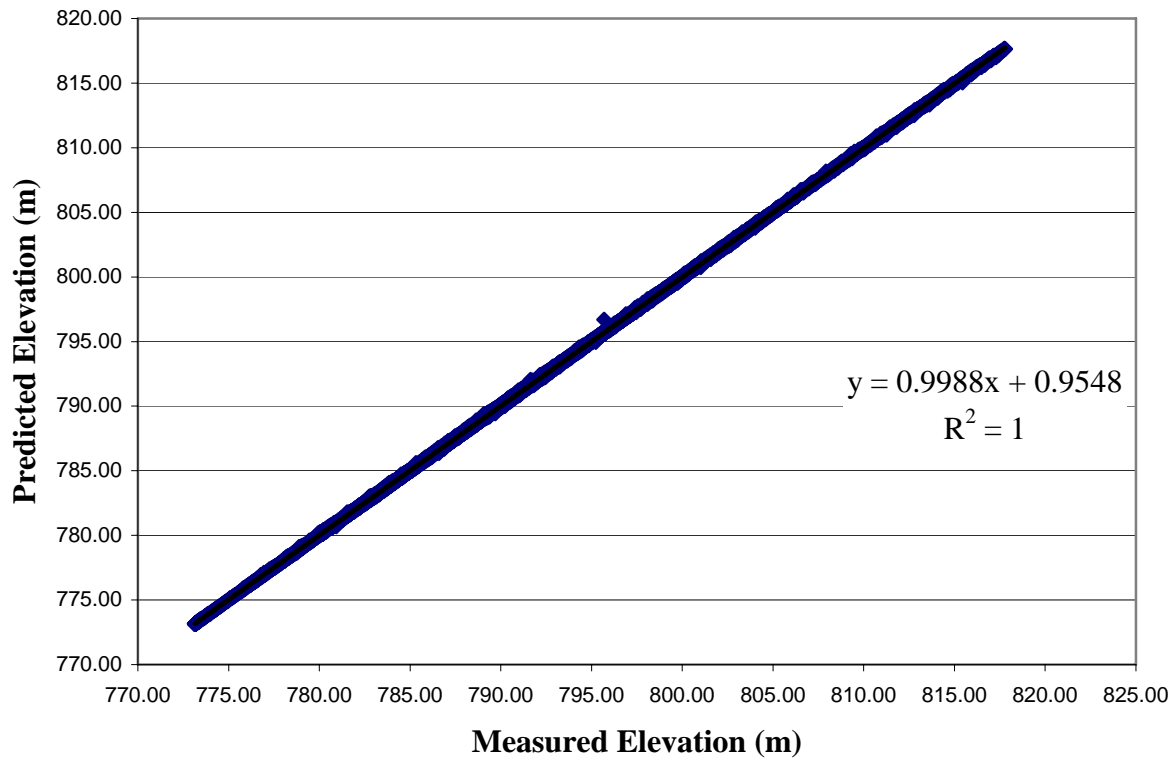


Figure 1.5. Cross validation of exact local polynomial interpolation of 30440 global positioning system survey elevation points on the Cunningham Agronomy Farm.

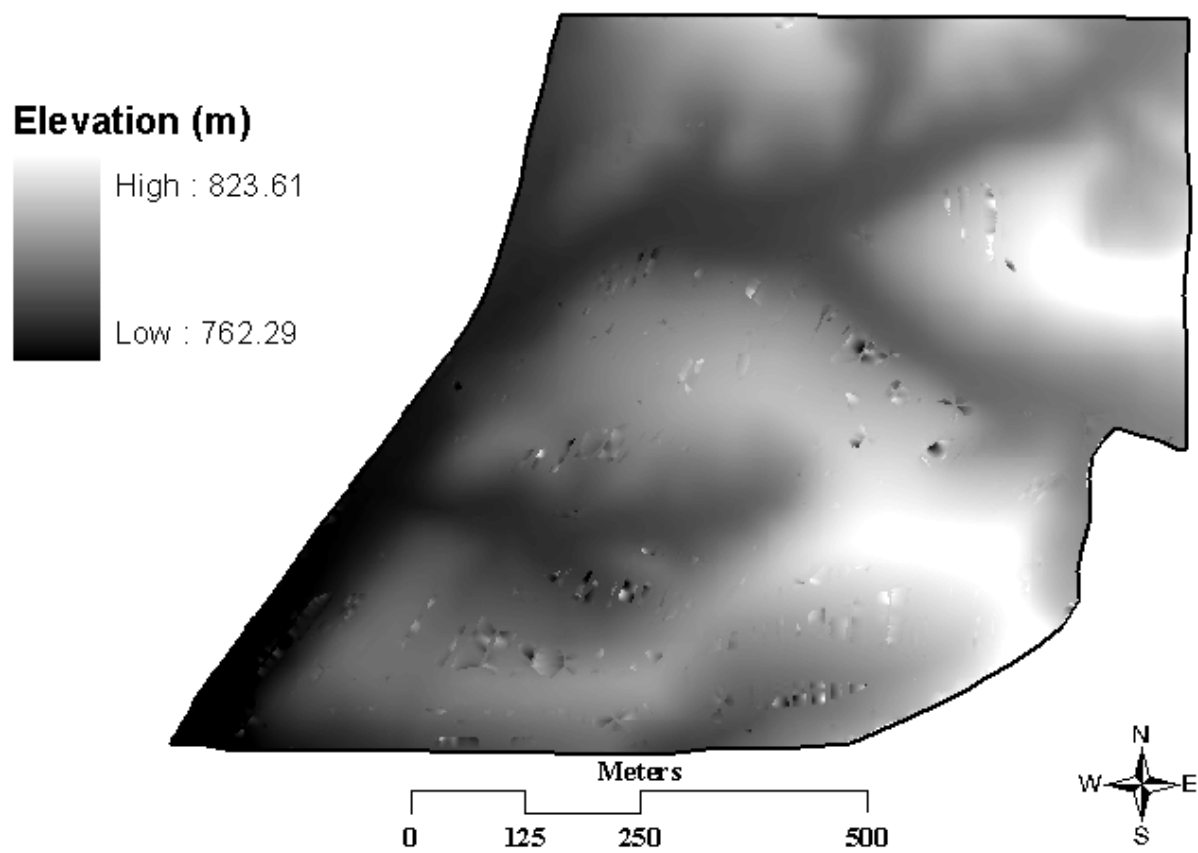


Figure 1.6. A 2-m digital elevation model created from 100% local and 0% global polynomial interpolation.

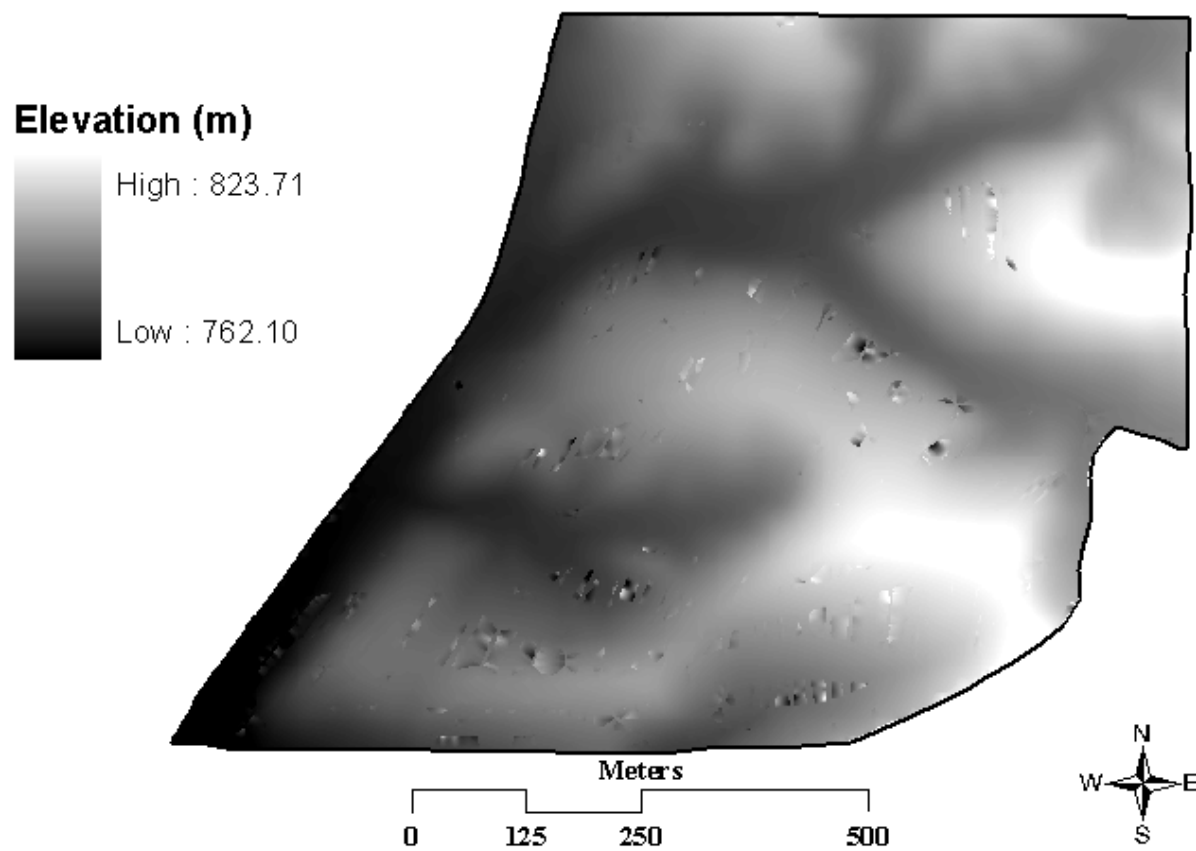


Figure 1.7. A 2-m digital elevation model created from 90% local and 10% global polynomial interpolation.

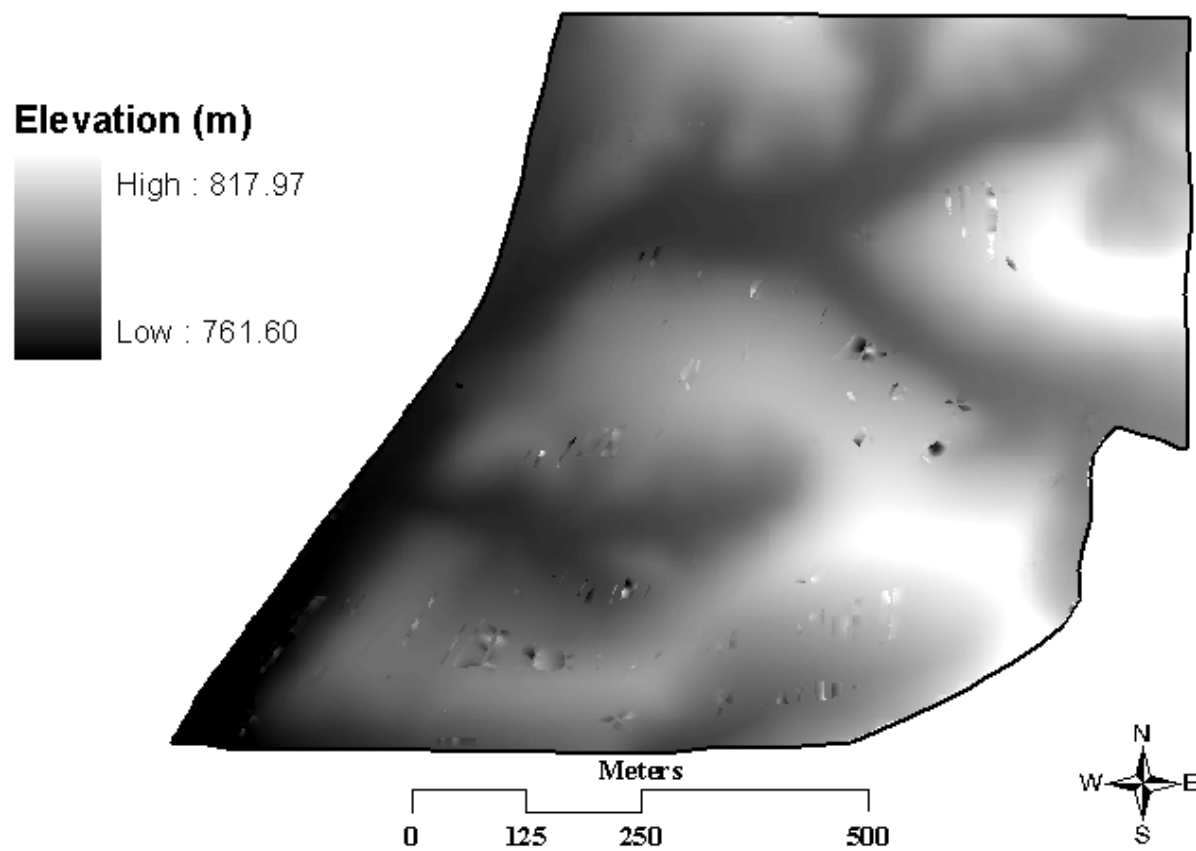


Figure 1.8. A 2-m digital elevation model created from 80% local and 20% global polynomial interpolation.

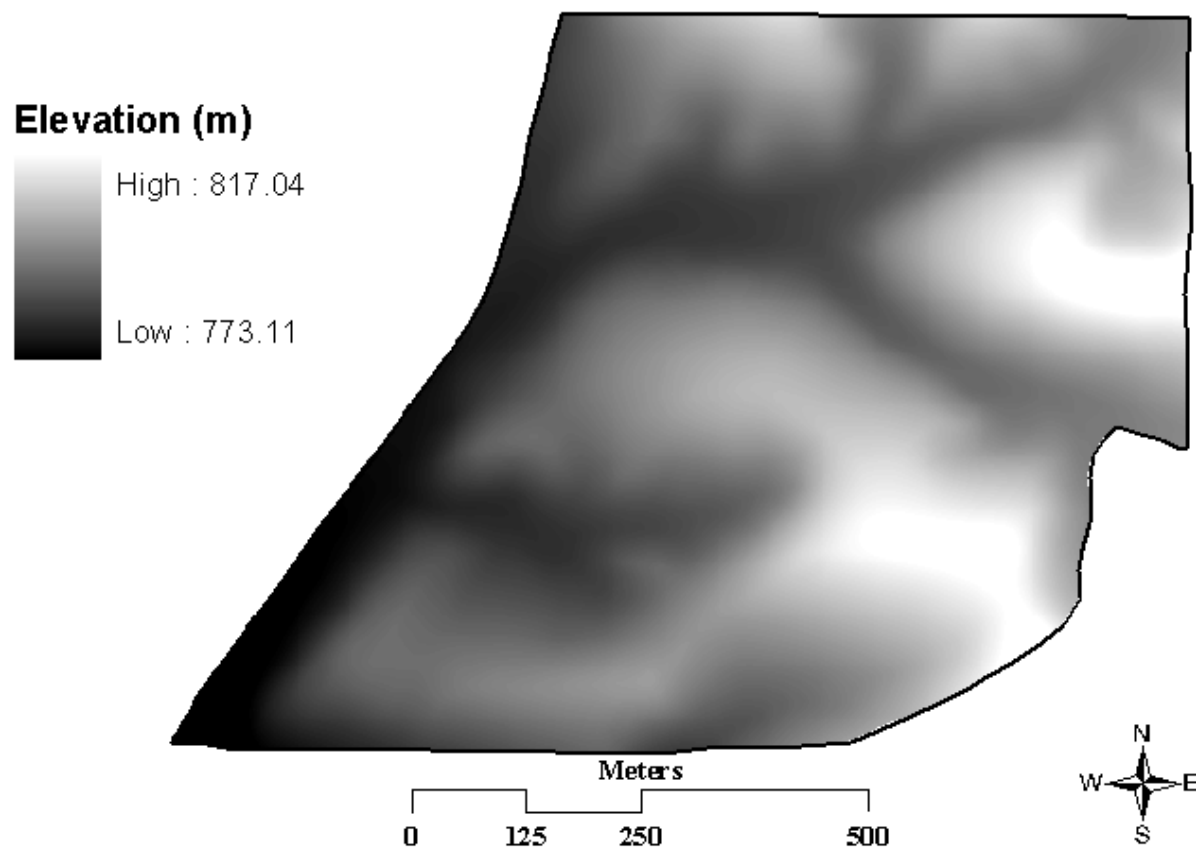


Figure 1.9. A 2-m digital elevation model created from 60% local and 40% global polynomial interpolation.

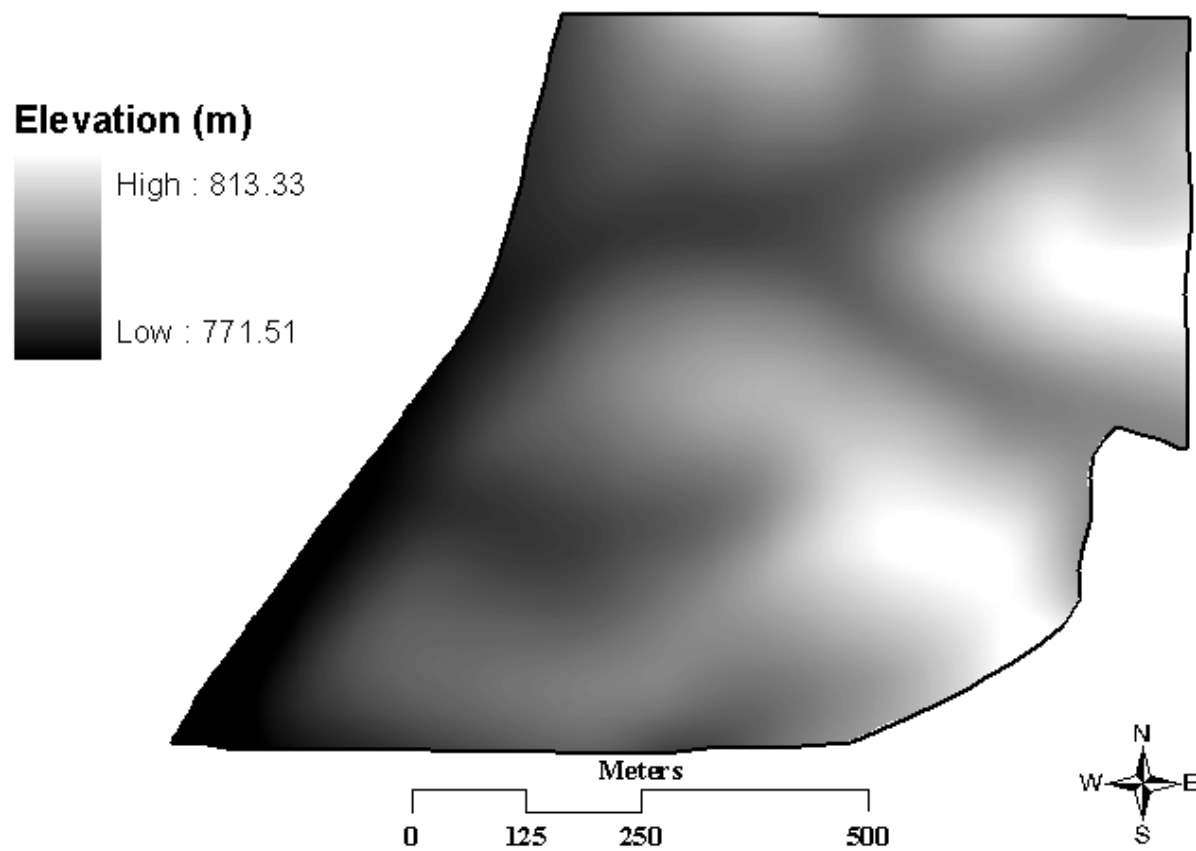


Figure 1.10. A 2-m digital elevation model created from 40% local and 60% global polynomial interpolation.

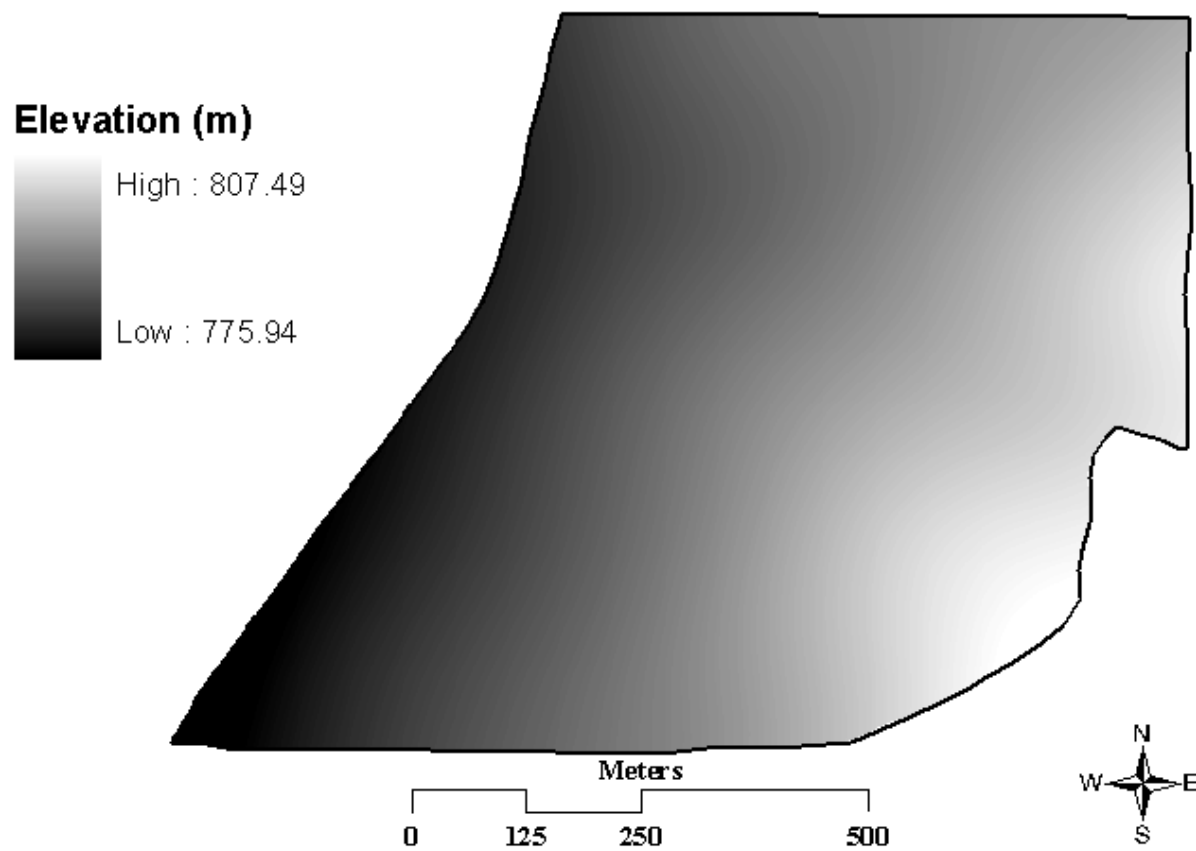


Figure 1.11. A 2-m digital elevation model created from 20% local and 80% global polynomial interpolation.

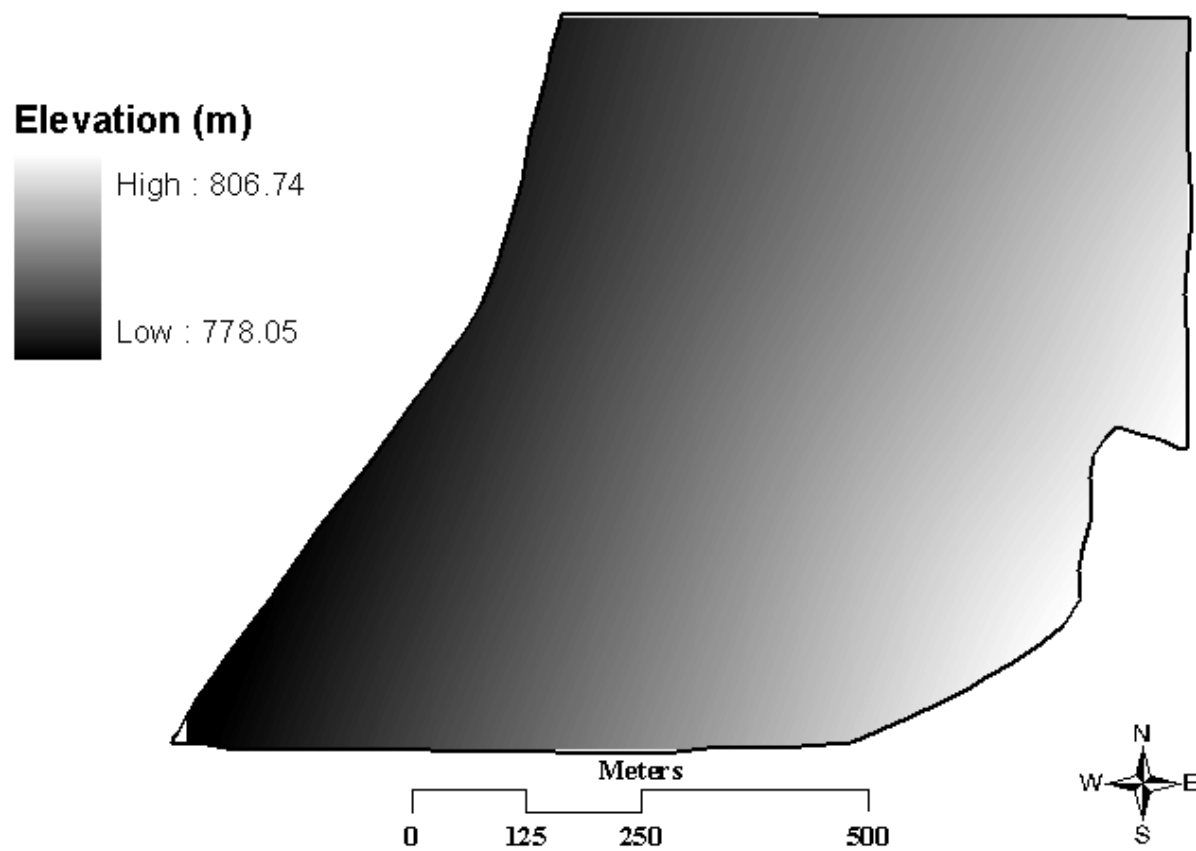


Figure 1.12. A 2-m digital elevation model created from 10% local and 90% global polynomial interpolation.

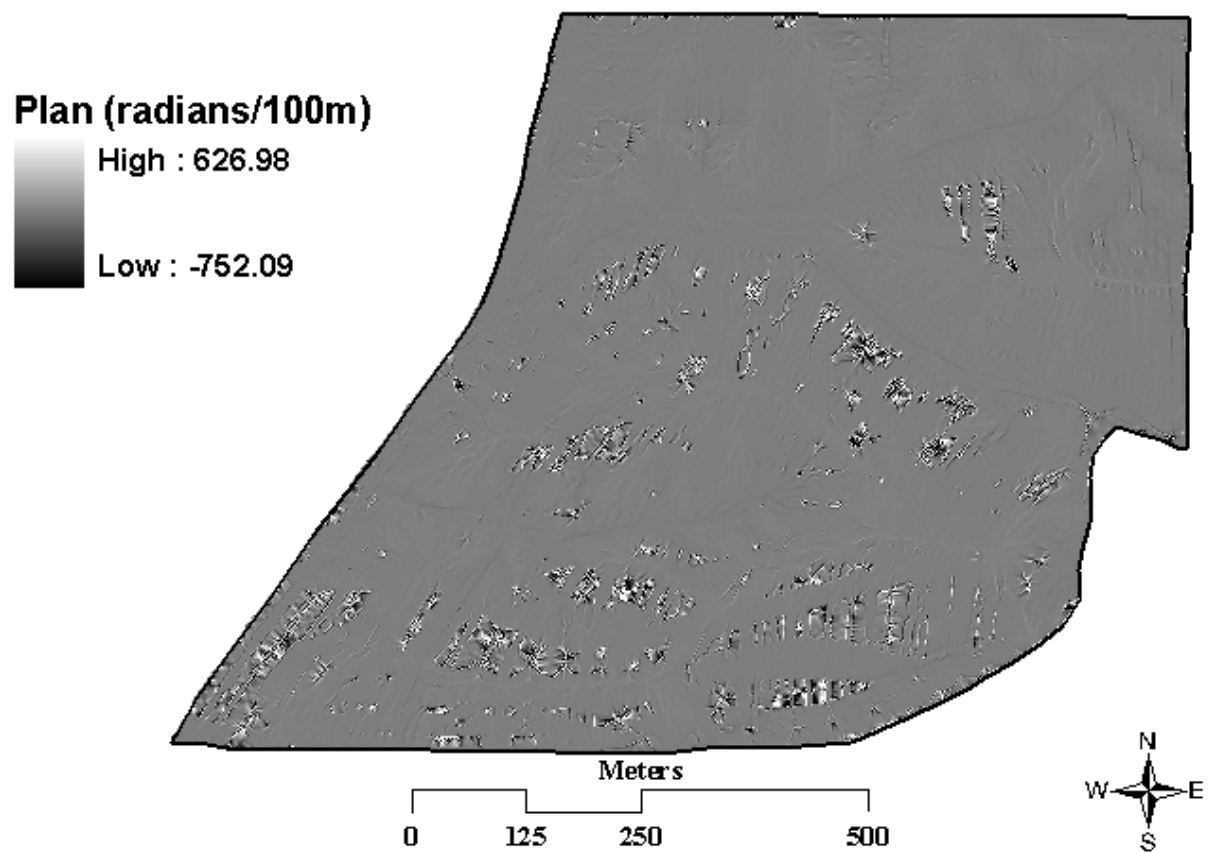


Figure 1.13. A plan curvature raster created from 100% local and 0% global polynomial interpolation of a 2-m digital elevation model.

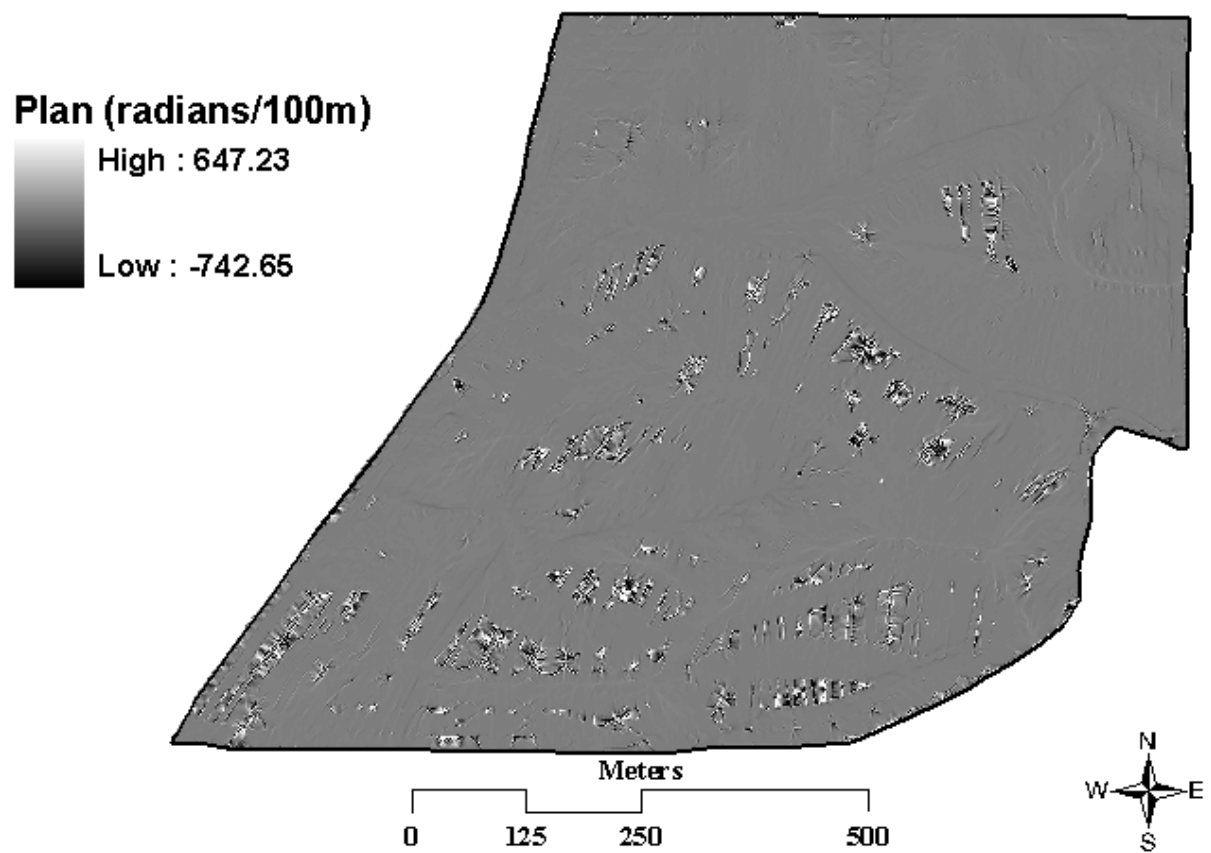


Figure 1.14. A plan curvature raster created from 90% local and 10% global polynomial interpolation of a 2-m digital elevation model.

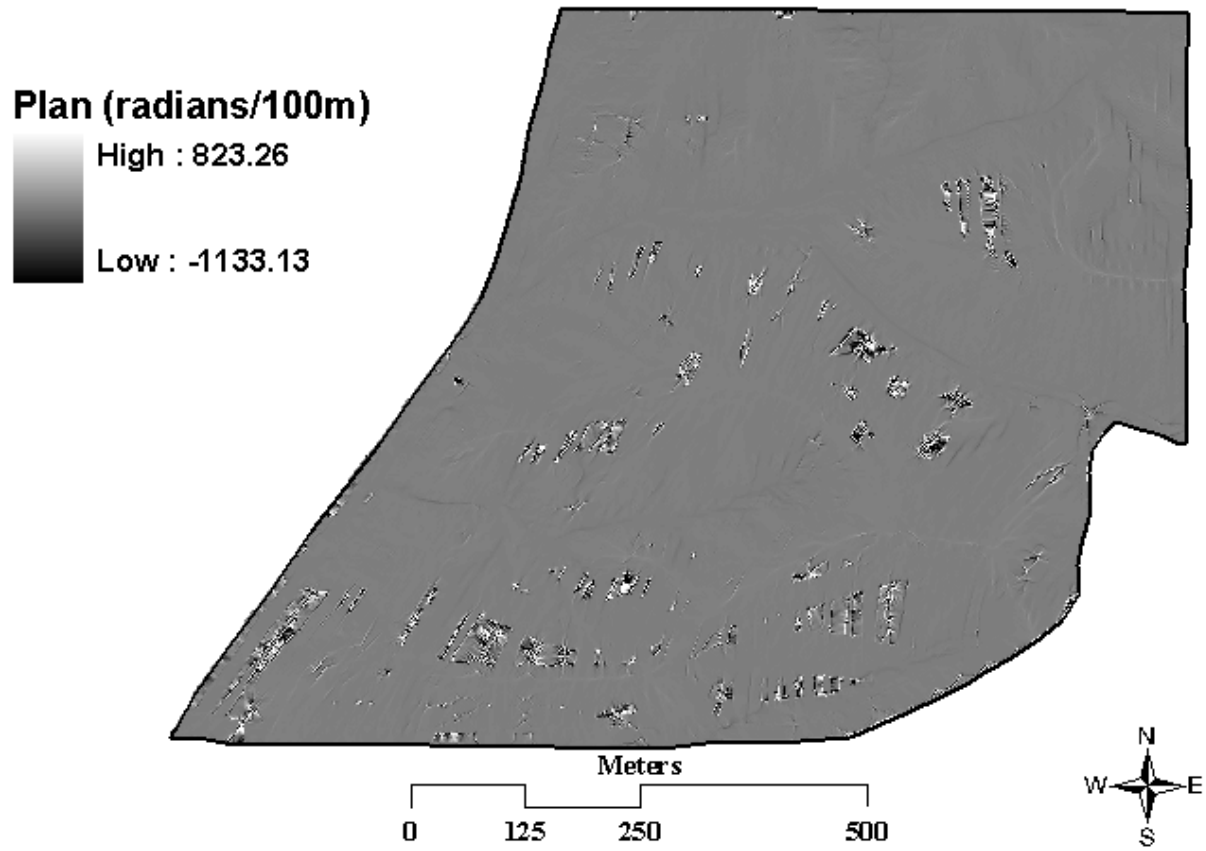


Figure 1.15. A plan curvature raster created from 80% local and 20% global polynomial interpolation of a 2-m digital elevation model.

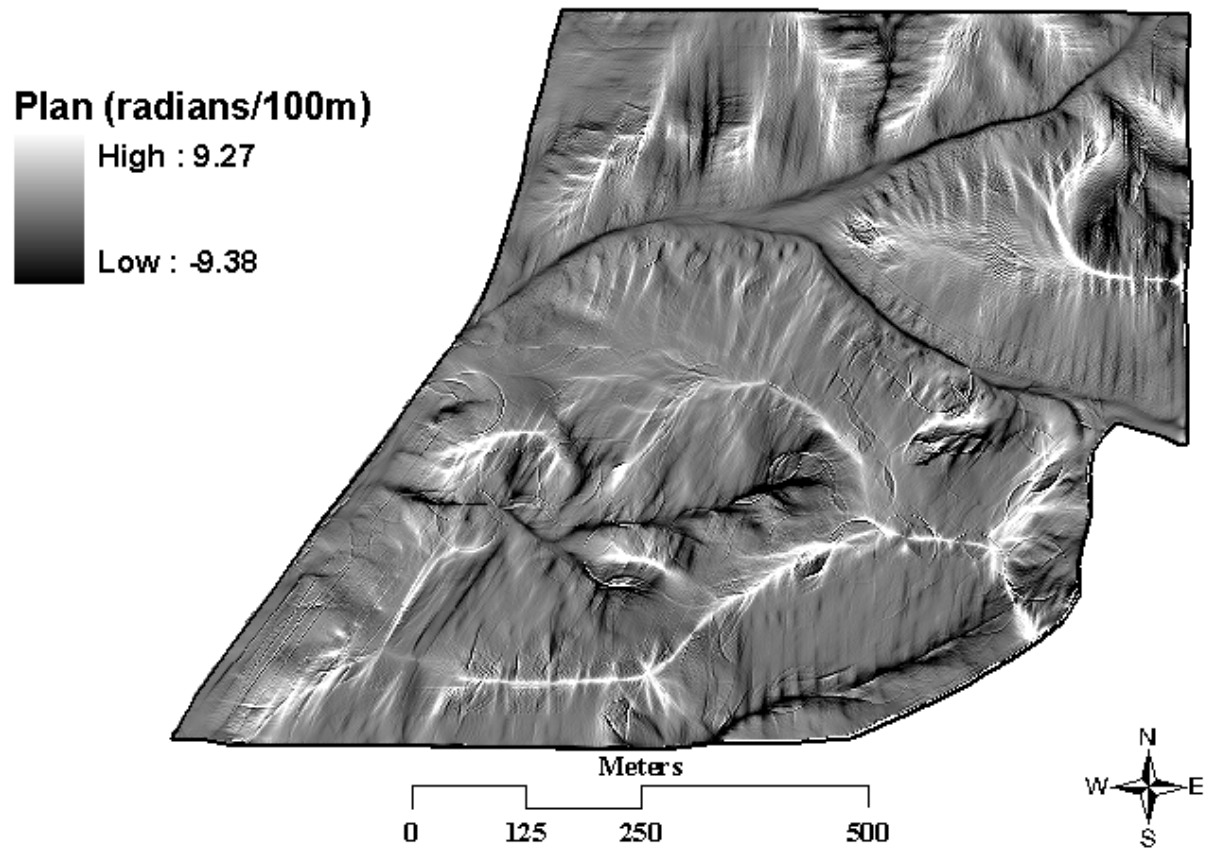


Figure 1.16. A plan curvature raster created from 60% local and 40% global polynomial interpolation of a 2-m digital elevation model.

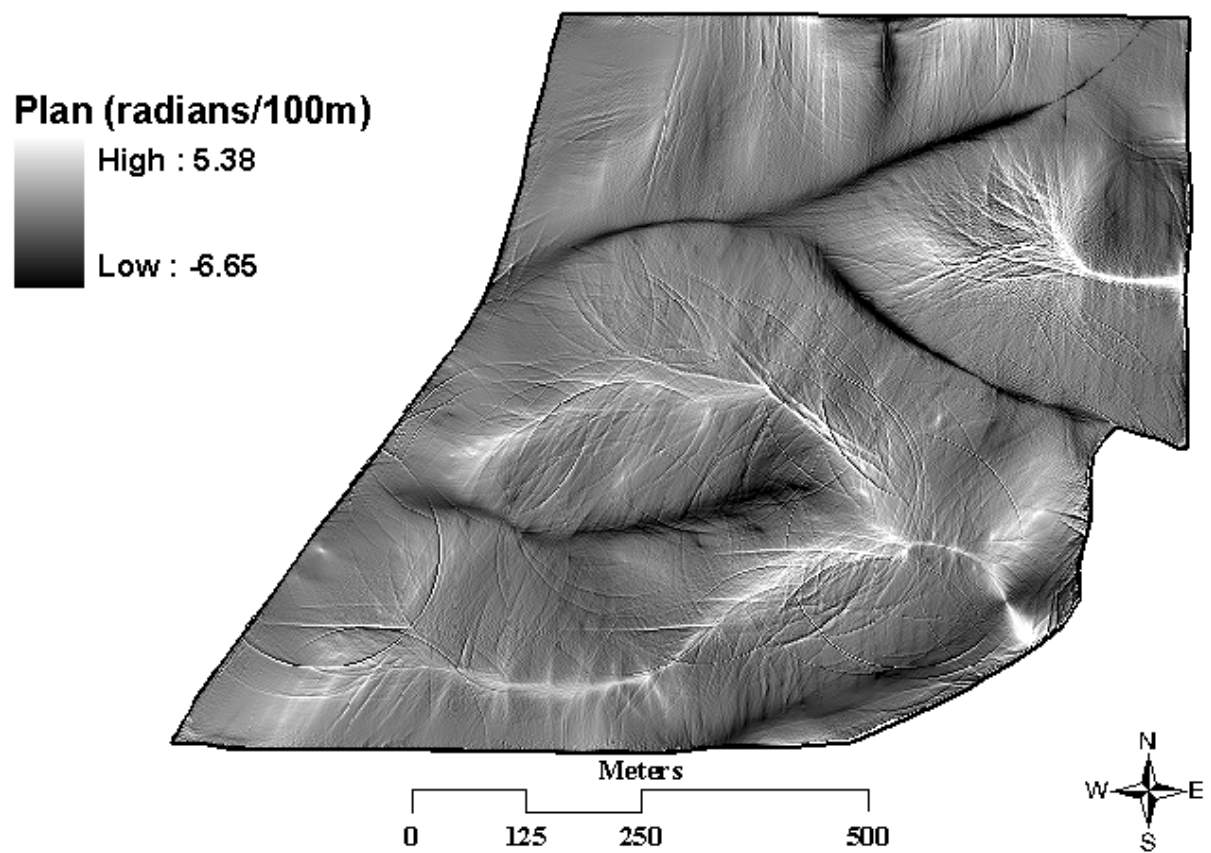


Figure 1.17. A plan curvature raster created from 40% local and 60% global polynomial interpolation of a 2-m digital elevation model.

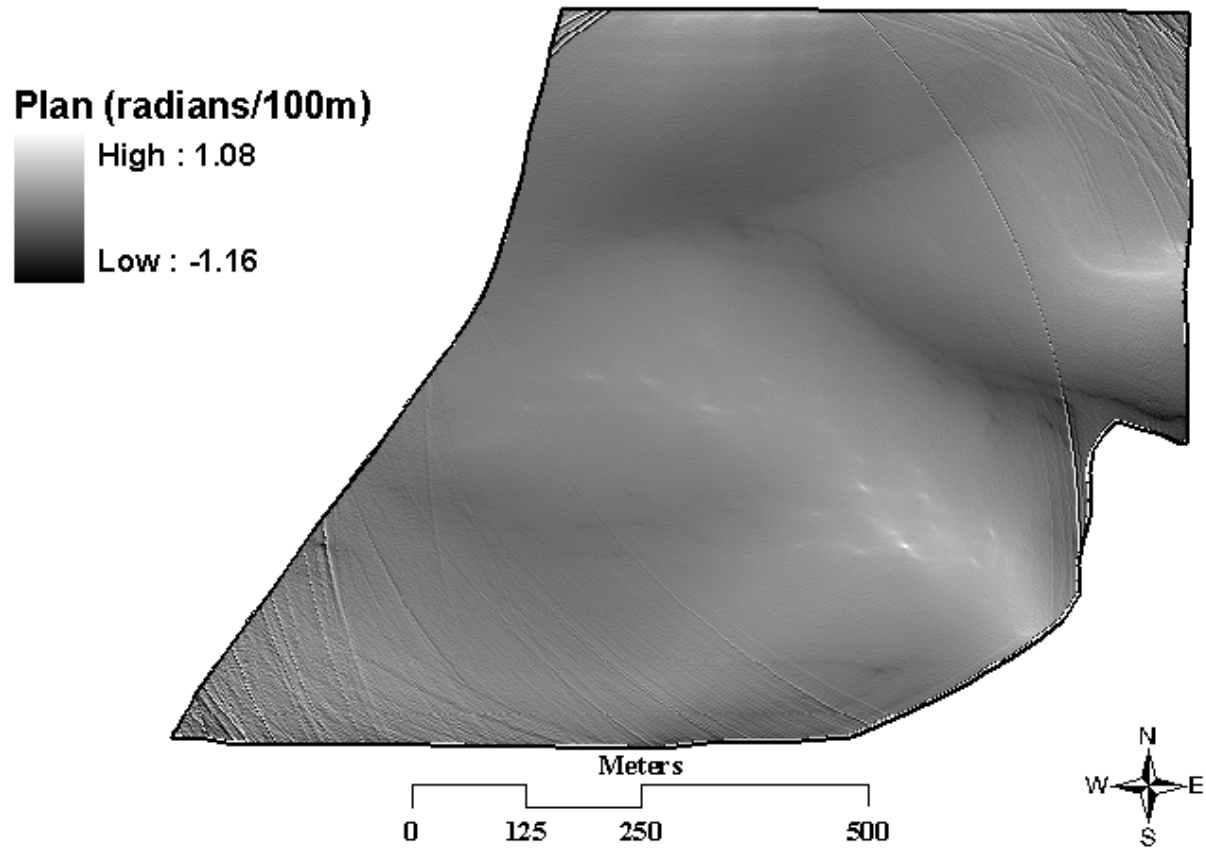


Figure 1.18. A plan curvature raster created from 20% local and 80% global polynomial interpolation of a 2-m digital elevation model.

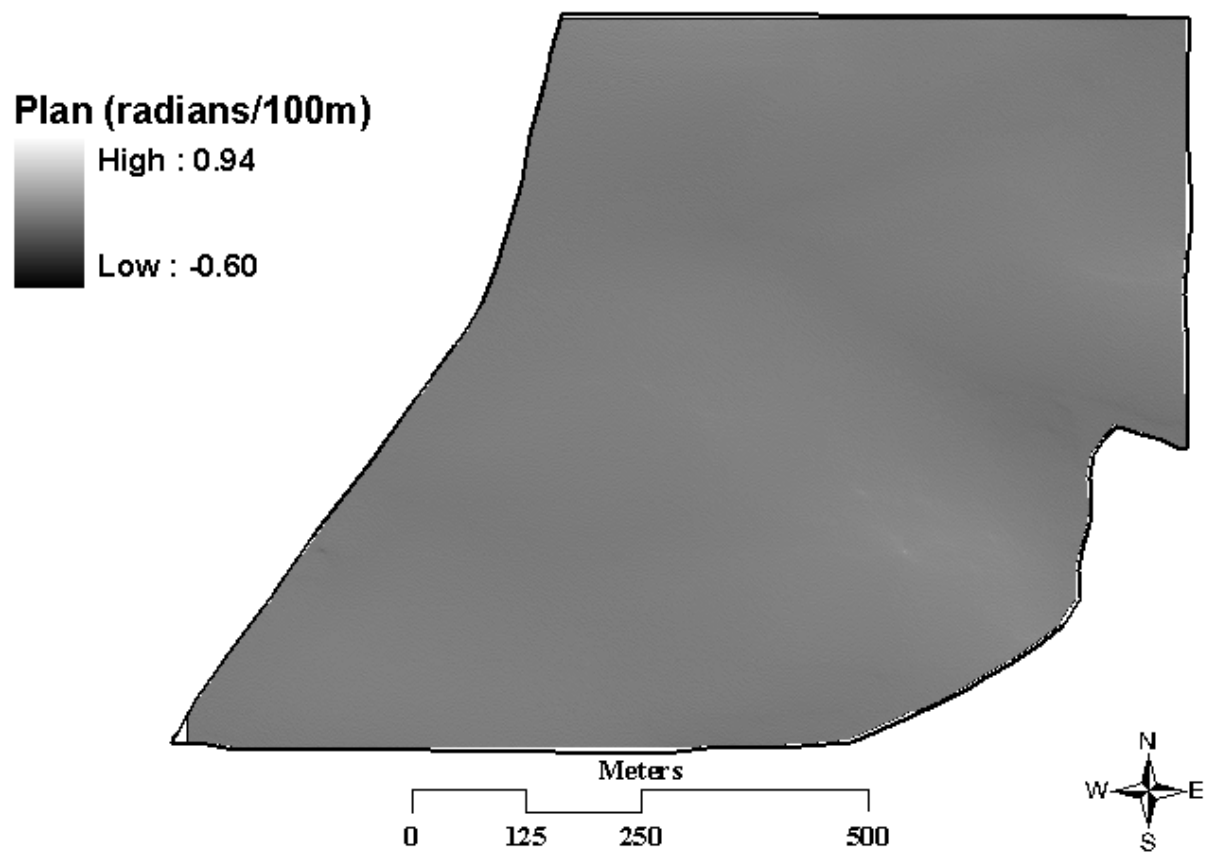


Figure 1.19. A plan curvature raster created from 10% local and 90% global polynomial interpolation of a 2-m digital elevation model.

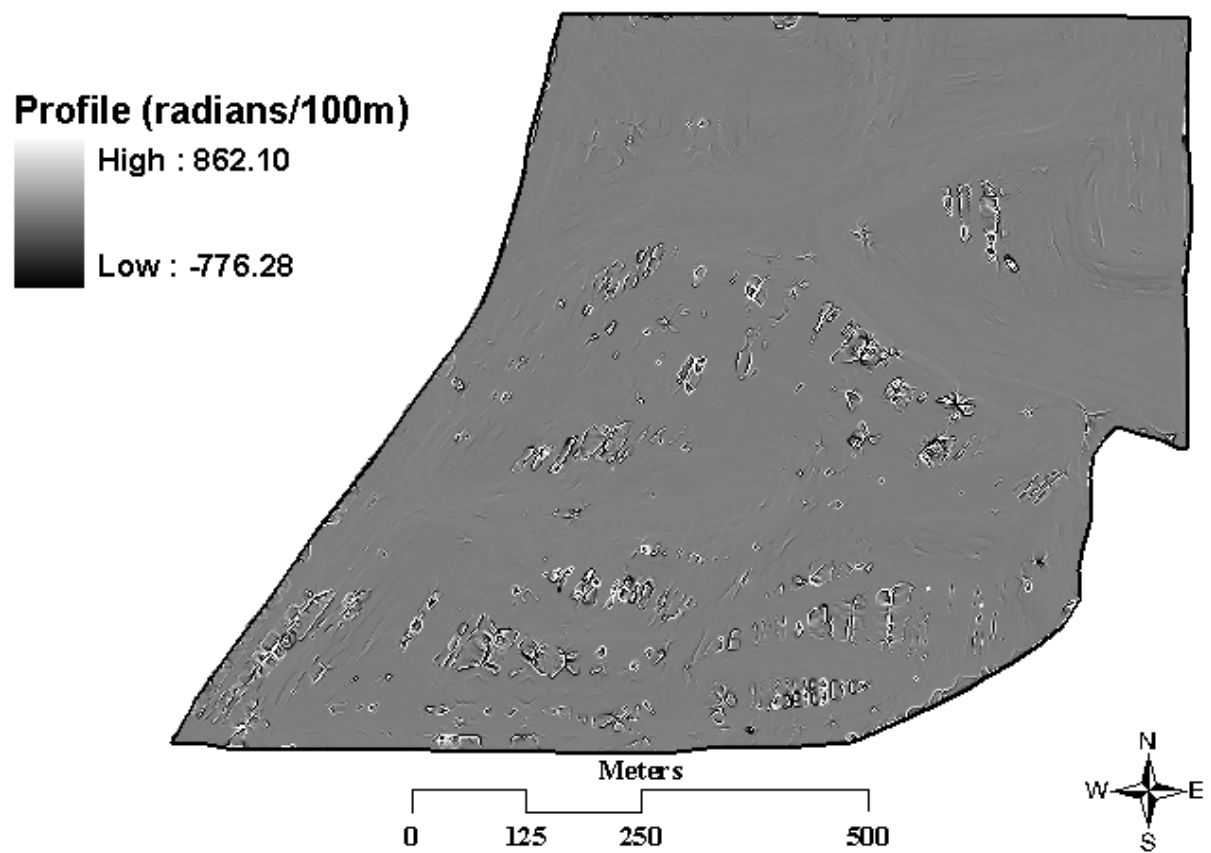


Figure 1.20. A profile curvature raster created from 100% local and 0% global polynomial interpolation of a 2-m digital elevation model.

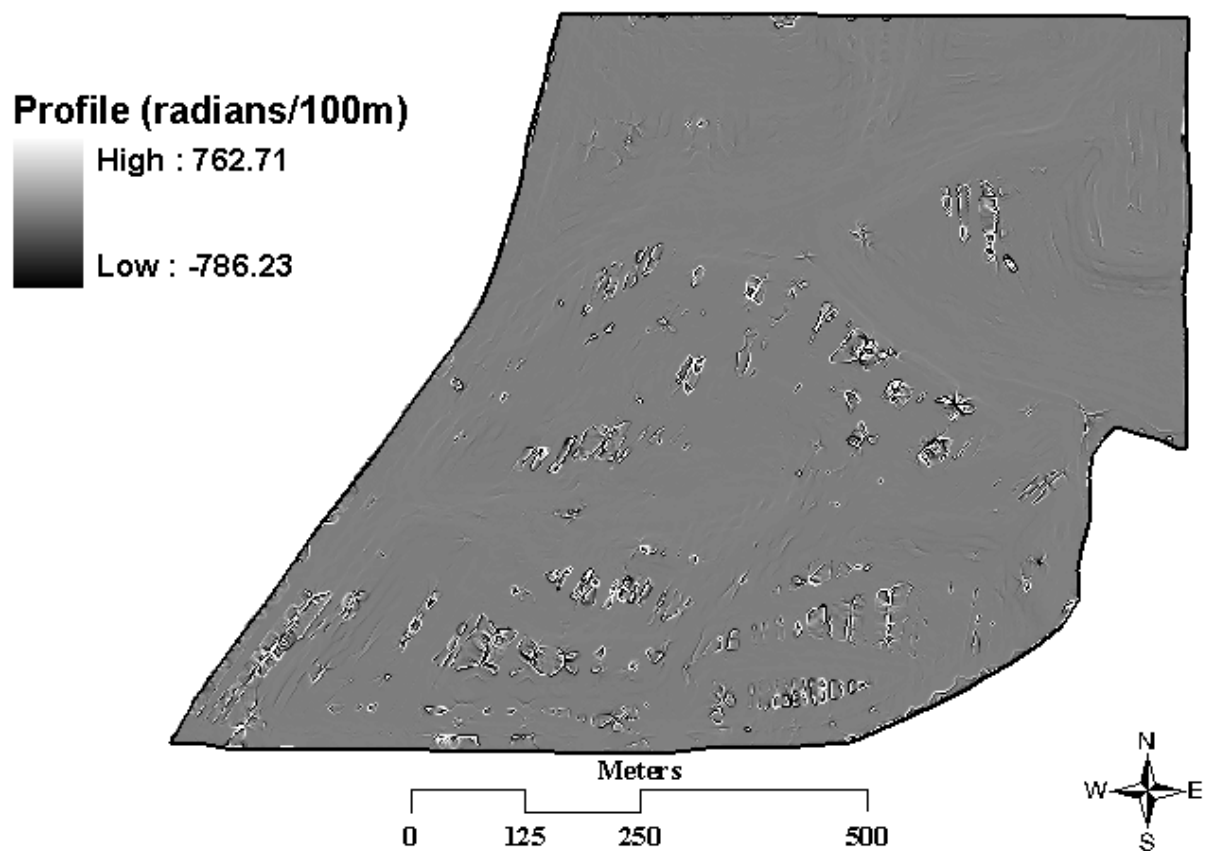


Figure 1.21. A profile curvature raster created from 90% local and 10% global polynomial interpolation of a 2-m digital elevation model.

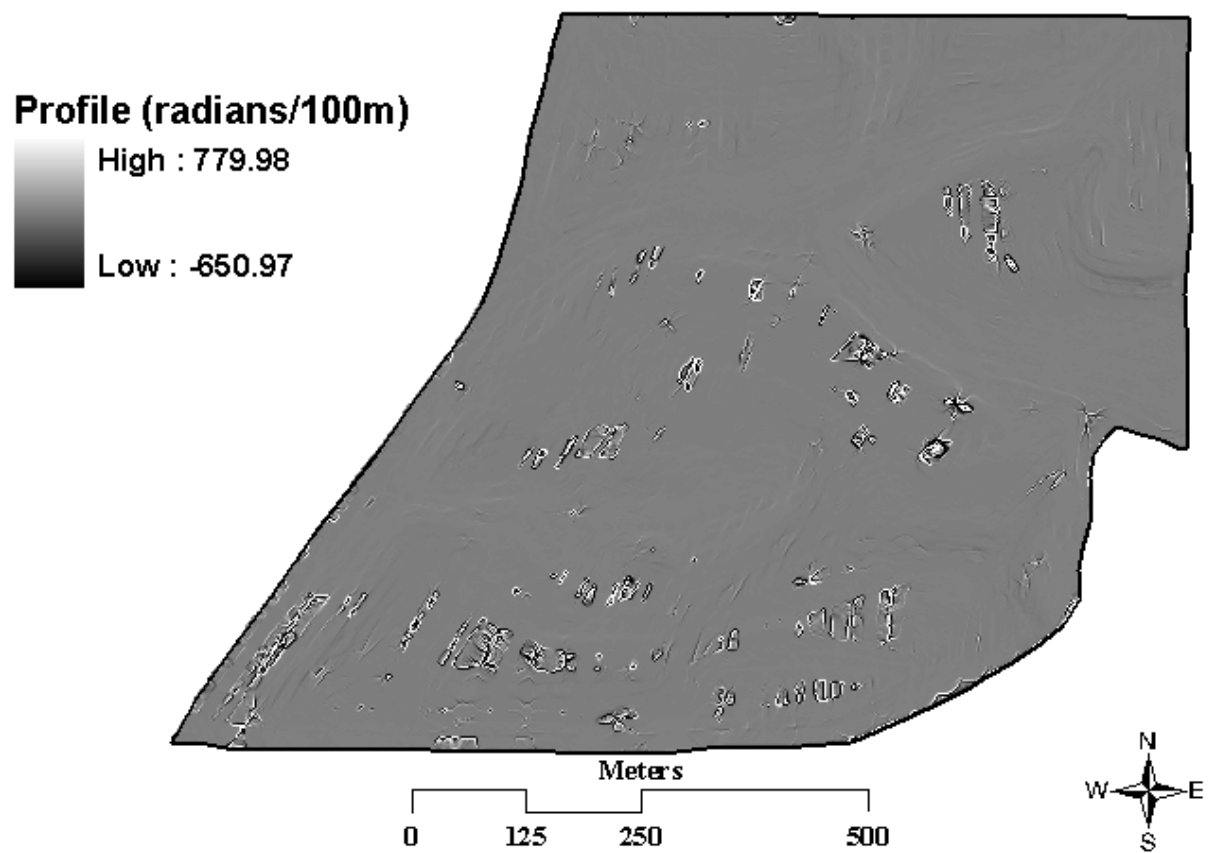


Figure 1.22. A profile curvature raster created from 80% local and 20% global polynomial interpolation of a 2-m digital elevation model.

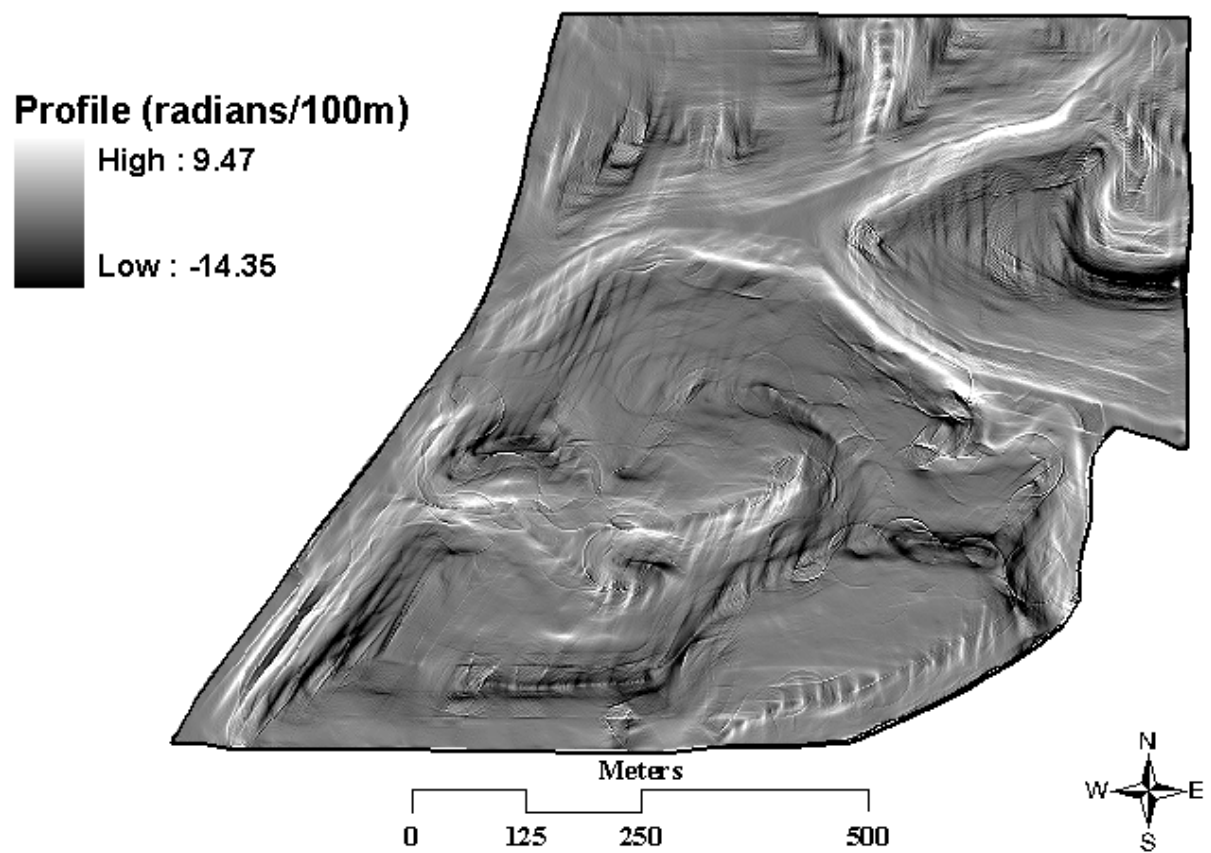


Figure 1.23. A profile curvature raster created from 60% local and 40% global polynomial interpolation of a 2-m digital elevation model.

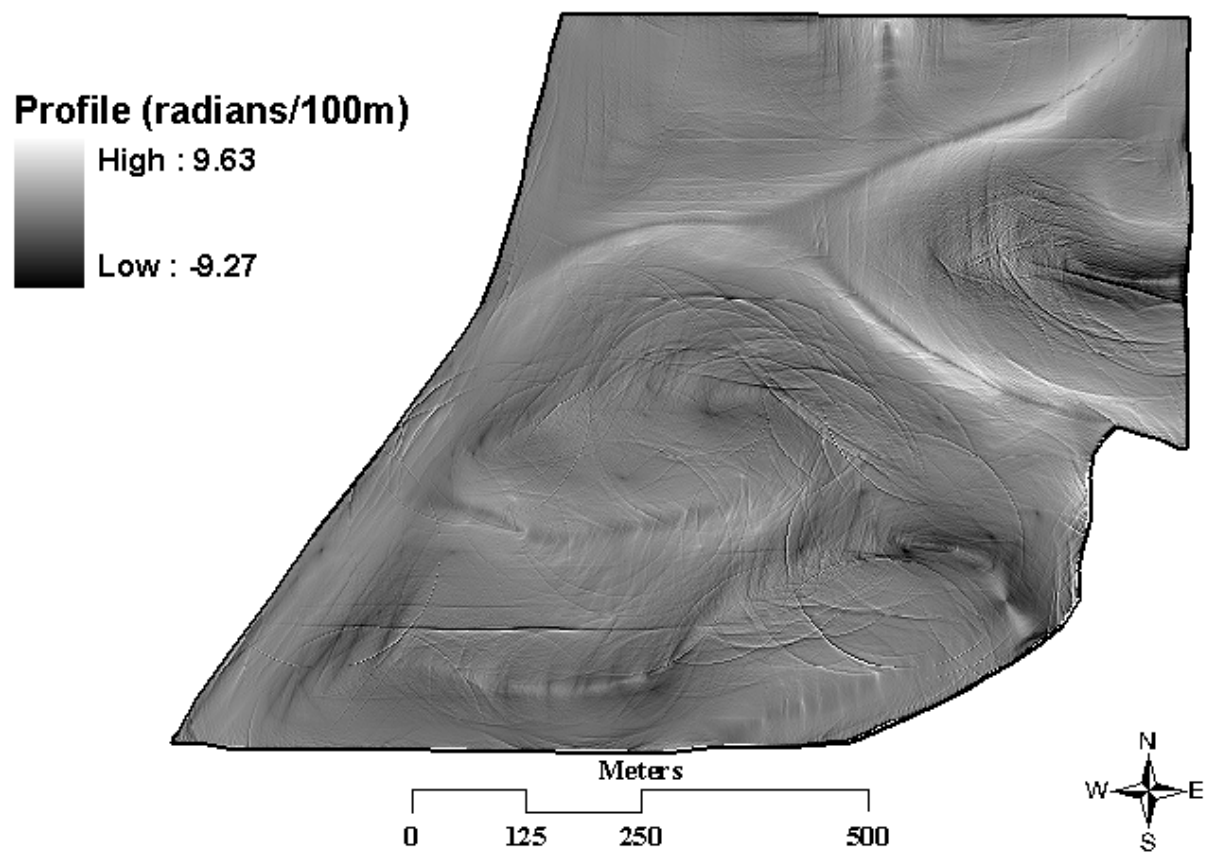


Figure 1.24. A profile curvature raster created from 40% local and 60% global polynomial interpolation of a 2-m digital elevation model.

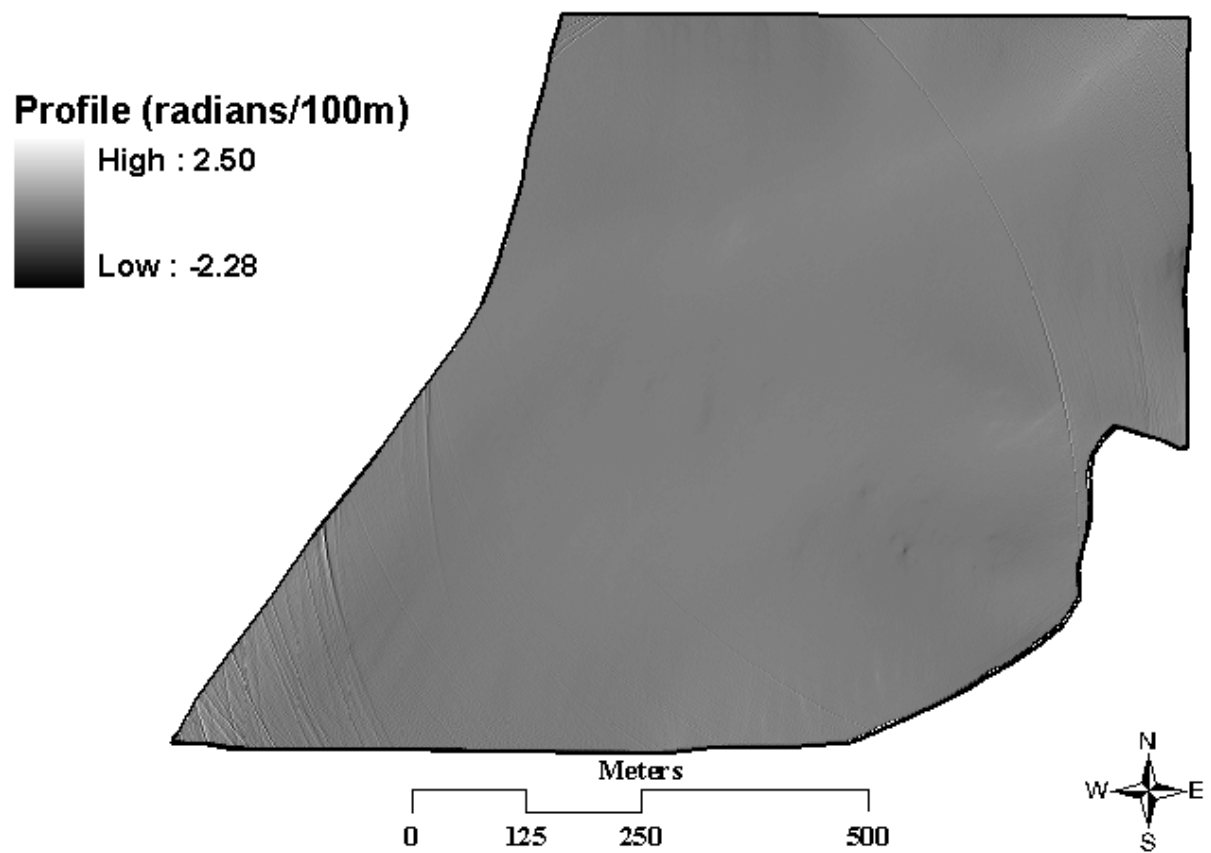


Figure 1.25. A profile curvature raster created from 20% local and 80% global polynomial interpolation of a 2-m digital elevation model.

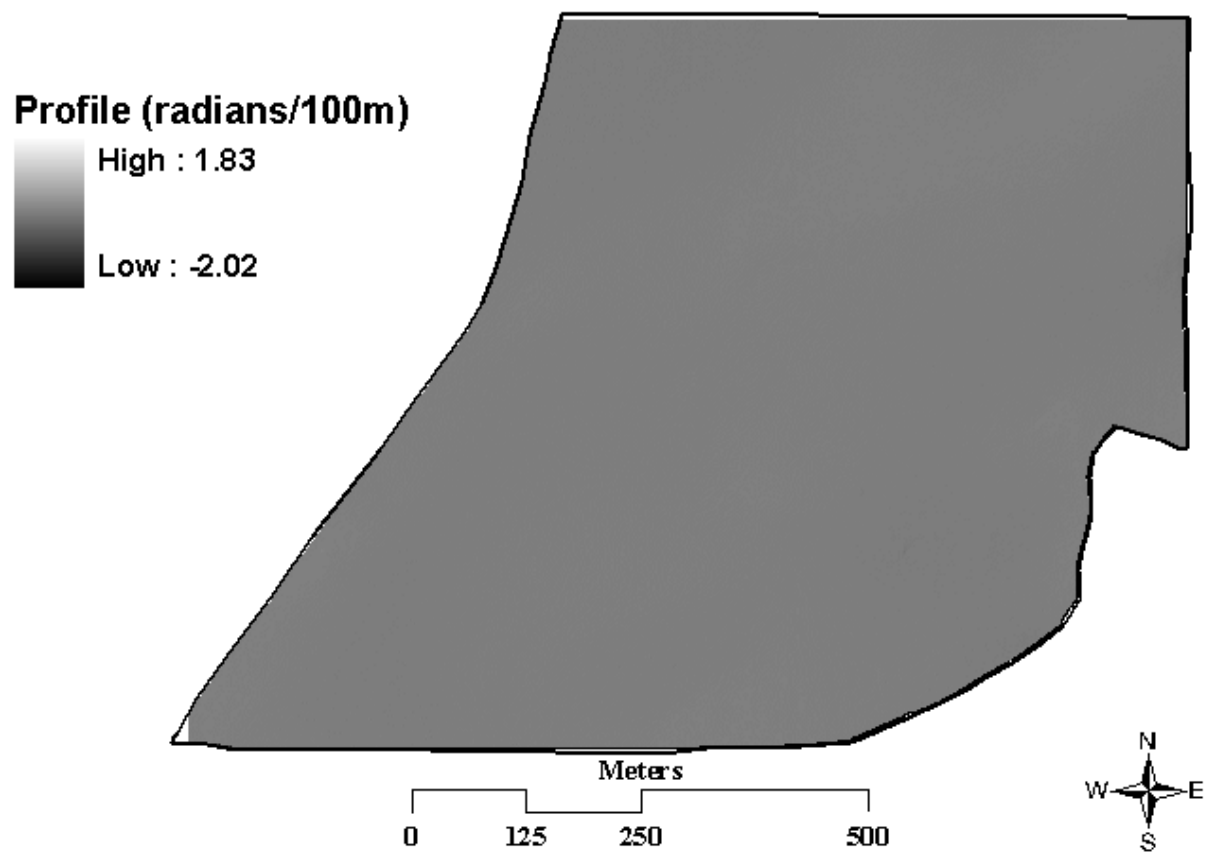


Figure 1.26. A profile curvature raster created from 10% local and 90% global polynomial interpolation of a 2-m digital elevation model.

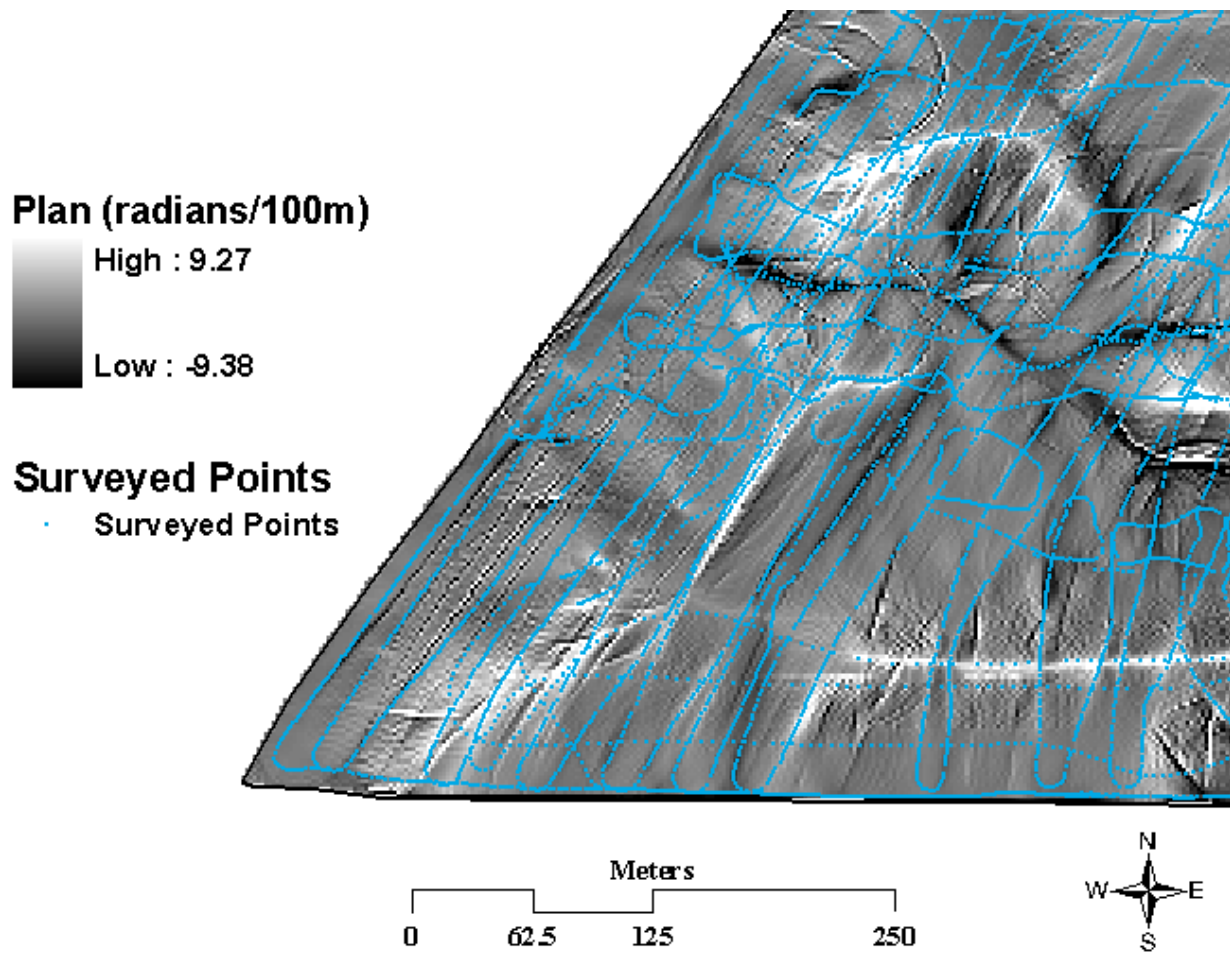


Figure 1.27. Close up of 2-m plan curvature raster created from 60% local and 40% global polynomial interpolation showing streaking created from collection method with survey points overlain.

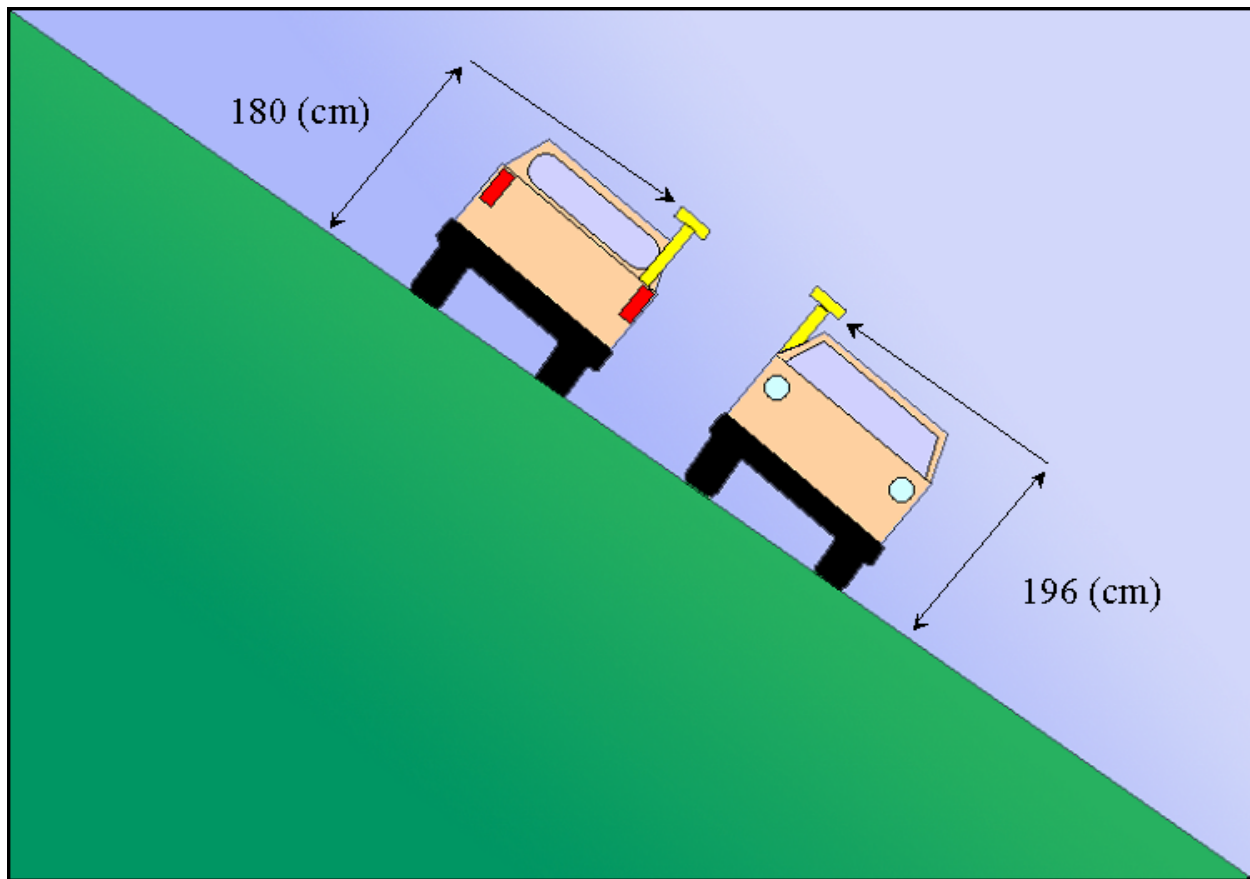


Figure 1.28. Diagram of antenna height differences due to sway of pickup truck on slopes when traveling in opposite direction

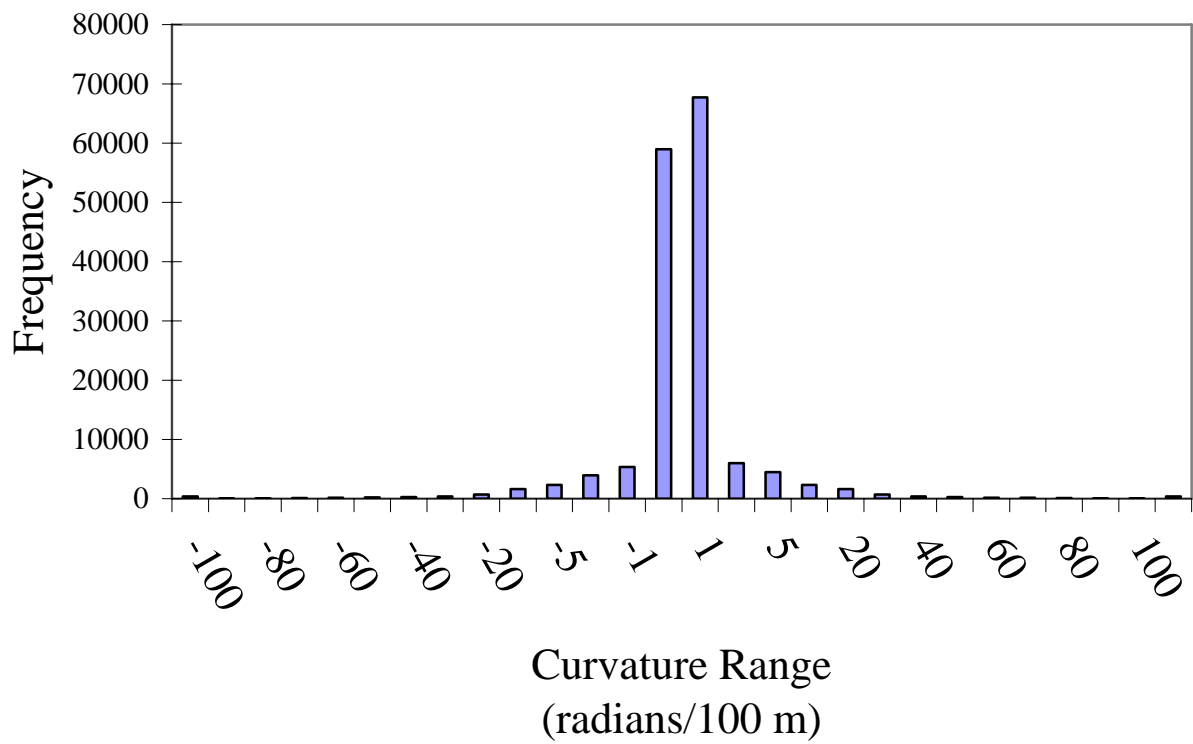


Figure 1.29. Frequency histogram of 2-m plan curvature raster created from 100% local polynomial interpolation.

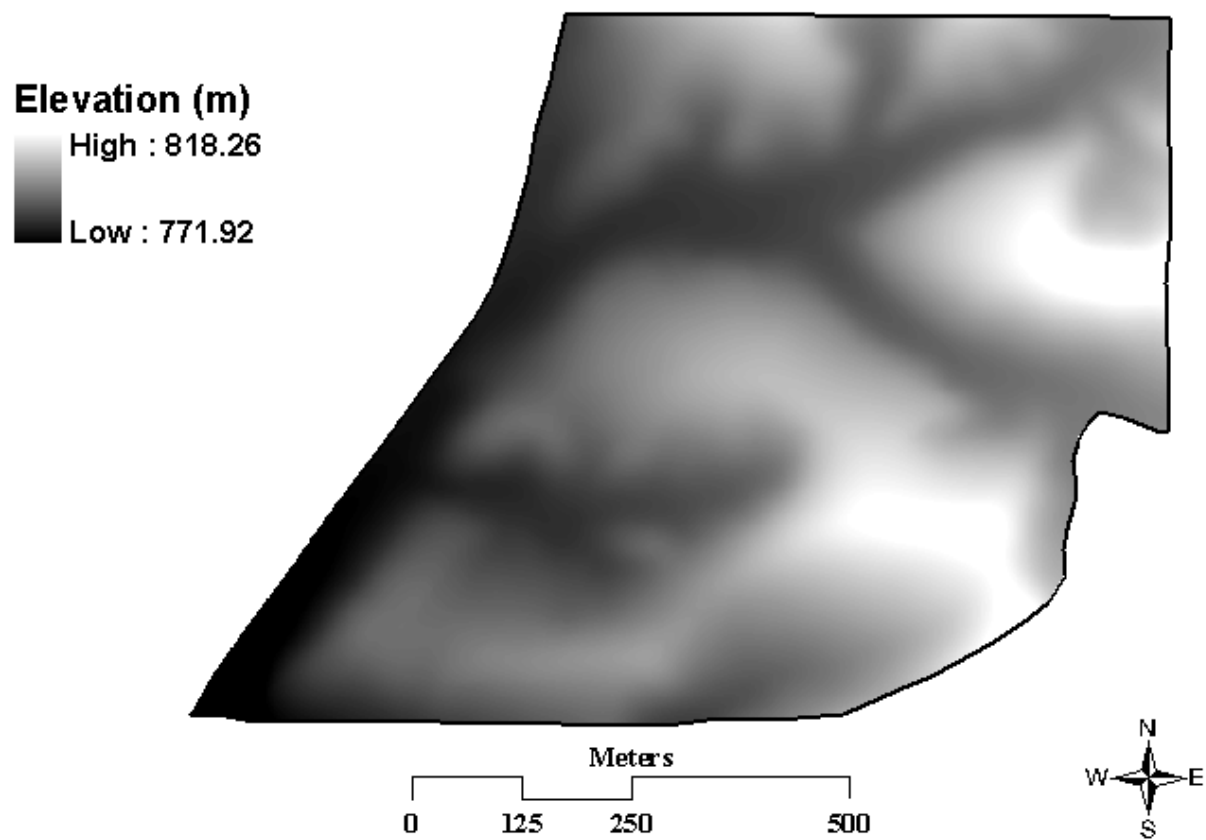


Figure 1.30. A 1-m digital elevation model created from 30% global and 70% local polynomial interpolation.

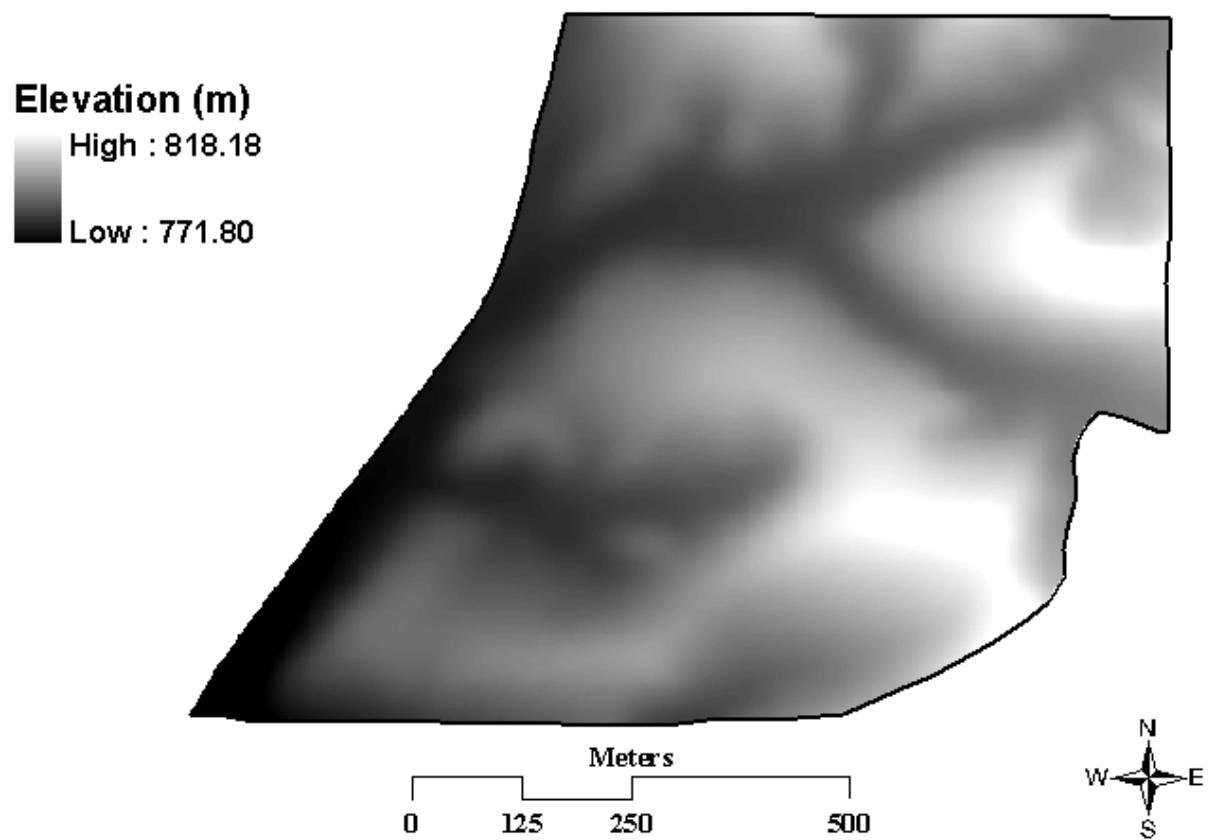


Figure 1.31. A 2-m digital elevation model created from 30% global and 70% local polynomial interpolation.

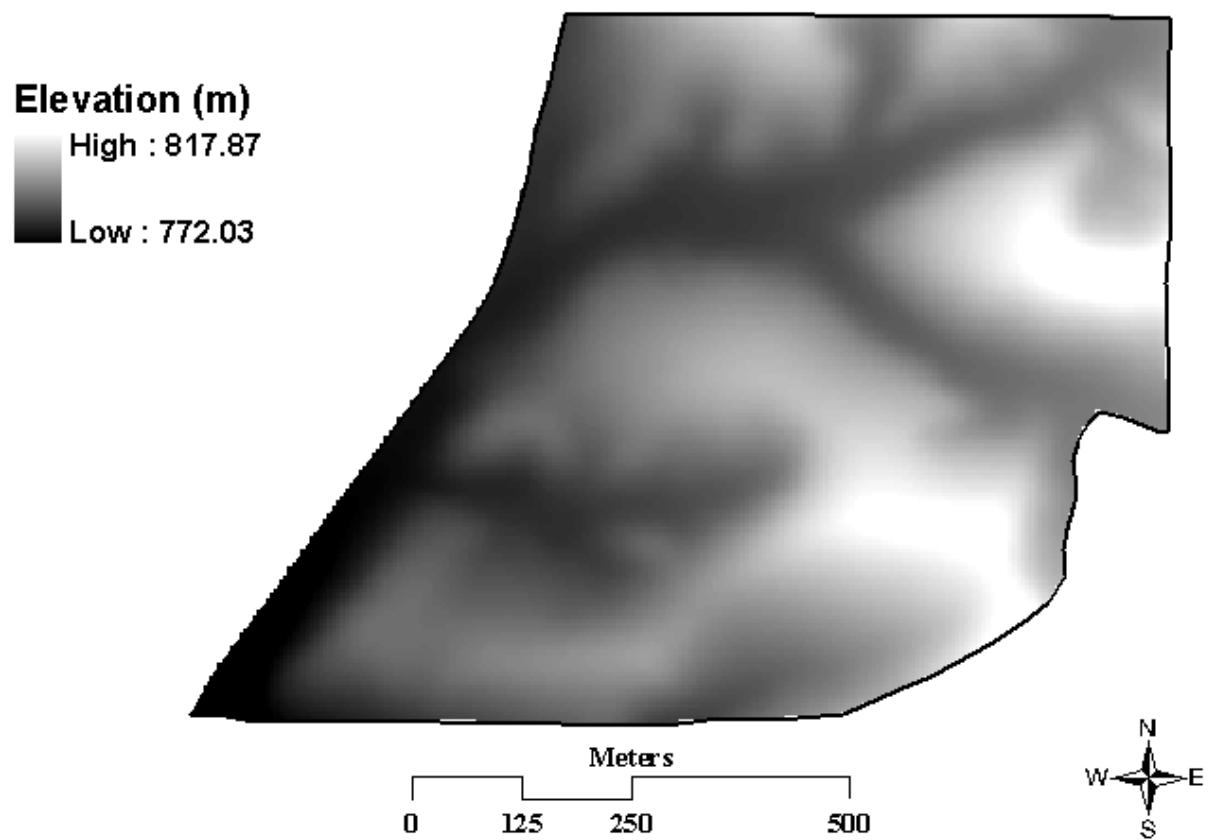


Figure 1.32. A 5-m digital elevation model created from 30% global and 70% local polynomial interpolation.

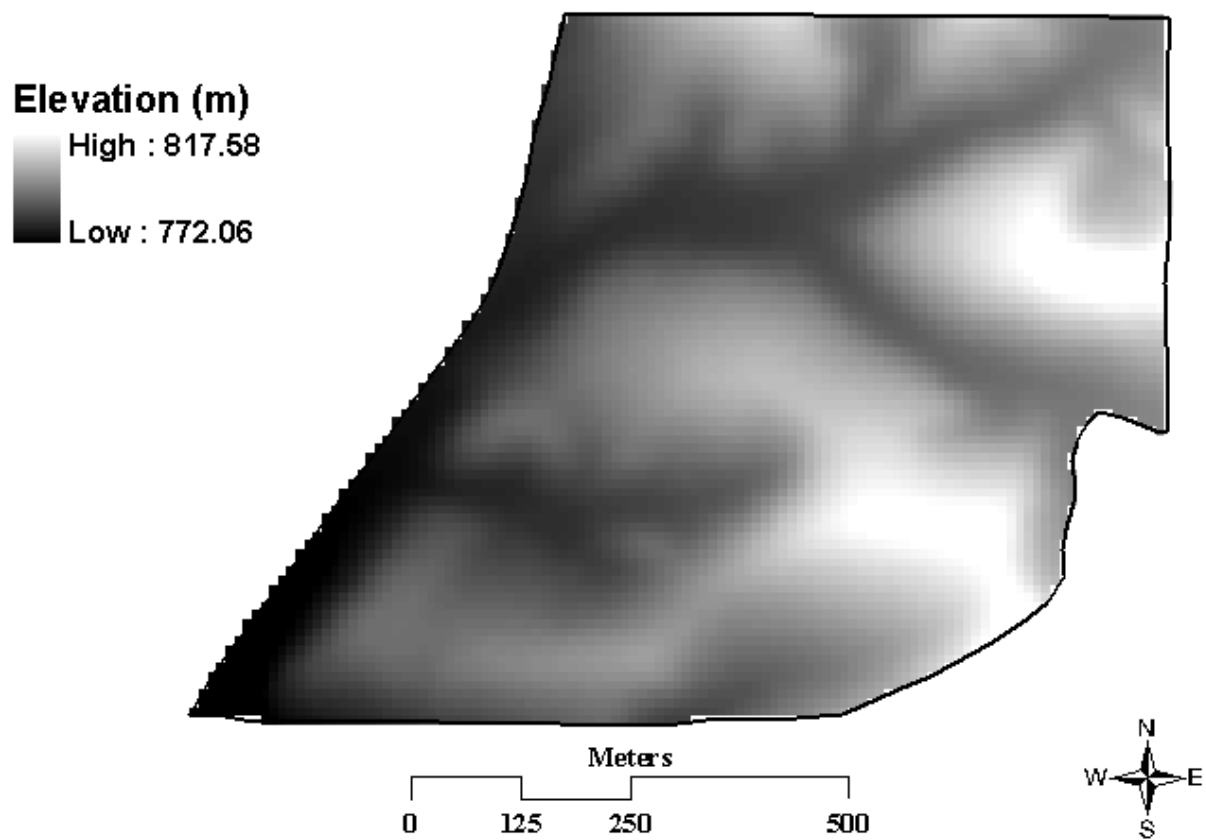


Figure 1.33. A 10-m digital elevation model created from 30% global and 70% local polynomial interpolation.

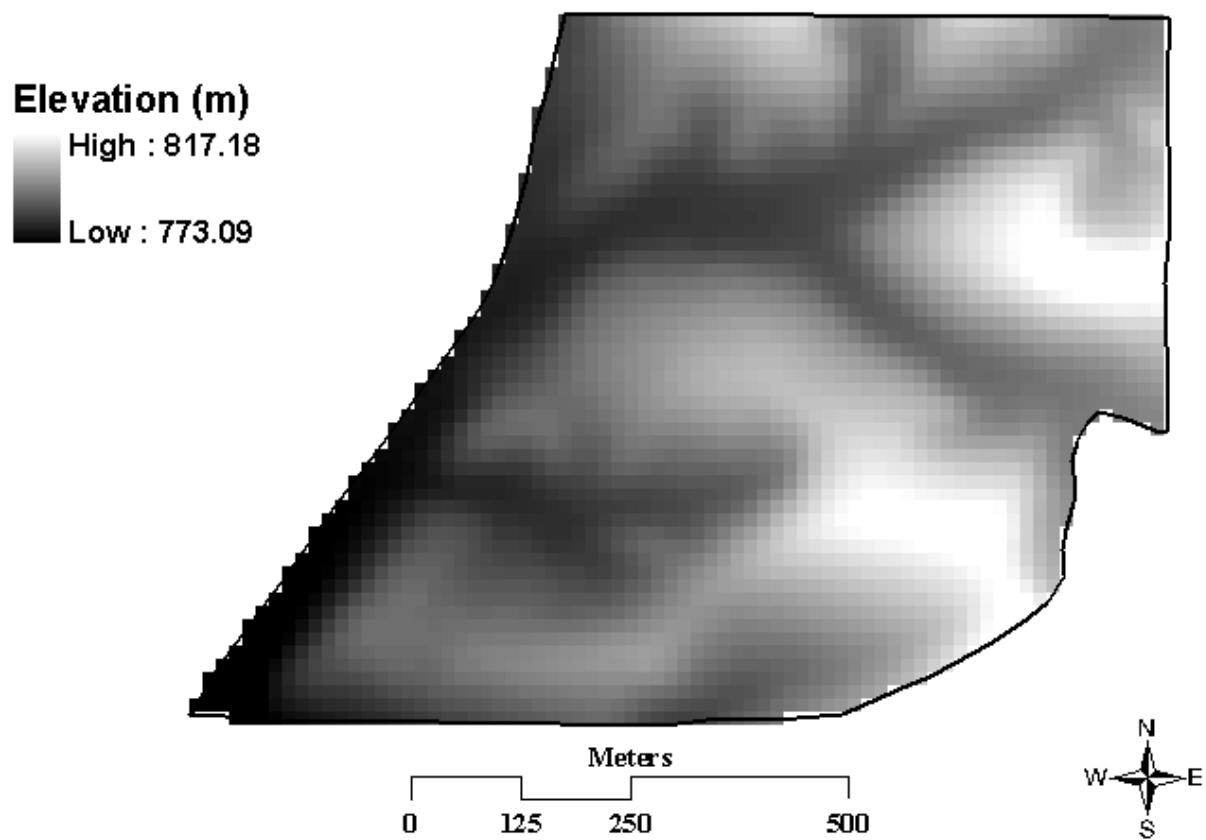


Figure 1.34. A 15-m digital elevation model created from 30% global and 70% local polynomial interpolation.

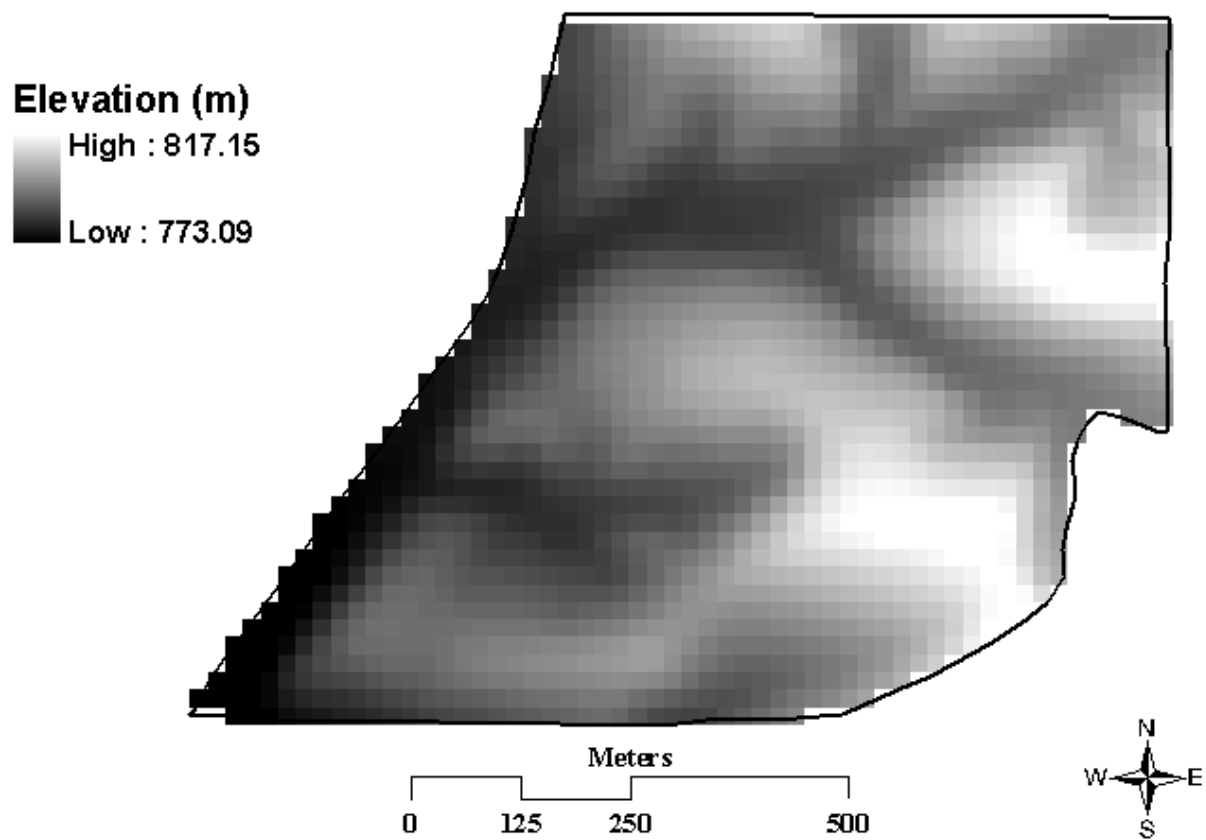


Figure 1.35. A 20-m digital elevation model created from 30% global and 70% local polynomial interpolation.

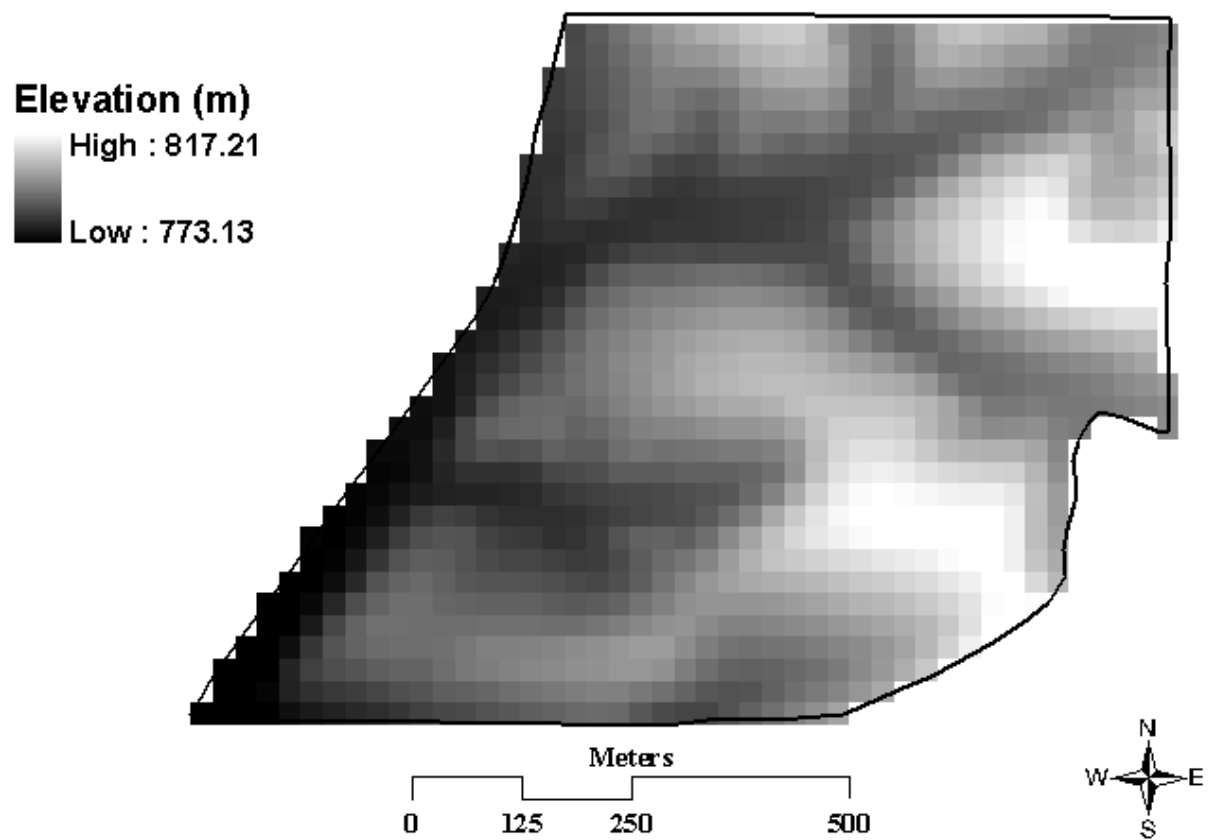


Figure 1.36. A 25-m digital elevation model created from 30% global and 70% local polynomial interpolation.

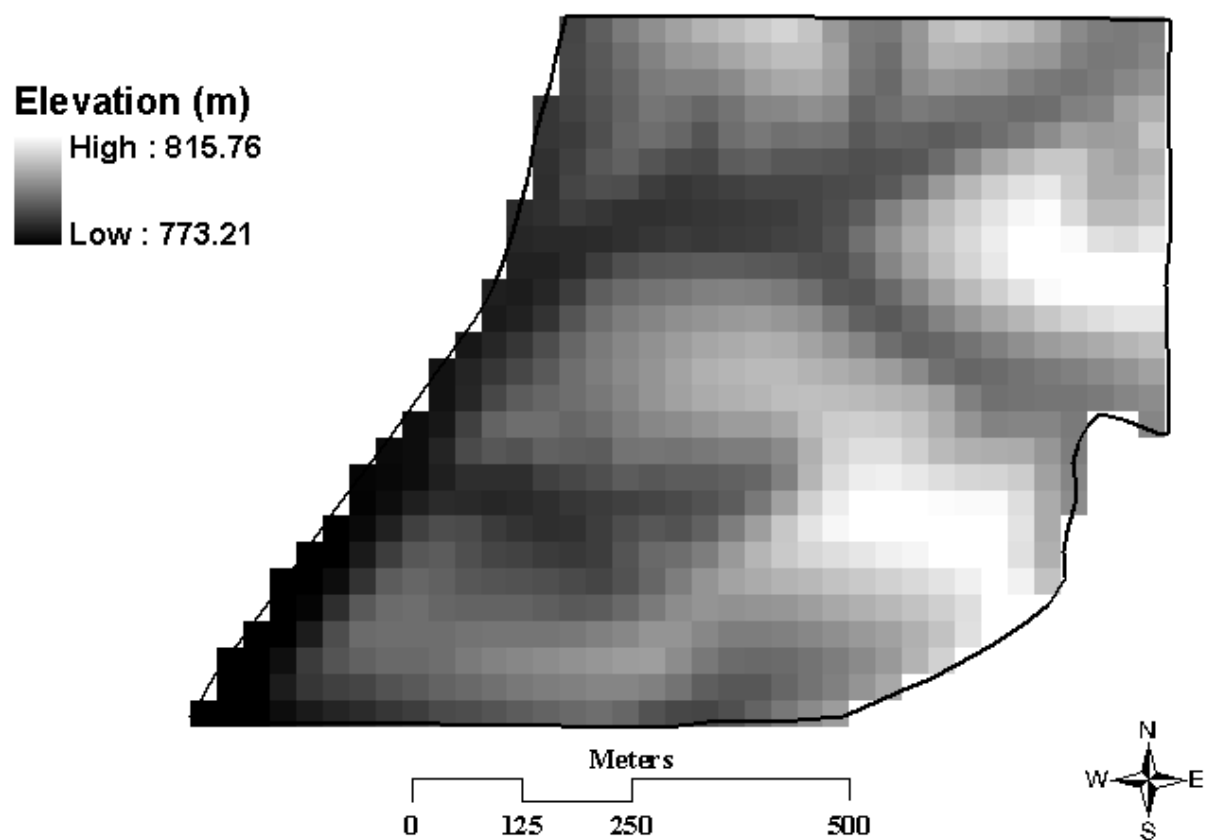


Figure 1.37. A 30-m digital elevation model created from 30% global and 70% local polynomial interpolation.

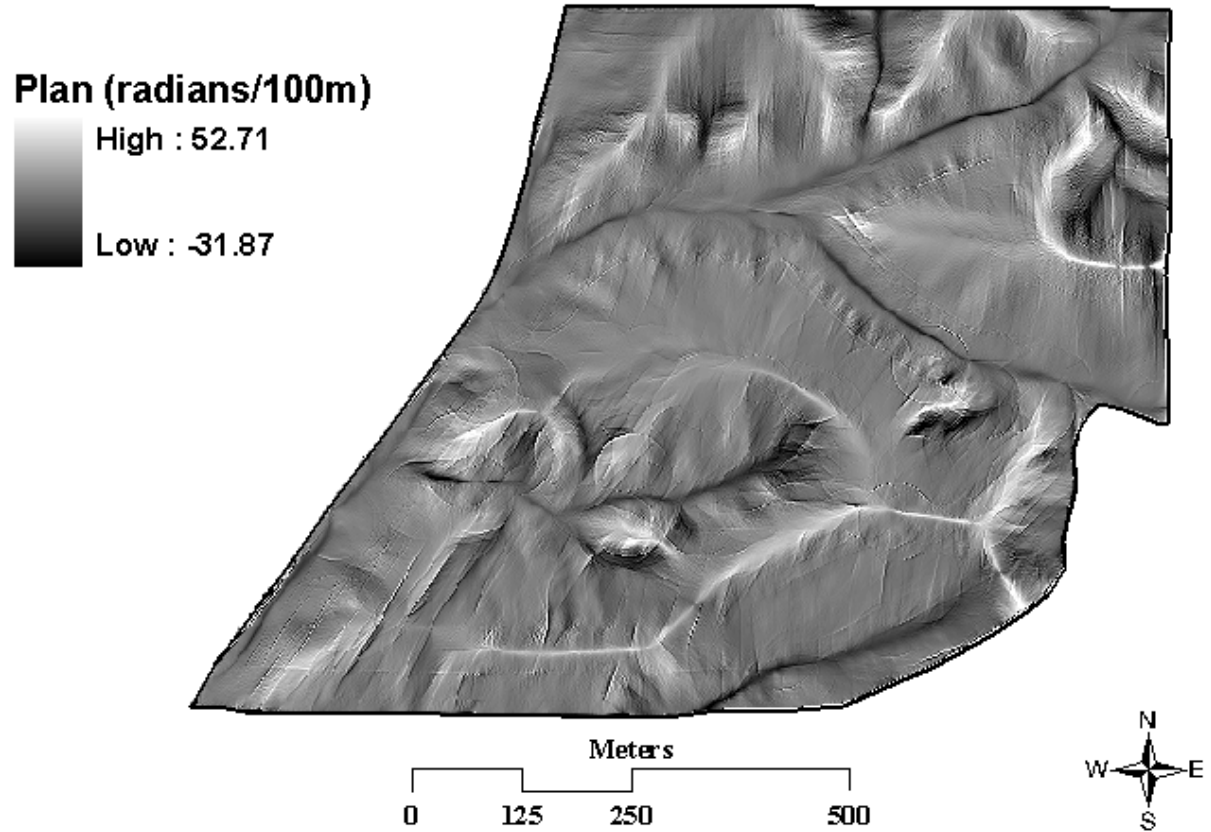


Figure 1.38. A plan curvature raster created from 70% local and 30% global polynomial interpolation of a 2-m digital elevation model.

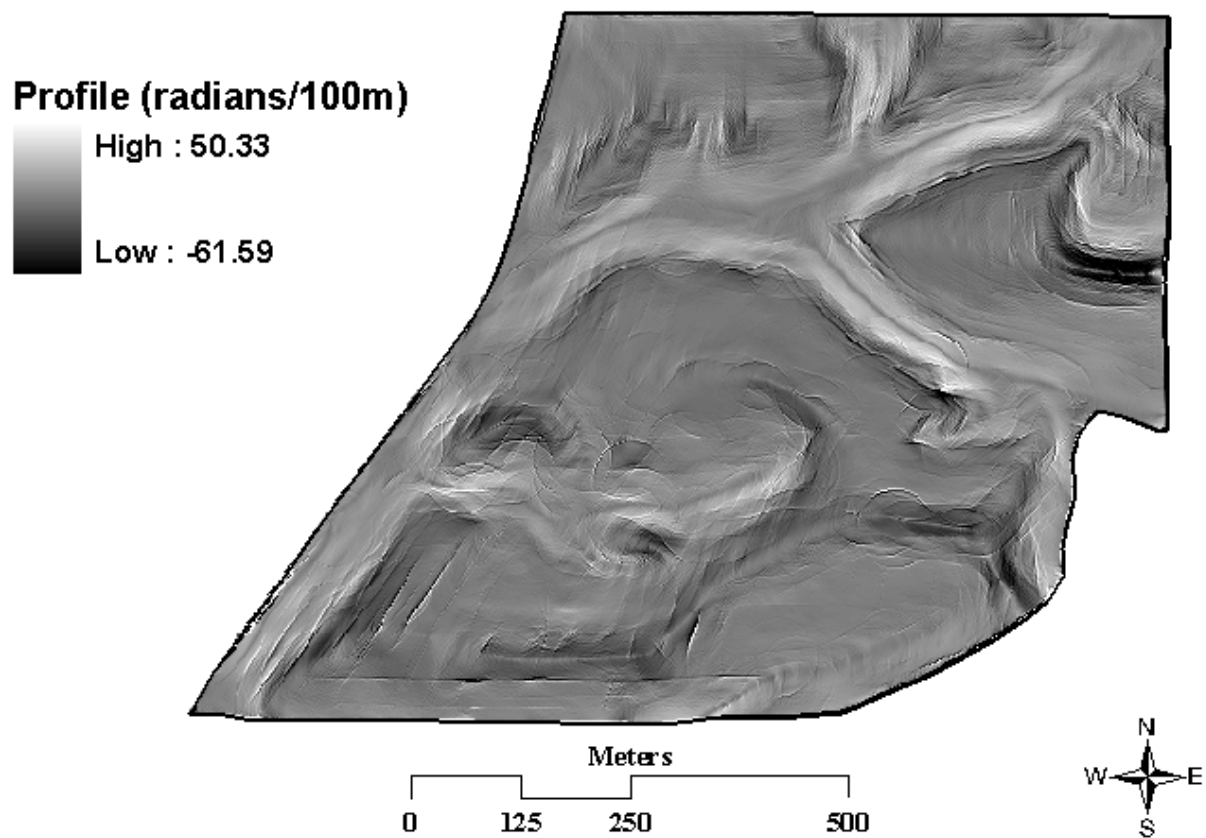


Figure 1.39. A profile curvature raster created from 10% local and 90% global polynomial interpolation of a 2-m digital elevation model.

1.7 References

- Desmet, P.J. 1997. Effects of interpolation errors on the analysis of DEMs. *Earth Surface Processes and Landforms* 22: 563-580.
- ESRI Inc. 2000. Using ArcGIS Geostatistical Analyst. ESRI Press. Redlands, CA
- ESRI Inc. 2002. How Curvature Works. ArcGIS 8.2 Online Help. ESRI. Redlands, CA.
- Friedman J.H. 1984. A variable span smoother. Department of Statistics, Stanford University, Technical Report LCS5.
- Isaaks, E.H., Srivastava, R.M. 1989. Applied Geostatistics. Oxford University Press Inc. 1989.
- Montana State University. 2004. Glossary of GPS Terms [Online]. Available at
<http://www.montana.edu/places/gps/lres357/glossary.html> (verified February 12, 2004.)
- National Resource Conservation Service. 1998. Field Book for Describing and Sampling Soils Version 1.1. NRCS, Salt Lake City, UT.
- Palouse Conservation Field Station. 2004. United States Department of Agriculture: Agricultural Research Service. Pullman, WA.
- Russell, E., Kumler, M., Ochis, H. 1995. Identifying and removing systematic errors in USGS DEMs, GIS in the Rockies Conference Proceedings, Denver, CO. September 25-27, 1995.
- Schoorl, J.M., Sonneveld, M.P., Veldkamp, A. 2000. Three-Dimensional Landscape Process Modeling: The Effect of DEM Resolution. *Earth Surface Processes and Landforms* 25: 1025-1034.
- Soil Conservation Service. 1980. Soil Survey of Whitman County, Washington. USDA Soil Conservation Service.

Thompson, J.A., Bell, J.C. Butler, C.A., 2001. Digital elevation model resolution: effects on terrain attribute calculation and quantitative soil-landscape modeling. *Geoderma* 100: 67-89.

Trimble Navigation 2001. TSC1 Asset Surveyor Software User Guide. Trimble Navigation Limited.

Wilson, J.P., Gallant, J.C. 2000. *Terrain Analysis Principles and Application*. John Wiley & Sons Inc.

Yao, H., Clark, R.L. 2000. Evaluation of Sub-Meter and 2 to 5 Meter Accuracy GPS Receivers to Develop Digital Elevation Models. *Precision Agriculture* 2: 189-200.

CHAPTER II: PREDICTING SOIL B_t HORIZONS FROM APPARENT SOIL ELECTRICAL CONDUCTIVITY AND TERRAIN ATTRIBUTES

2.1 Introduction

Terrain attributes and apparent soil electrical conductivity (EC_a) can be gathered rapidly and provide detailed field-scale information applicable to designing precision agricultural systems. Terrain attributes derived from digital elevation models (DEM) have been utilized to predict various soil attributes (Moore et al., 1993). Slope, catchment area, solar insolation, and curvature have been used to predict soil horizon boundaries (Boer et al., 1996). Curvature convexity has been linked to surface erosion processes (Pennock, 2003). Slope was utilized with vegetation maps and types of granite as predictors for creating detailed maps of soil texture (Mertens et al., 2001). Slope, aspect, plan curvature, and profile curvature have been utilized for the prediction of subsoil clay percentage, depth to solum, and depth to bedrock (Odeh et al., 1995). Soil moisture levels have been linked to surface curvature, with greater moisture levels in areas of concavity and lesser in areas of convexity (Girgin et al., 1997). Topsoil organic matter has been modeled using wetness index, aspect, and slope as the main attributes for prediction (Cook et al., 1996). Although terrain attributes have proven useful as predictors of soil properties, the resolution of the DEM affects the derived terrain attributes (Thompson, et al., 2001).

Like terrain attributes, EC_a data have also been used to create a better understanding of soil properties. Apparent electric conductivity has successfully predicted soil textural discontinuities (James et al., 2003), while also being used to predict clay content, cation

exchange capacity, and soil moisture (McNeill, 1992). Topsoil and water table depths have also been found to correlate with EC_a readings (Sudduth et al., 2000, Sherlock et al., 2003).

Resolution of terrain attributes and EC_a data can affect their capabilities to predict soil properties. As resolution size increases, terrain attribute range and variance decreases as derived values approach the mean of the data (Isaaks and Srivastava, 1989). Prediction of soil hydromorphic boundaries utilizing catchment area deteriorated as terrain attribute resolution becomes courser (Chaplot et al., 2000). Map quality of soil carbon at 100-m resolution substantially lessened compared to 30-m or 61-m resolutions (Mueller et al., 2003). Thompson et al. (2001) reported that slope decreased and landscape features diminished as resolution decreased from a 10-m to 30-m DEM. Prediction of soil erosion, a function of slope, has been shown to increase with coarser resolution DEMs (Schoorl et al., 2000).

Soil properties are important for the creation of management zones for precision agriculture. In the Palouse, subsurface Bt horizons contain greater accumulation of clay (Soil Survey Manual, 1998) and can reduce rooting depth and root access to available water (Pan and Hopkins, 1991). In the Palouse, the Bt horizon is thought to be a relic from previous loess deposition and subsequent pedogenesis (McDonald and Bussaca, 1992). The ability to predict the presence of Bt horizons may aid in the creation of precision agriculture systems. The objectives of this study are to: (1) evaluate the utility of terrain attributes and EC_a data to predict Bt horizon presence or absence using data from DEMs created at various resolutions; and (2) create and evaluate the accuracy of mapped zones that predict the presence or absence of Bt horizons.

2.2 Materials and Methods

2.2.1 Horizon Information

A 30.48-m grid was superimposed over the southern 36.4 hectares of the Washington State University (WSU) Cunningham Agronomy Farm (CAF). A random point was generated in each cell of the grid using MapInfo (RedHen Software Inc.) creating 369 geo-referenced points (Figure 2.1). In the fall of 1998 and 1999, every other point, 184 of the 369, were soil sampled with a tractor mounted hydraulic driven probe. Intact soil cores, 1.52 m long and 5.08 cm in diameter were collected from the 184 points and described using methods in the Soil Survey Manual (1998). The soil descriptions, including presence or absence of Bt horizons, were converted into digital format with coordinates, UTM WGS84 zone 11N, and imported into a database (Microsoft Access 2000).

2.2.2 Terrain Attributes

A series of increasing raster cell size DEMs, 1-m, 2-m, 5-m, 10-m, 15-m, 20-m, 25-m, and 30-m, were created using a Local Polynomial Interpolation (LPI) with 30% global and 70% local polynomial influence. Terrain attributes derived from the resulting DEMs were slope, aspect, curvature, global solar insolation, flow direction, flow accumulation, specific catchment area, and wetness index using ArcGIS 8.2 (ESRI) with the exception of global solar insolation (Table 2.1). Global solar insolation was calculated using Solar Analyst Extension for ArcView 3.0 (HemiSoft Inc). For this project, global solar insolation was calculated based on a combination of direct and diffuse solar radiation.

To combine the 184 geo-referenced points of horizon data with terrain attributes, a point file of the 184 core locations was overlain on each of the created terrain attribute rasters: 1-m, 2-

m, 5-m, 10-m, 15-m, 20-m, 25-m, and 30-m. The value of each individual raster cell that was under a given point was extracted and placed into the database for that point. The created database has Bt horizon presence or absence along with terrain attribute values for all of the raster cell sizes.

2.2.3 Apparent Electrical Conductivity

A survey of EC_a was conducted using an EM38 (Geonics Limited, 2000) coupled with a Trimble Ag 132 Differential GPS (DGPS), UTM WGS84 zone 11N. The EM38 is an electrical conductivity sensor that continuously measures EC_a. It is sensitive to fluctuations in electrical conductivity due to soil salinity, clay content, soil water content, and cation exchange capacity (McNeill, 1992). When operated in the vertical dipole mode, the effective measurement depth is about 1.5 m (Sudduth et al., 2001). Any conductive substance within 3 m of the EM38 can influence its measurements; therefore, the unit was placed in the end of a 4 m polyvinyl chloride (PVC) pipe attached to an all terrain vehicle (ATV). The ATV was driven in a north-south, east-west grid across the 36.4 hectares of the CAF. The readings from the EM38 were coupled with location data provided by the DGPS every second using the HGIS (StarPal 1997) software package. The EC_a survey was conducted twice, once in the spring, March 25, 2000, and once in the fall, September 14, 2000, following spring barley harvest. The output text files were imported into Geostatistical Software Library (GSLIB, Deutsch and Journel, 1992) where interpolation of both the spring and fall EC_a data was accomplished using ordinary kriging (OK).

For data to be analyzed with GSLIB, duplicate data must be removed. In the survey of the spring and fall data, duplicate values occurred when the ATV was stopped for a period of time while data was still being logged. In addition, when the GPS values are rounded to their

appropriate reading accuracy, 1 m, duplicate data were created. Duplicate data were removed from both the spring and fall data sets before OK.

Ordinary kriging of the spring data did not require any further post-collection processing once the duplicate data were removed. A single exponential structure was used for modeling of the spring EC_a data with a range of 78m and 348m in the x and y directions respectively. The rotation was 11.4° counter clockwise, from the 0° north, about the vertical z-axis with a nugget of 0.003. The kriging of the fall data, however, required more post-collection processing before an acceptable interpolation could be accomplished. When the EC_a data was collected, it was not published that the EM38 unit EC_a values would drift as the unit temperature increased by 0.4 mS m⁻¹ °C⁻¹ (Geonics Limited, 2004). There are various techniques to model drift, but they are all utilized while collecting the data (Sudduth et al., 2001). Since the drift problem was unknown at the time of collection, these methods were not implemented. On the day data were collected in the fall of 2000, the air temperature changed from 13.9°C to 28.9°C, while in the spring of 2000 the temperature changed from 1.1°C to 10.0°C. Although both changes in temperature are sufficient to create substantial drift, the temperature change in the spring did not likely occur during the survey period, whereas the fall's data collection occurred during the day when temperature change was more probable.

Removal of drift from the fall data was necessary in order to achieve accurate modeling using OK. Attempts to model drift with time such as cokriging EC_a values with time and conditional expectation (Friedman, 1984) were all tried; however, none produced satisfactory results. The removal of all east-west data collected at later times in the survey, 3725 points, was the final solution used to remove data most affected by drift. A single exponential structure was used for ordinary kriging of the fall data with a range of 63m and 32m in the x and y directions,

respectively. The rotation was 1.5° clockwise, from 0° north, about the vertical z-axis with a nugget of 0.028. Interpolation of both the spring and fall EC_a data was modeled for 1-m, 2-m, 5-m, 10-m, 15-m, 20-m, 25-m, and 30-m raster cell sizes. The output of GSLIB is an ASCII file of the data, which was imported into ArcGIS 8.2 (ESRI) where the rasters were created. The EC_a data for all raster sizes were combined with the soil and terrain attribute data for the 184 cores using the same extraction method used for the terrain attribute data.

2.2.4 Indicator Kriging of Bt Horizon Presence or Absence

Indicator Kriging (IK) was done on the presence or absence of Bt horizons on the 184 cores in GSLIB. The purpose of IK mapping of the Bt horizon was to create a reference map to which prediction maps created from terrain attributes and EC_a could be compared. Two spherical structures were utilized for the modeling of Bt horizon presence or absence, with a nugget of 0.344. The first structure had a range 180m and 65m for x and y, respectively, with a rotation of 48.3° counter clockwise, from 0° north, about the vertical z-axis. The second structure had a range of 2579m and 140m for x and y, respectively, with a rotation of 9.9° clockwise, from 0° north, about the vertical z-axis. The GSLIB output was imported into ArcGIS 8.2 (ESRI, 2002) where a 1-m raster was created.

2.2.5 Classification and Regression Tree (CART) Analysis

The CART analysis was developed by Brieman, et al. (1984) as a multivariate analysis tool for a single response variable. It allows for the usage of predictor variables (i.e. terrain attributes, EC_a) to separate the response variable (i.e. Bt horizon) into groups based on the response variable's sums of squares. To create these groups, CART analyzes all the predictor variables available and finds the value of the predictor variable that maximizes the quantity SST-

SSL-SSR where SST is the total sums of squares, SSL is the resulting left group sums of squares, and SSR is the resulting right group sums of squares. When maximization of SST-SSL-SSR is achieved, the response variable is split into a left group, where all the response variables have values less than the split value, and a right group, where all the response variables have a value greater than the split value. The groups that the CART analysis creates are the most homogeneous groupings of the response variable within the group, and the most heterogeneous groupings of the response variable between groups. Each grouping made from the splitting of a group is then analyzed, as it's own group, and split in the same manner as the original group. Each group can only be split into two resulting groups forming a bivariate tree.

The bivariate tree is made up of two types of nodes: (1) parent nodes, represented in figures as ovals, and (2) terminal nodes, represented in figures as rectangles. If the node is a parent node, the CART analysis splits it based on a predictor variable and value. If a node is a terminal node, the CART analysis did not split it because the maximization of the quantity SST-SSL-SSR resulted in a value below a designated threshold, or the splitting of a node resulted in a node containing less than the minimum number of observations designated for a node.

The advantages of CART are its simplicity, speed, and virtual lack of assumptions (Rossi, Per. Comm.). The predictor variables can be either categorical or continuous values. The CART analysis does not require distribution assumptions. Although CART has been traditionally used in economics (Howieson, 1991), it has also been used for ecological analysis (Gottschalk et al., 1998). Soil property classification by CART is relatively new, but it has been used effectively for the prediction of soil series boundaries (Mertens et al., 2001).

For this project, the Bt horizon was the response variable coded as 1 for presence and 0 for absence. Slope, aspect, curvature, global solar insolation, flow direction, flow accumulation,

specific catchment area, wetness index, and EC_a data for all raster sizes were used as predictor variables. The CART analysis was run on 147 of the 184 cores, following the removal of 37 cores (20% of the data set) randomly selected as a validation group for assessing CART performance. The CART analysis quantity SST-SSL-SSR threshold limit used was 0.001 and the minimum number of cores allowed per node was 9 (6% of the data). Two scenarios were created for the CART analysis: (1) prediction of Bt horizon presence or absence using all the terrain and EC_a data; and (2) prediction of Bt horizon presence or absence using only terrain data.

The output of CART was used to create a bivariate tree diagram from which results could be interpreted. Terminal nodes were chosen for mapping based on their percentage of Bt presence, which was selected as an average of at least 85%, and when grouped, having a total representation of Bt presence of 70%. The selected nodes of interest were mapped using ArcGIS 8.2 (ESRI 2002) based on the split values calculated by CART. Once the nodes were mapped, the resulting areas are referred to as zones.

Validation of the CART analysis was done in two ways: (1) using the 37 validation cores to assess output accuracy; and (2) using the IK map mean values for areas of Bt presence created by the zones. The first method was done by overlaying a point file of the 37 validation cores on the map of the CART zones. The value of the zone map was extracted for each point in the same manner as the terrain attributes and EC_a data. The second method for validation was to use a representation of presence or absence of Bt horizons, in this case, the IK map of Bt presence or absence. The zones that were created from the CART output based on nodes of interest were overlain onto the IK map. The values for the IK map were extracted into a new map only for the areas where the CART zones overlapped the IK map. The maps created from the extraction were analyzed for the distribution and mean of the IK values.

2.3 Results and Discussion

2.3.1 Indicator Kriging of Bt Horizon

The probability of having a Bt horizon is represented by the IK raster (Figure 2.2) and ranges in value from 0 to 1. The IK raster values represent the probability of having a Bt horizon (Figure 2.2). The mean value of the raster map was 0.44, which is equivalent to 44% of the data having a Bt horizon present. The original data had 45% of the total cores containing a Bt horizon and the similar percentage of the IK map indicates that a globally unbiased interpolation was achieved.

Presence of the Bt horizon within the 1.52 m sample depth occurred in a variety of different landscapes. Low lying areas tended to have a Bt horizon present in every aspect, however, this is not true in all instances. The presence of Bt horizon on hilltops was relatively sparse with the exception of one south-facing slope where the Bt horizon is present until the summit of the hill. Once the summit is crossed and the slope becomes north facing, the Bt horizon is not present until the draw is approached. Since Bt horizon presence is dispersed throughout draws and hill slopes, no apparent correlation between landscape position and Bt horizon presence is visibly discernable from the IK map.

2.3.2 Terrain Attributes

The influence of raster resolution on terrain attributes separated into two categories: (1) large impact, where resolution changes effected either maximum or minimum values by 20% or more; and (2) small impact, where resolution changes effected either maximum or minimum values by 5% or less (Tables 2.2-2.12). The terrain attributes that raster cell size had a large impact on, greater than 20%, were: slope, curvature, and wetness, whereas raster cell size had a

small impact on elevation, aspect, global solar insolation, flow direction, flow accumulation, and specific catchment.

Maximum values for slope decreased from 45.1 to 13.4 degrees as raster cell size increased from 1 to 30-m (Table 2.3). Curvature ranges were also reduced as cell size increased. The maximum value for plan curvature decreased from 203.16 to 0.81 radians per 100 m, while the minimum values increased from -154.49 to -0.71 radians per 100 m (Table 2.5-2.7). The maximum value for profile curvature decreased from 207.88 to 0.82 radians per 100 m, while the minimum values increased from -227.10 to -1.25 radians per 100 m. The maximum value for tangential curvature decreased from 122.48 to 0.10 radians per 100 m, while the minimum values increased from -109.46 to -0.09 radians per 100 m. Wetness index maximum values also decreased from 20.1 to 14.2 as raster cell size was increased from 1 to 30-m, while the minimum remained 0.

The large reduction in range from the 1 to 2-m rasters for slope, curvature, and wetness index, may be partially due to DEM error. As described in Chapter 1, there was error present in the DEM due to GPS measurement error, the collection method, and interpolation method. These errors were minimized through choice of interpolation method and increasing raster cell size; however, error still exists in the DEM and curvature error areas at the 1-m resolution level approached 9%. To ensure that DEM error did not affect the CART analysis, the values for the attributes were checked to see if any unrealistic values existed for the 184 core locations, none were found (data not shown).

The attributes that were affected the most by the increase in raster cell size from 1 to 30-m are the attributes that utilize slope in their calculation. Plan and profile curvature are the rate of change in slope (Wilson and Gallant, 2000), and tangential curvature is plan curvature

multiplied by the sine of the slope. Wetness index, defined as the log of specific catchment area divided by the tangent of the slope, is also influenced by slope changes (Wilson and Gallant, 2000). As the values of slope are reduced when cell size is increased, all the attributes that utilize slope will also be decreased.

Elevation, aspect, global solar insolation, flow accumulation, and specific catchment area were minimally affected as raster cell size increased from 1 to 30-m. Although flow accumulation and specific catchment area have values that decrease as cell size is increased, the decrease is due to the change in individual cell size of the DEM. As the DEM cell size increases from 1 to 2-m, there is a 400% increase in surface area covered by the individual cell. A raster cell with a size of 30-m covers 900 times the surface area as a 1-m raster cell. For attributes that utilize numbers of contributing cells, increasing the size of the cell will decrease the number of cells contributing; however, the cells that are contributing are much larger in area. Flow accumulation is the number of cells that flow into a given cell; specific catchment (A_s) is a measure of upslope area per unit cell width (Wilson and Gallant, 2000). To derive A_s , the flow accumulation value is multiplied by the area of the raster cell, divided by the length of the cell side. For the 30-m raster the calculation would be $345 * 900/30$. This gives the value of 10350 m^2/m . Since the calculation of A_s is based on the cell size, A_s will always decrease as the cell size increases; however, when put on the same area scale, the range of values is similar. If the A_s value for the 30-m DEM is multiplied by 30, the number of 1-m cells covered by the side of a 30-m cell, the value is $310500 m^2/m$. This value is similar to the 1-m value of $325980 m^2/m$. Therefore, the effects of changes in resolution can be misleading when evaluating attributes that are based on the number of contributing cells. In the calculations of flow accumulation and specific catchment area, there was very little change in maximum and minimum values when

going from 1 to 30-m even though the range of values indicate otherwise.

Terrain attribute values for each of the 184 locations for raster sizes 2 to 30-m were plotted against the 1-m value to assess effects of raster size (Figures 2.13-2.23). Similar to what the reductions of ranges in Tables 2.2-2.12 indicated, slope derived attributes had the largest reductions in value with increasing raster cell. Since slope is a fundamental attribute used in the calculation of erosion potential (Wilson and Gallant, 2000), the reduction in value would change the prediction value for erosion potential for a given DEM. This is important for the prediction of Bt horizon since erosion in the Palouse dictates how close the Bt horizon is to the surface (Busacca et al., 1985).

2.3.3 Apparent Electrical Conductivity

The EC_a surveys collected 10331 data points in the spring of 2000, and 10037 data points in the fall of 2000. The area covered during both surveys was the south 37.5 hectares, averaging 1 point every 36.30 m² in the spring and 37.36 m² in the fall. The maximum, minimum, and mean value of spring data was 71.70, 13.80, and 30.57 mS/m, respectively. The maximum, minimum, and mean values of fall data were 68.70, 9.10, and 23.44 mS/m, respectively.

Reported values of EC_a vary depending on soil conditions at measurement times. A range of 28.4 to 77.0 mS/m was reported for data collected in April near Centralia, Missouri (Sudduth et al., 2001). In March of 1998, EC_a readings ranging from 0.4 to 48.0 mS/m were reported for Cambridgeshire, UK (James et al., 2003). Both of these reported ranges are similar to the data collected during the two EC_a surveys for this study.

The spring EC_a data values were on average 23% higher than the fall data. This trend is

attributed to soil conductivity increases from greater soil water content in the spring as compared to the fall (Rhoades et al., 1976). Although spring EC_a values were higher, the OK maps of the spring and fall data show similar trends (Figures 2.24, 2.25). Mapped areas where relative EC_a readings were higher in the spring are similar to higher relative EC_a readings in the fall. Sudduth et al., (2003) found a correlation between increased soil clay content and higher values of EC_a values. When visual comparison of the EC_a maps and IK map of Bt horizon presence are made, the higher EC_a values in the spring and fall appear to correspond with Bt horizon presence.

When raster cell sizes increased, the minimum and maximum values for EC_a in both spring and fall increased and decreased, respectively (Tables 2.13, 2.14). The maximum value for the spring EC_a decreased from 71.70 to 53.84 mS/m as raster cell size increase from 1 to 30-m, respectively, a decrease of 25%. The maximum value for the fall EC_a decreased from 68.70 to 50.45 mS/m as raster cell size increased from 1 to 30-m, respectively, a decrease of 27%. Reduction in maximum values and increasing of minimum values is a common affect for increasing cell size (Isaaks and Srivastava, 1989). The spring and fall EC_a data (Figures 2.26, 2.27) had a decrease in EC_a values, for the ones above the mean, for each increase in raster size. The lower EC_a values, ones below the mean EC_a value, increased with every increase in raster size. When relating EC_a ranges to Bt presence or absence, decreasing the overall EC_a range by increasing raster cell size could have an affect on prediction capabilities.

2.3.4 Classification and Regression Tree

2.3.4.1 Prediction of Bt Horizon Utilizing Apparent Soil Electrical Conductivity and Terrain Attributes

For the CART analysis containing EC_a and terrain attributes, the response variable was

split into 19 different nodes (Figure 2.28). The first node was split based on spring EC_a at the 5-m level, 30.48 mS/m. This was the only time EC_a data was used by CART for the splitting of a node; however, the two child nodes produced were distinctly different. Node two, where all cores had a 5-m EC_a value less than 30.48mS/m, had only 32% of the total Bt cores in it, whereas node three had 68%. The presence of Bt horizon being correlated with higher spring EC_a values in Palouse soils is indicated by the splitting attribute and value of node one.

The nodes chosen for further analysis from the CART output using terrain attributes and EC_a data were five, six, and 13. When total number of Bt cores for the three nodes were combined, they represented 50 of the 68 cores (74%) with a Bt horizon. The average percentage of Bt presence in the three nodes was 87%. Although node six is a parent node and was split on 1-m global solar insolation, the two child nodes, 10 and 11, are both high percentage terminal nodes and nothing is gained by individually mapping them over mapping node six.

Global solar insolation was the only attribute used to create a node of interest at two resolutions, 25 and 30-m. Although global solar insolation was the only attribute used twice to create a node of interest, it does indicate that terrain attributes created from multiple resolution DEMs may be necessary to create zones with high likelihood of having a Bt horizon. The only splitting attribute used to create nodes of interest at a finer resolution than 10-m was the 5-m spring EC_a data. The EC_a data is not a derived terrain attribute from a DEM, and the usage of a 10-m DEM for creating terrain attributes for prediction of Bt horizons may suffice when coupled with EC_a data of a finer resolution.

The nodes of interest were mapped based on split attributes and corresponding split values of EC_a and terrain attributes identified by the CART analysis (Figures 2.29). The area of the zone created by mapping nodes five, six, and 13 was 35% of the total area of the map. The

zones created tended to be aggregated spatially with little scattering of the zones.

2.3.4.2 Analysis Utilizing Terrain Attributes

The CART analysis utilizing only the terrain attribute data, split the response variable into 21 nodes (Figure 2.30). The first node was split based on 30-m profile curvature. Cores having values less than -0.025 radians per 100 m went to node two, while values greater than -0.025 went to node three. Although profile curvature was also used to split node 11, its greatest influence was as the first split attribute for nodes two and three, with 24% and 76% of the Bt cores captured in each nodes, respectively. The nodes chosen for mapping from the CART analysis just using terrain attributes were four, seven, 14, and 20. When these terminal nodes are combined, 47 of the 68 cores with a Bt horizon (69%) were in the four nodes. The average percentage of Bt horizon presence in the nodes was 90%.

Plan curvature was used by the CART analysis as a splitting attribute at the 1-m, 10-m, 15-m, and 25-m, 40% of the total number of split attributes. Profile curvature was utilized as a splitting attribute at both 2 and 30-m resolutions. Of the split attributes in the CART analysis using only terrain attributes, 70% of the split attributes were curvature attributes. Wetness index and elevation were the only other terrain attributes used for a split. For the nodes of interest, plan curvature values were used at 1, 10, and 15-m resolutions. Plan curvature usage as a splitting attribute alone indicates that the usage of DEMs at multiple resolutions ranging from 1 to 15-m may be needed to predict Bt horizon presence in Palouse soils when only using terrain attributes.

Positive curvature values are areas with convex shape, while concave shapes have negative curvature values. The splitting of node one was -0.025 radians per 100 m for the 30-m

profile curvature, a slight concavity. The average value for 30-m profile curvature for node three was 0.19 radians per 100 m, a slight convexity. When nodes 14 and 20 were mapped, concave plan curvature values were used for splitting. Drawing the conclusion that concavities were more important than convexities is difficult from the analysis. Soil erosion is influenced by convergent and divergent flows created by surface curvature, and eroded soils in the Palouse have a higher clay content closer to the surface (Busacca et al., 1985), but from this analysis both concave and convex curvature influenced Bt horizon prediction.

The area of the zone created by mapping nodes four, seven, 14, and 20 was 37% of the total area of the map. The zones created from mapping tended to make large areas with little scattering of the zones, with zone four being an exception. Zone four, based on a 30-m profile curvature and a 1-m plan curvature, tended to be scattered throughout the map.

2.3.5 Validation of Classification and Regression Tree

The mapped zones for the CART analysis, using terrain attributes and EC_a as predictors, had a mean IK value of 0.62. A frequency histogram of the IK values for the zones shows the frequency increasing as the IK values approach 1 (Figure 2.32). When validation cores were used to assess results from this CART analysis, Bt horizon presence was correctly predicted 58% of the time (Table 2.15).

The CART analysis that used terrain attributes had a mean IK value of 0.53. A frequency histogram of the IK values for the zones shows the frequency increasing as the IK values approach 1 (Figure 2.33). When validation cores were used to assess results from this CART analysis, Bt horizon presence was correctly predicted 69% of the time (Table 2.15).

Indicator kriging validation between the zones created by CART for EC_a and terrain

attribute data compared to terrain attribute data alone, there was a 9% increase in Bt presence prediction using EC_a data coupled with terrain attributes. Apparent soil electrical conductivity data has been strongly correlated to soil properties, including depth to Bt (Sudduth et al., 2000). This corroborates the CART analysis' usage of 5-m spring EC_a as the primary attribute for the prediction of Bt horizon presence.

Validation of the CART analysis using a validation set of cores was 11% higher for the analysis using terrain attributes alone. This is a reversal of the validation results from IK mapping. The differences in validation ranges for the two analyses is a function of the extrapolation of CART nodes into mapped zones. The deviation suggests that the use of terrain attributes alone may not give satisfactory results when extrapolating to larger areas despite high validation for cores.

2.4 Conclusion

The prediction of Bt horizon presence by the CART analysis found 5-m spring EC_a data as the main attribute indicating Bt presence when coupled with terrain attributes. The use of EC_a data as the primary splitting value for the classification of Bt horizon presence shows a strong indication that EC_a data is a valuable tool for prediction of Bt horizon presence. When no EC_a data was used, 30-m profile curvature was the primary predictor for Bt horizon presence. Once the primary split was done, curvature attributes were utilized by CART as splitting attributes 70% of the time. In situations when EC_a data are not available, curvature attributes were useful for Bt horizon prediction.

The CART analysis utilized plan curvature, profile curvature, and wetness index multiple times as the splitting attribute for the same CART analysis, but at different resolutions, indicating

that changes in values of terrain attributes at different resolutions can influence the prediction of Bt horizons. Producing DEMs and EC_a rasters at a variety of resolutions were necessary for Bt horizon prediction using CART.

Mapping the bivariate tree output from the CART analysis allowed for relatively easy zone mapping of nodes of interest. These mapped zones from CART were compared to an IK map and a validation core set in order to assess the predictive capabilities of the CART zones. The zones created from the CART analysis utilizing EC_a data and terrain attributes achieved accuracies of 58% and 62% for core validation and IK mapping, respectively. The zones created from the CART analysis utilizing terrain attributes achieved accuracies of 69% and 53% for core validation and IK mapping, respectively. The dissimilar validation results from the CART analysis using only terrain attribute data indicate difficulty in extrapolating the output nodes into mapped zones. Consistency in the validation of the CART analysis using EC_a and terrain attribute data indicates a better extrapolation into mapped zones.

2.5 Tables

Table 2.1. Terrain attributes, their units, and importance calculated from digital elevation models for classification and regression tree analysis.

Terrain Attribute	Units	Importance
Slope	degrees	Overland and subsurface flow
Aspect	degrees	Solar insolation and evapotranspiration
Plan Curvature	radians / 100 m	Converging and diverging flow
Profile Curvature	radians / 100 m	Flow acceleration
Tangential Curvature	radians / 100 m	Alternative measure of flow convergence
Global Solar Insolation	W/m ²	Irradiance incidence
Flow Direction	direction	Direction of flow
Flow Accumulation	no. cells	Contributing cell from flow
Specific Catchment Area	m ² /m	Runoff volume
Wetness Index	-	Zones of saturation

Table 2.2. Elevation values for decreasing resolution of digital elevation models.

<u>Raster Cell Size</u>	<u>Maximum</u>	<u>Minimum</u>	<u>Mean</u>
--m--	----- m -----		
1	818.26	771.92	793.51
2	818.17	771.80	793.49
5	817.87	772.03	793.52
10	817.58	772.06	793.48
15	817.18	773.09	793.47
20	817.15	773.09	793.44
25	817.21	773.13	793.44
30	815.76	773.20	793.45

Table 2.3. Slope values for decreasing resolution of digital elevation models.

<u>Raster Cell Size</u>	<u>Maximum</u>	<u>Minimum</u>	<u>Mean</u>
--m--	----- degrees -----		
1	45.1	0.0	6.5
2	27.2	0.0	6.4
5	19.5	0.0	6.4
10	18.5	0.0	6.2
15	16.5	0.0	6.0
20	15.2	0.0	5.8
25	13.8	0.0	5.5
30	13.4	0.0	5.3

Table 2.4. Aspect values for decreasing resolution of digital elevation models.

<u>Raster Cell Size</u>	<u>Maximum</u>	<u>Minimum</u>	<u>Mean</u>
--m--	-----degrees-----		
1	360	0	212
2	360	0	212
5	360	0	212
10	360	0	212
15	360	0	212
20	360	0	214
25	360	0	216
30	360	0	215

Table 2.5. Plan curvature values for decreasing resolution of digital elevation models.

<u>Raster Cell Size</u>	<u>Maximum</u>	<u>Minimum</u>	<u>Mean</u>
--m--	-----radians/100 m-----		
1	203.16	-154.49	0.03
2	52.71	-31.87	0.03
5	3.58	-6.35	0.03
10	1.98	-1.74	0.03
15	1.16	-0.91	0.03
20	1.31	-1.00	0.03
25	1.53	-0.92	0.03
30	0.81	-0.71	0.03

Table 2.6. Profile curvature values for decreasing resolution of digital elevation models.

<u>Raster Cell Size</u>	<u>Maximum</u>	<u>Minimum</u>	<u>Mean</u>
--m--	-----radians/100 m-----		
1	207.88	-227.10	0.03
2	50.33	-61.58	0.03
5	60.25	-7.22	0.03
10	2.39	-2.48	0.03
15	1.24	-1.92	0.03
20	1.00	-1.60	0.03
25	0.98	-1.61	0.03
30	0.82	-1.25	0.03

Table 2.7. Tangential curvature values for decreasing resolution of digital elevation models.

<u>Raster Cell Size</u>	<u>Maximum</u>	<u>Minimum</u>	<u>Mean</u>
--m--	-----radians/100 m-----		
1	122.48	-109.46	0.00
2	14.81	-13.97	0.00
5	1.07	-1.04	0.00
10	0.22	-0.29	0.03
15	0.13	-0.16	0.00
20	0.12	-0.14	0.00
25	0.09	-0.13	0.00
30	0.10	-0.09	0.00

Table 2.8. Global solar insolation values for decreasing resolution of digital elevation models.

<u>Raster Cell Size</u>	<u>Maximum</u>	<u>Minimum</u>	<u>Mean</u>
--m--		WH/m ²	
1	1919257	750182	1634025
2	1914986	1030157	1634464
5	1909891	1160087	1635251
10	1904607	1190598	1637299
15	1899033	1236064	1638947
20	1896218	1266946	1639358
25	1888511	1334846	1670505
30	1887423	1323353	1673962

Table 2.9. Flow direction values for decreasing resolution of digital elevation models.

<u>Raster Cell Size</u>	<u>Maximum</u>	<u>Minimum</u>	<u>Mean</u>
--m--			
1	128	1	28
2	128	1	28
5	128	1	28
10	128	1	27
15	128	1	27
20	128	1	27
25	128	1	27
30	128	1	27

Table 2.10. Flow accumulation values for decreasing resolution of digital elevation models.

<u>Raster Cell Size</u>	<u>Maximum</u>	<u>Minimum</u>	<u>Mean</u>
--m--	-----no. Raster Cells-----		
1	325980	0	331
2	81505	0	205
5	13063	0	77
10	3341	0	41
15	1561	0	29
20	870	0	22
25	562	0	18
30	345	0	11

Table 2.11. Specific catchment area values for decreasing resolution of digital elevation models.

<u>Raster Cell Size</u>	<u>Maximum</u>	<u>Minimum</u>	<u>Mean</u>
--m--	----- m^2/m -----		
1	325980	0	331
2	163010	0	411
5	65312	0	307
10	33410	0	412
15	23415	0	431
20	17400	0	444
25	14050	0	442
30	10350	0	340

Table 2.12. Wetness index values for decreasing resolution of Digital elevation models.

<u>Raster Cell Size</u>	<u>Maximum</u>	<u>Minimum</u>	<u>Mean</u>
--m--			
1	20.1	0.0	5.5
2	18.3	0.0	5.5
5	16.7	0.0	5.5
10	16.0	0.0	5.4
15	14.8	0.0	5.3
20	14.5	0.0	5.3
25	14.0	0.0	5.2
30	14.2	0.0	5.1

Table 2.13. Apparent soil electrical conductivity values for spring 2000 for decreasing resolution.

<u>Raster Cell Size</u>	<u>Maximum</u>	<u>Minimum</u>	<u>Mean</u>
--m--	-----mS/m-----		
1	71.70	13.80	30.03
2	71.02	14.14	30.04
5	69.76	14.81	30.07
10	66.81	15.50	30.12
15	66.22	17.76	30.17
20	62.65	17.32	30.24
25	58.01	19.43	30.24
30	53.84	19.71	30.28

Table 2.14. Apparent soil electrical conductivity values for fall 2000 for decreasing resolution.

<u>Raster Cell Size</u>	<u>Maximum</u>	<u>Minimum</u>	<u>Mean</u>
--m--	-----mS/m-----		
1	68.70	9.10	22.78
2	67.00	10.67	22.80
5	64.30	10.97	22.88
10	61.00	11.30	22.99
15	57.95	11.52	23.09
20	57.71	12.27	23.27
25	54.38	12.72	23.34
30	50.45	12.77	23.41

Table 2.15. Classification and regression tree validation results from core set.

<u>CART Analysis</u>	<u>Zones</u>	<u>Total Predicted</u>	<u>Correct</u>	<u>Percentage Correct</u>
		-no.-	-no.-	-%-
Terrain attributes and EC _a	5,6,13	12	7	58
Terrain Attributes	4,7,14,20	16	11	69

2.6 Figures

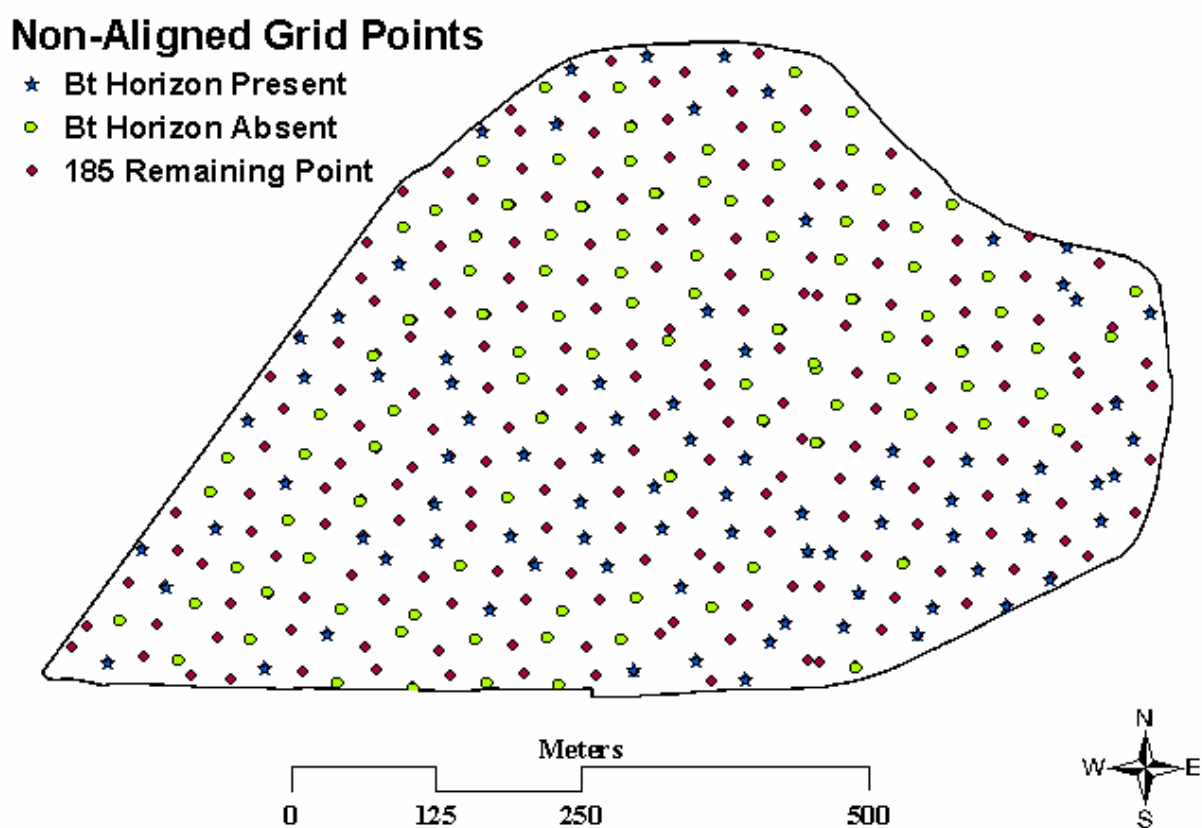


Figure 2.1. The 369 random points created from a 30.48-m grid superimposed on the Cunningham Agronomy Farm with indication of Bt horizon presence of absence.

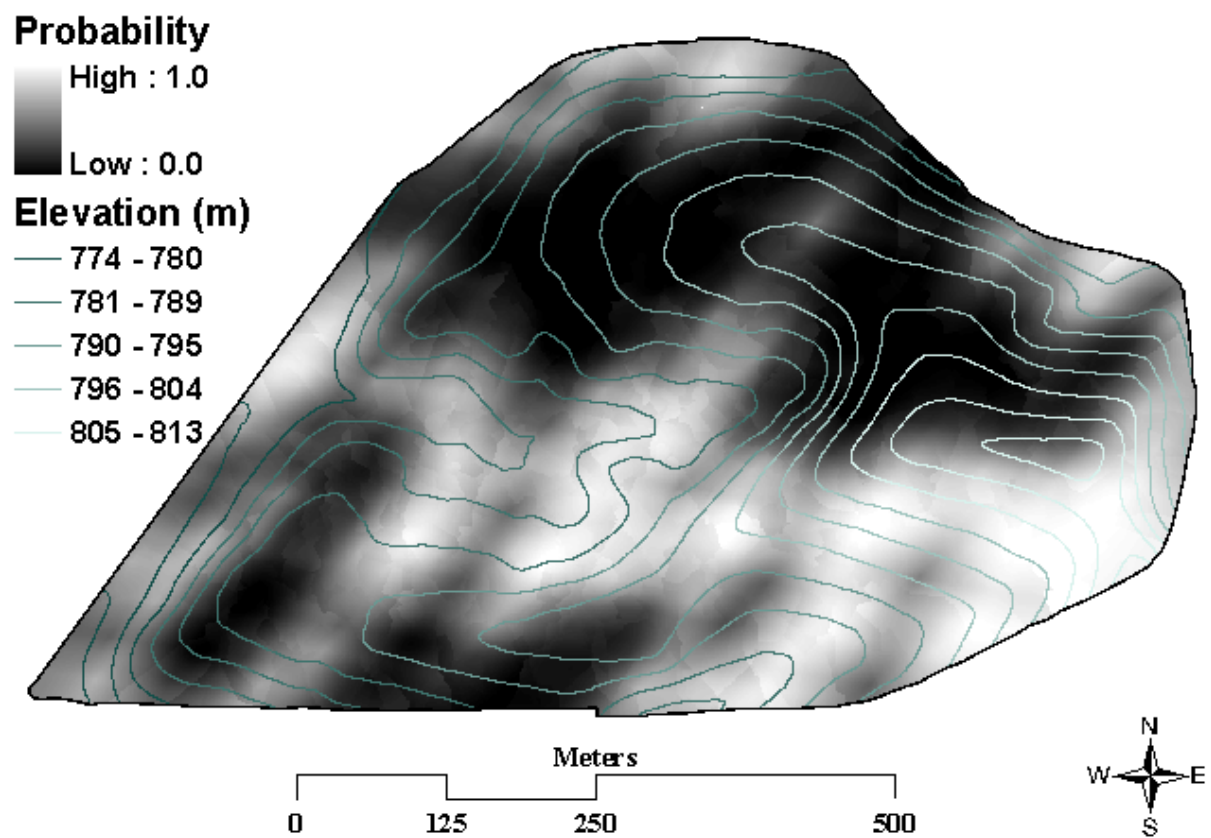


Figure 2.2. Indicator kriging of the probability of Bt horizon presence and elevation contours from 2-m digital elevation model.

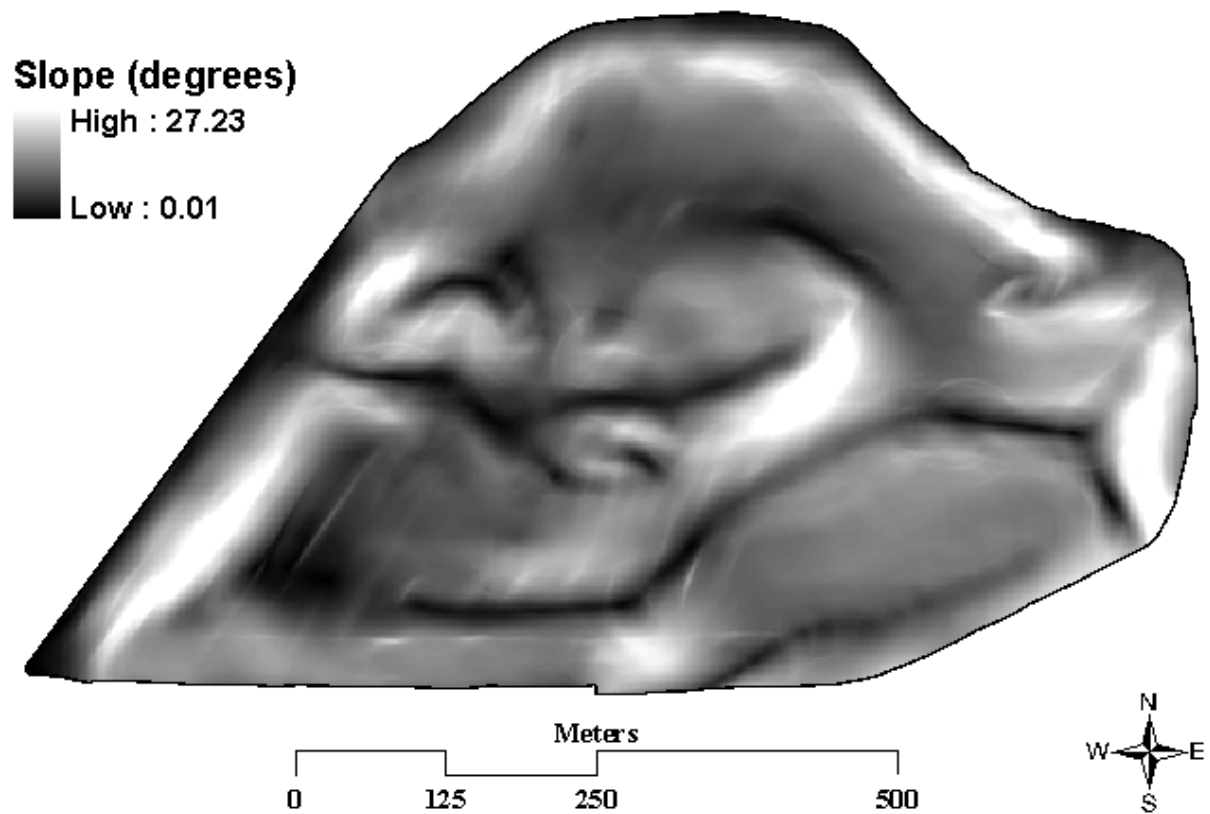


Figure 2.3. Slope map created from 2-m digital elevation model for 36.4 ha Cunningham Agronomy Farm.

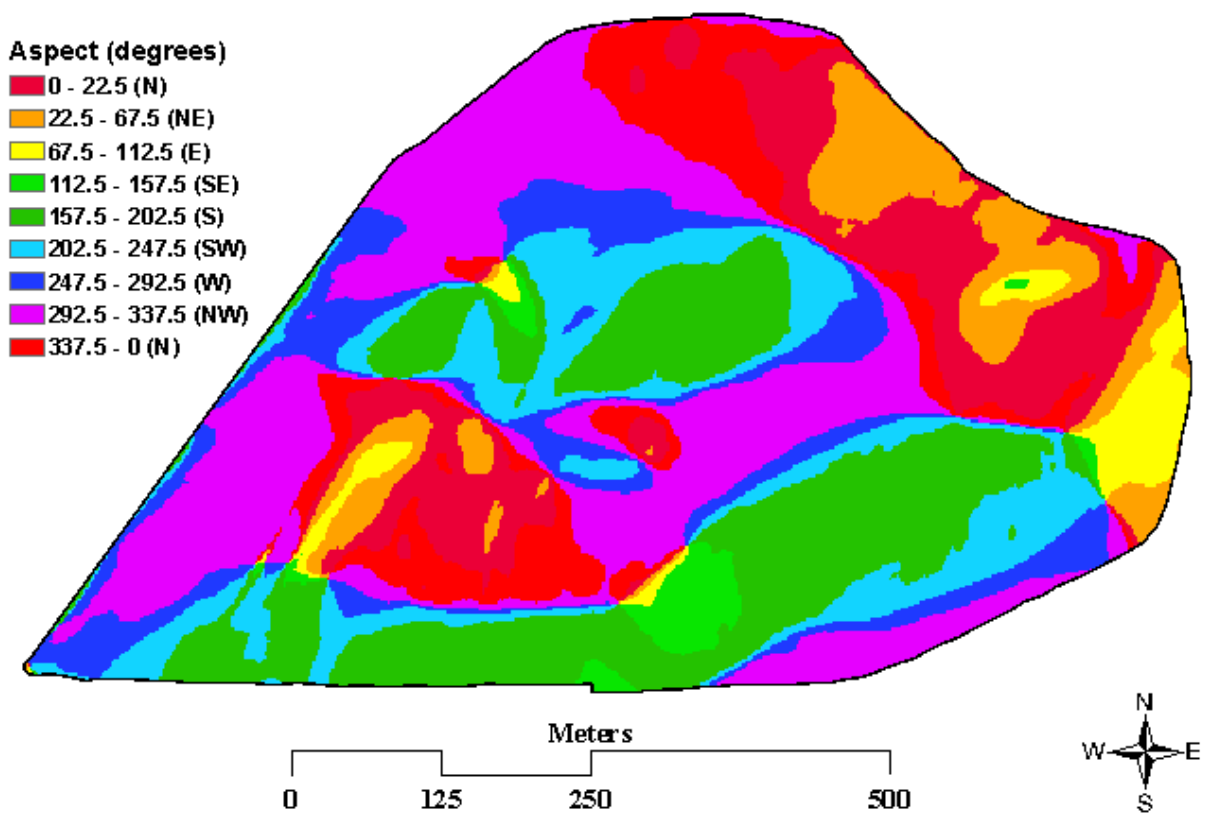


Figure 2.4. Aspect map created from 2-m digital elevation model for 36.4 ha Cunningham Agronomy Farm.

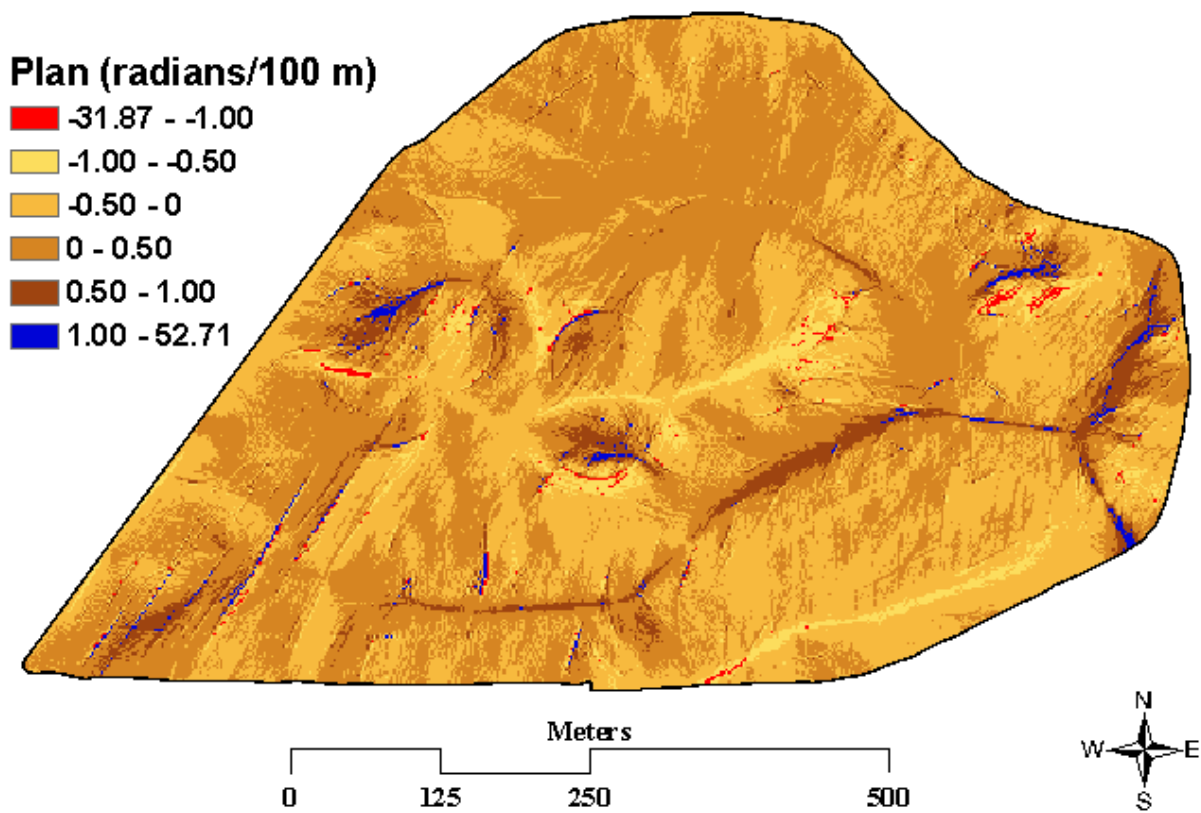


Figure 2.5. Plan curvature map created from 2-m digital elevation model for 36.4 ha

Cunningham Agronomy Farm.

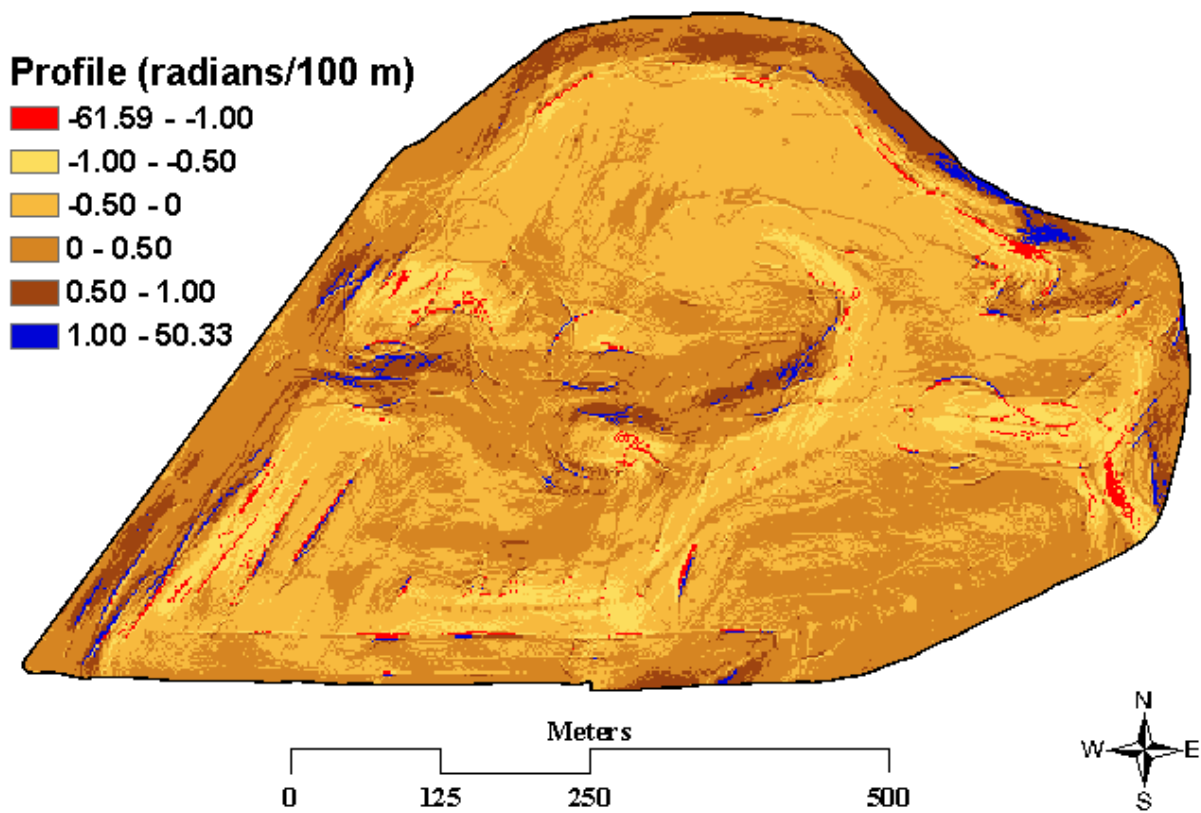


Figure 2.6. Profile curvature map created from 2-m digital elevation model for 36.4 ha

Cunningham Agronomy Farm.

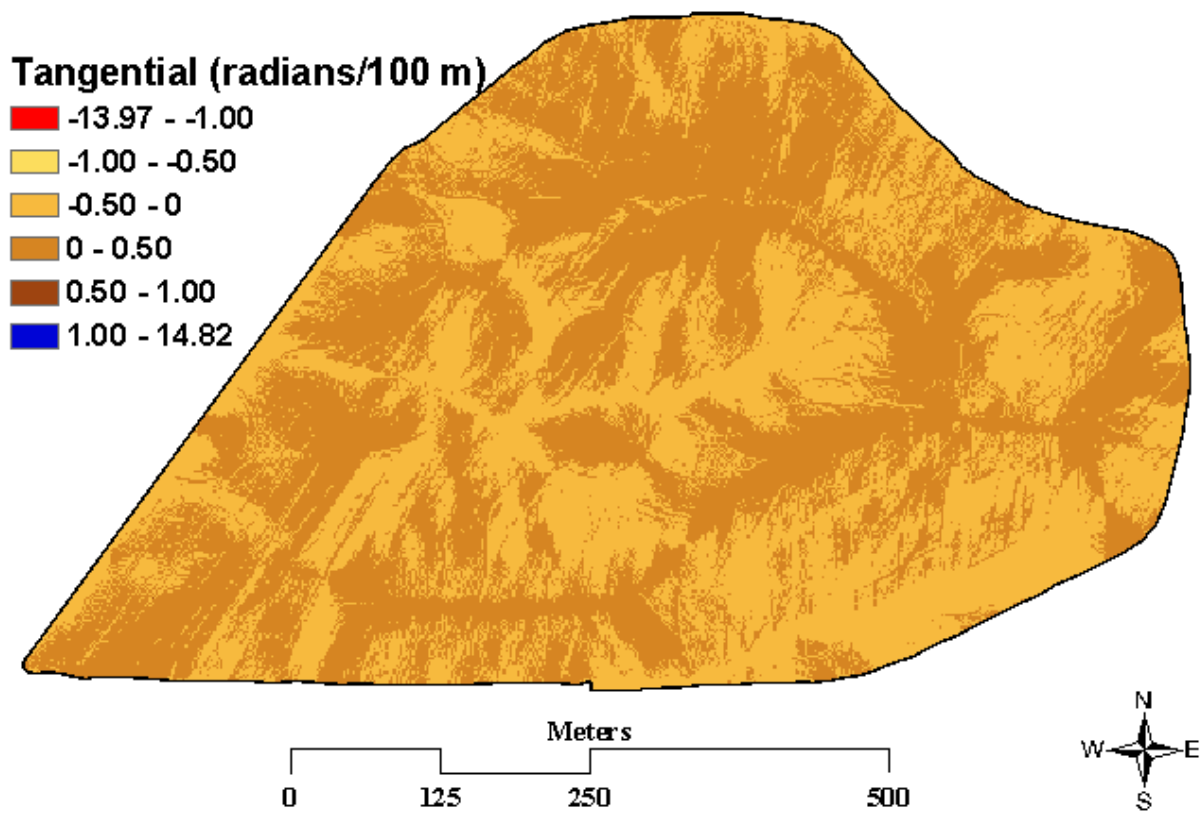


Figure 2.7. Tangential curvature map created from 2-m digital elevation model for 36.4 ha

Cunningham Agronomy Farm.

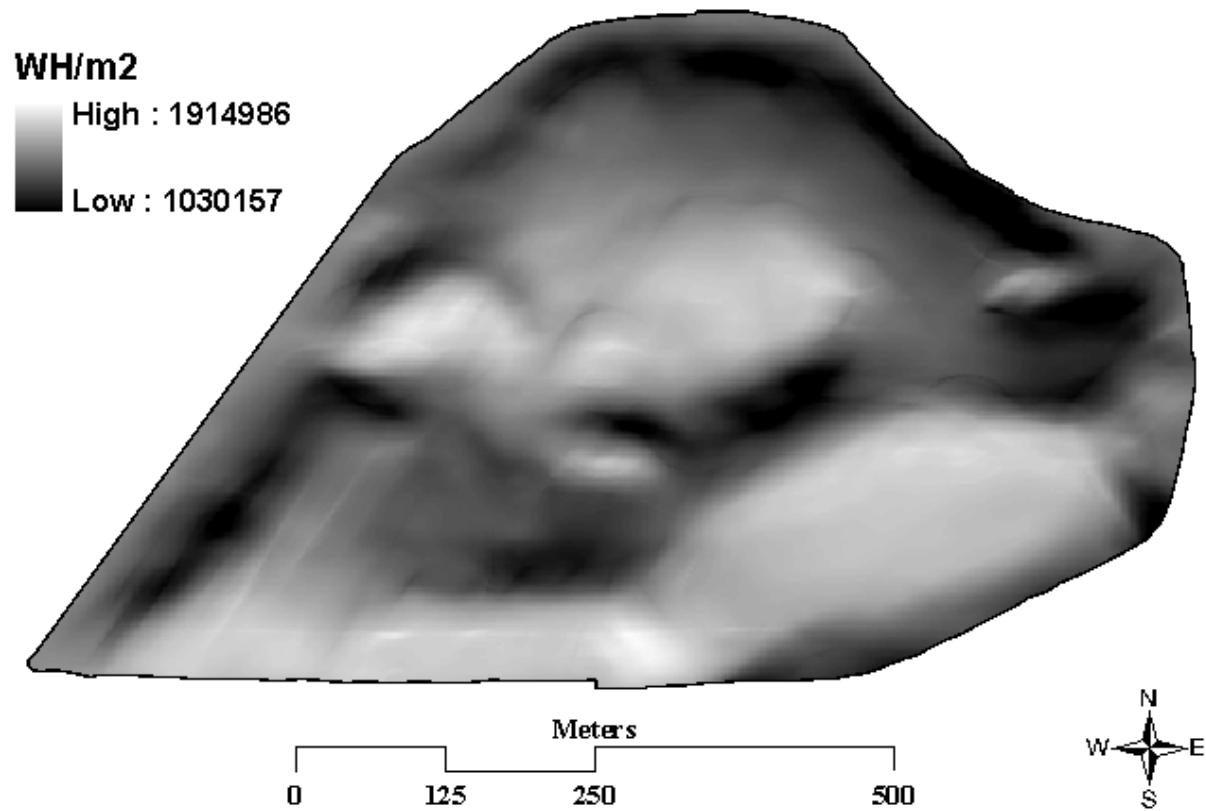


Figure 2.8. Global solar insolation map created from 2-m digital elevation model for 36.4 ha

Cunningham Agronomy Farm.

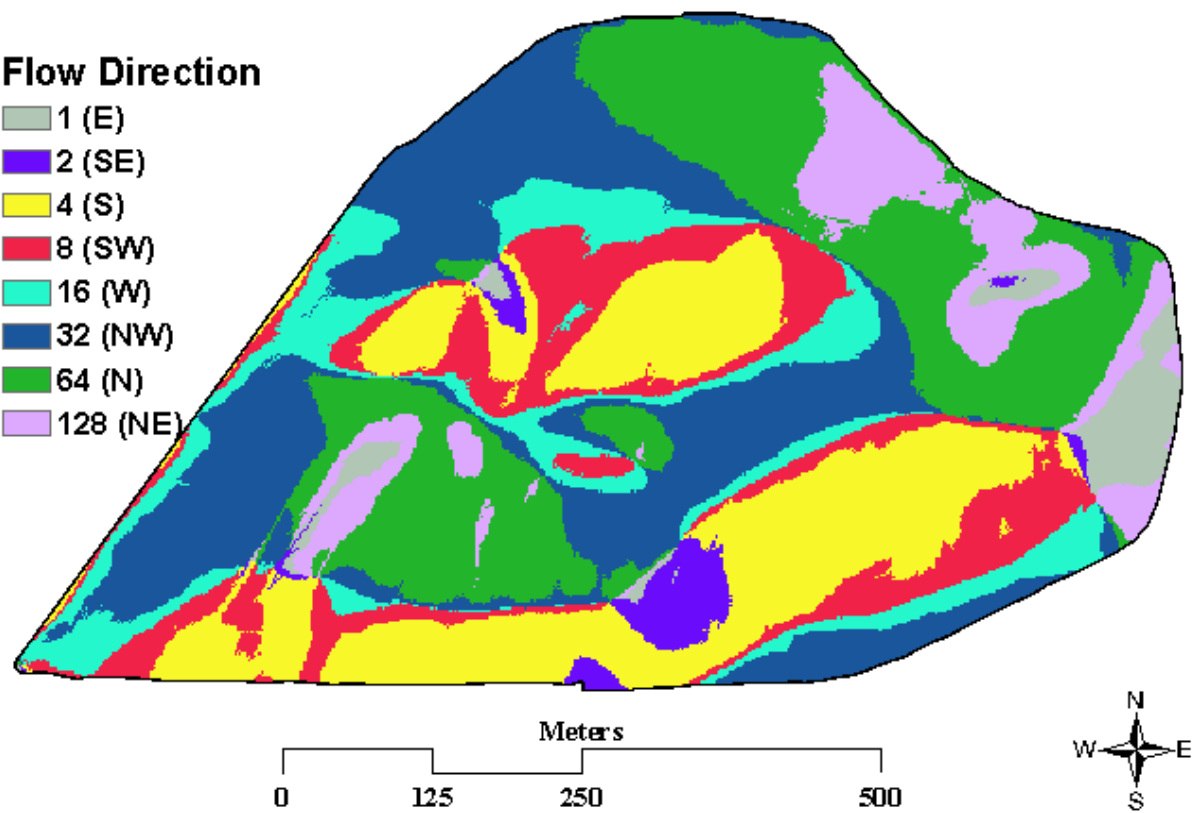


Figure 2.9. Flow direction map created from 2-m digital elevation model for 36.4 ha

Cunningham Agronomy Farm.

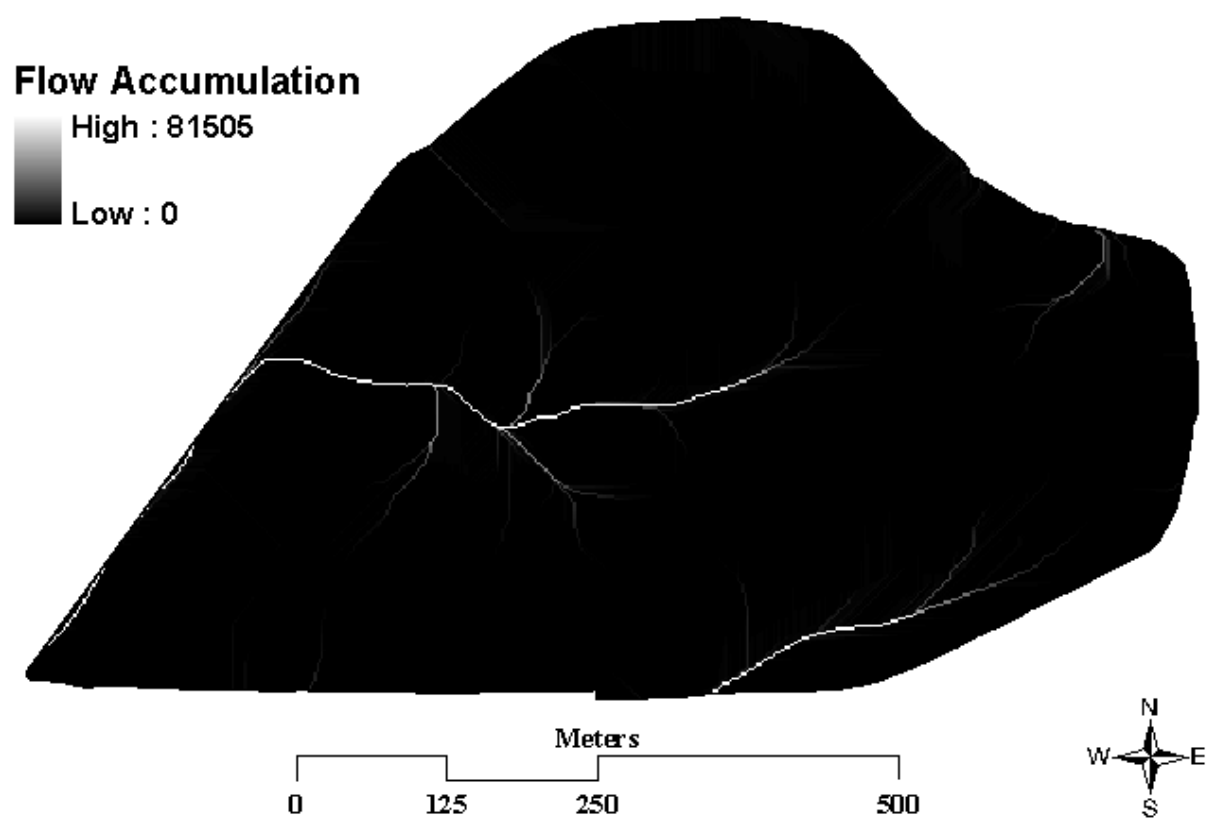


Figure 2.10. Flow accumulation map created from 2-m digital elevation model for 36.4 ha

Cunningham Agronomy Farm.

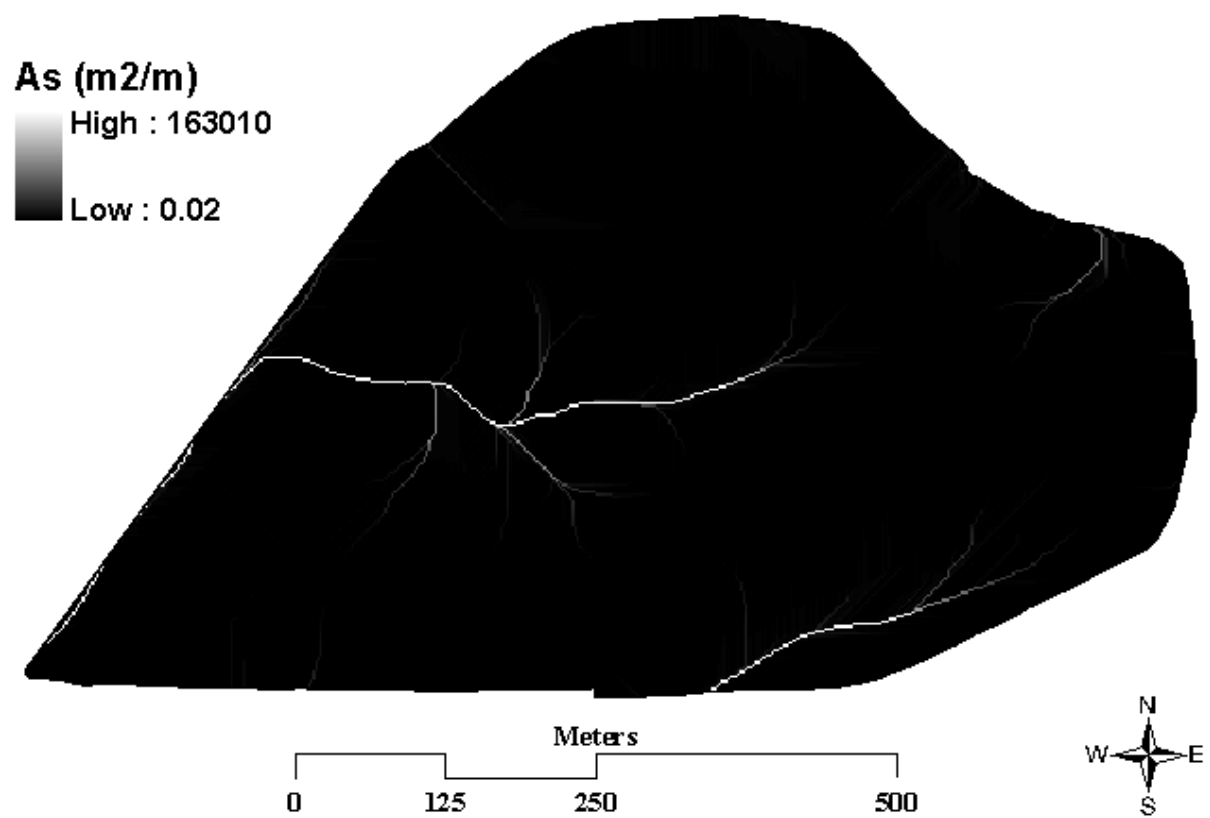


Figure 2.11. Specific catchment area (A_s) map created from 2-m digital elevation model for 36.4 ha Cunningham Agronomy Farm.

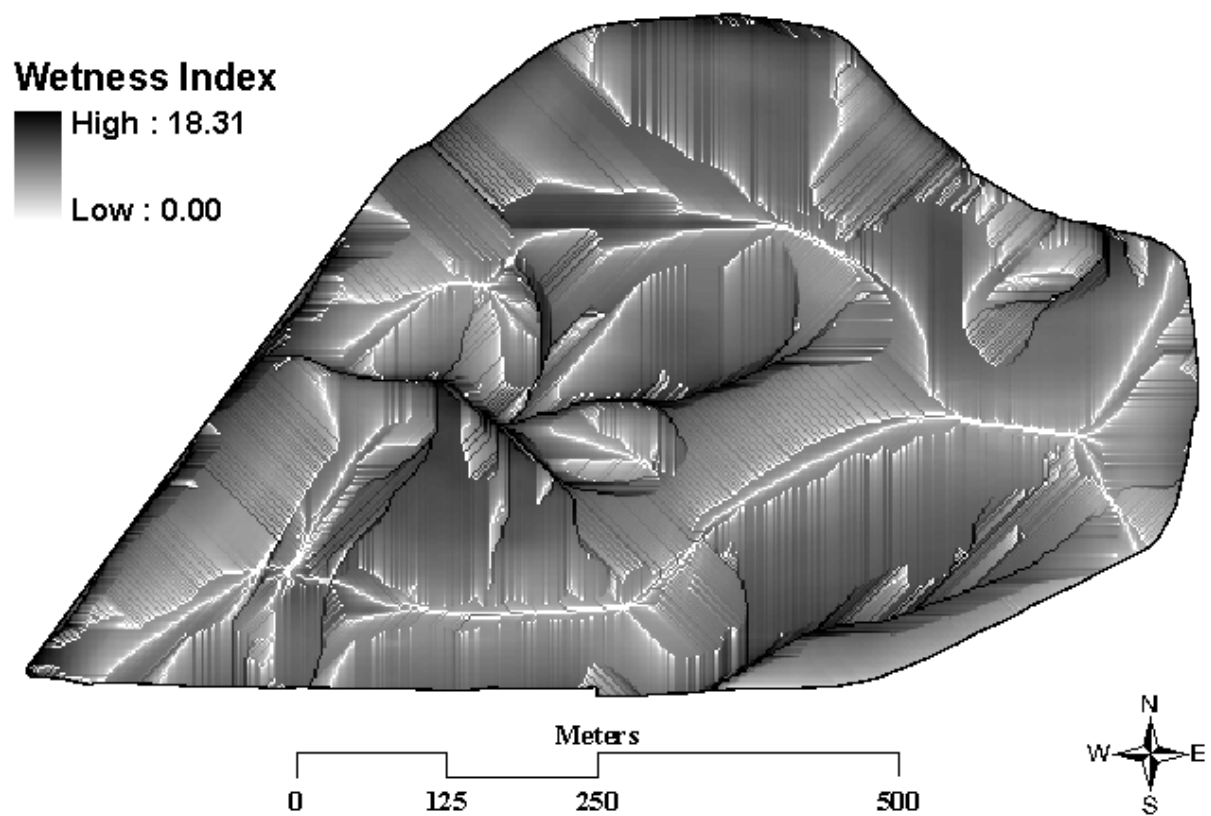


Figure 2.12. Wetness index map created from 2-m digital elevation model for 36.4 ha

Cunningham Agronomy Farm.

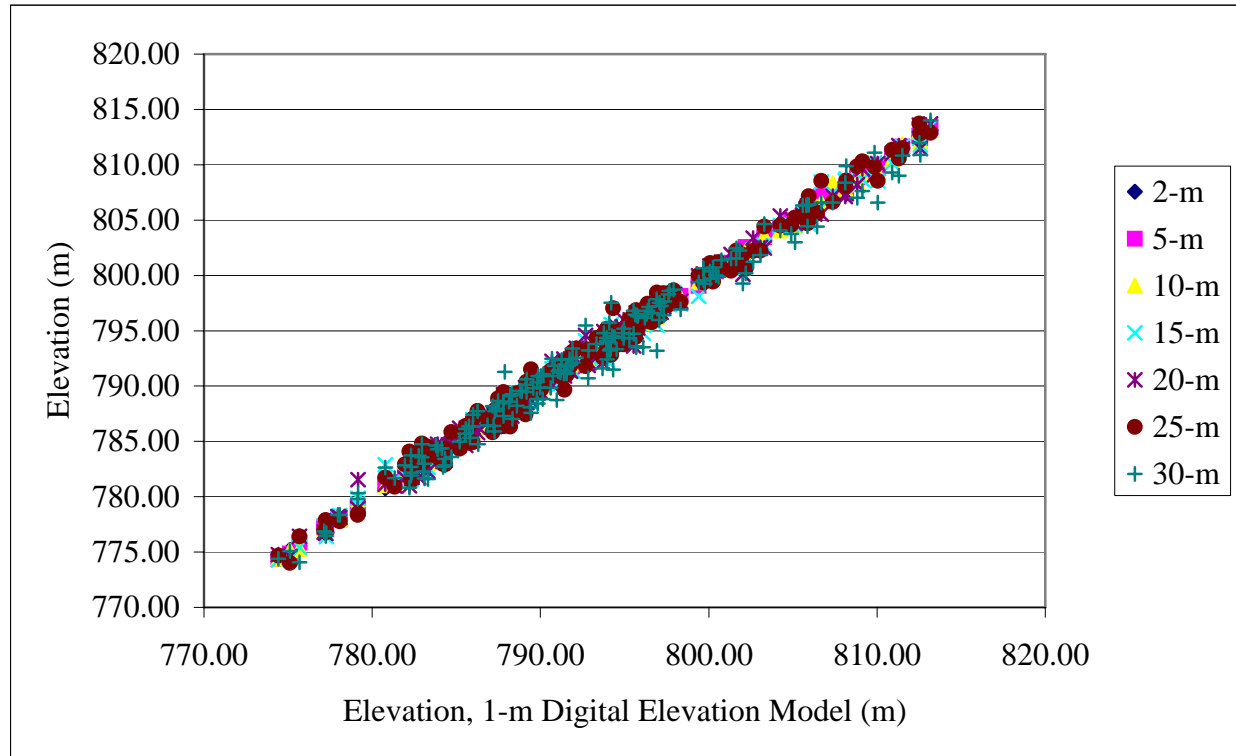


Figure 2.13. Graph of 1-m digital elevation model elevation data for 184 core locations *versus* increasing raster cell sizes.

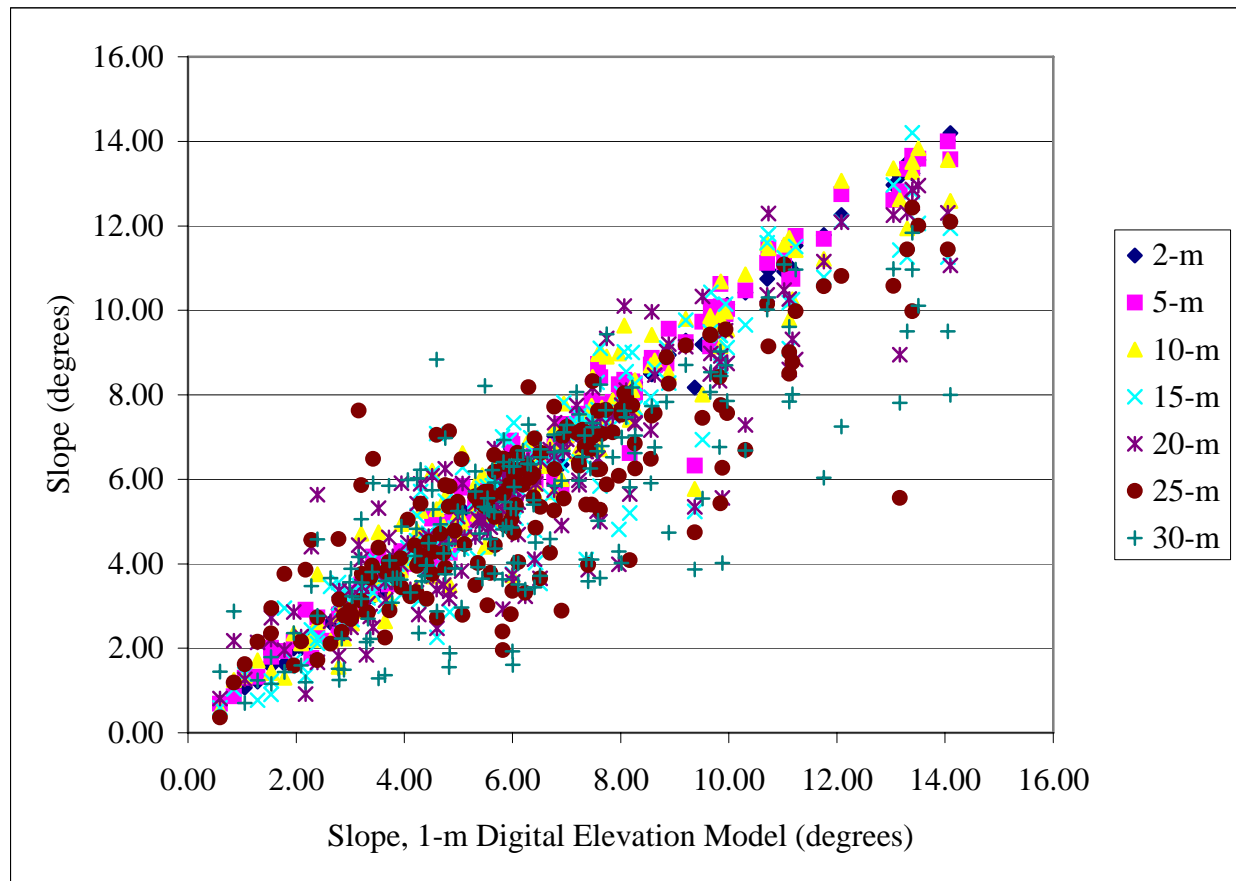


Figure 2.14. Graph of 1-m digital elevation model slope data for 184 core locations *versus* increasing raster cell sizes.

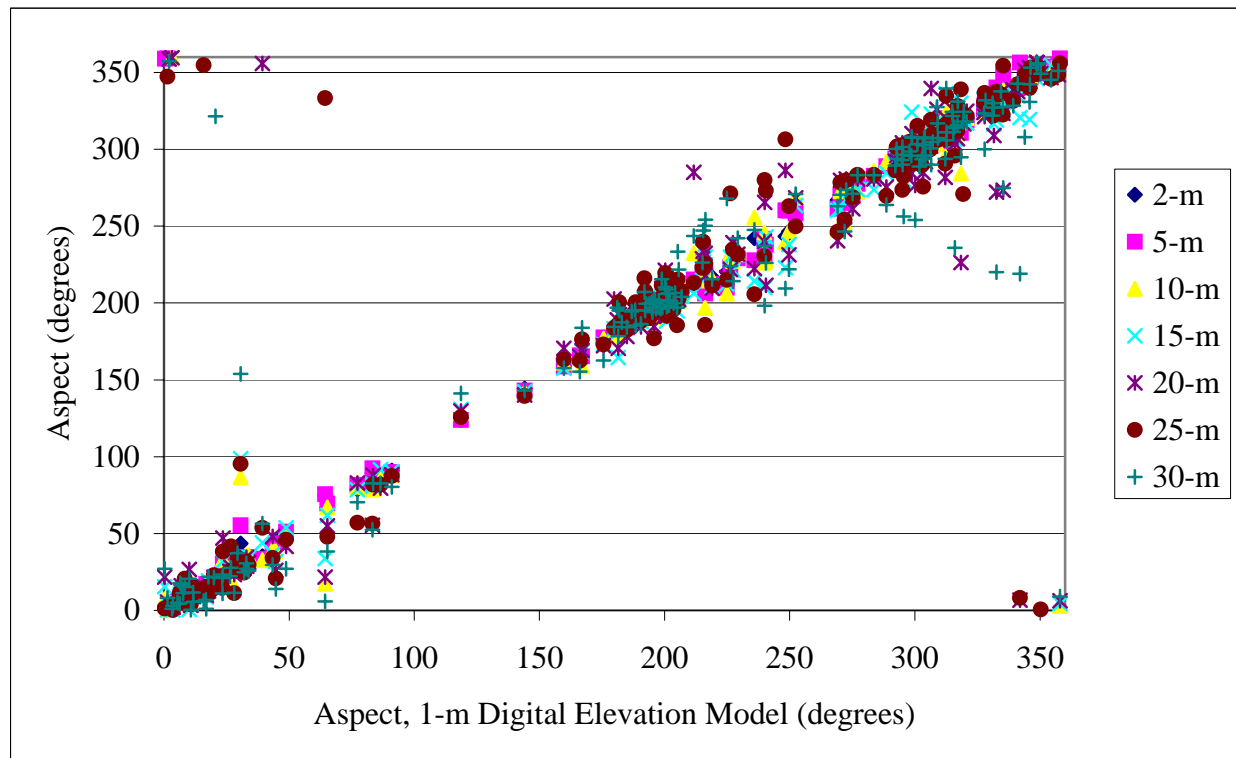


Figure 2.15. Graph of 1-m digital elevation model aspect data for 184 core locations *versus* increasing raster cell sizes.

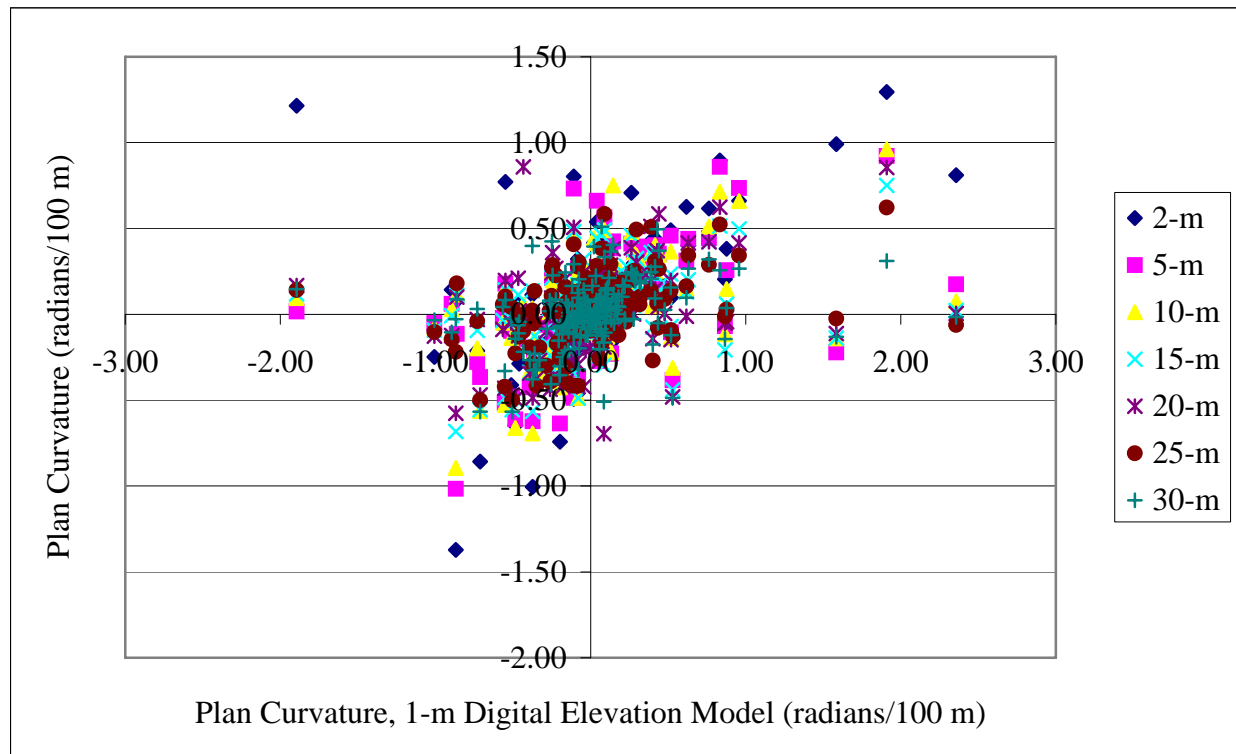


Figure 2.16. Graph of 1-m digital elevation model plan curvature data for 184 core locations *versus* increasing raster cell sizes.

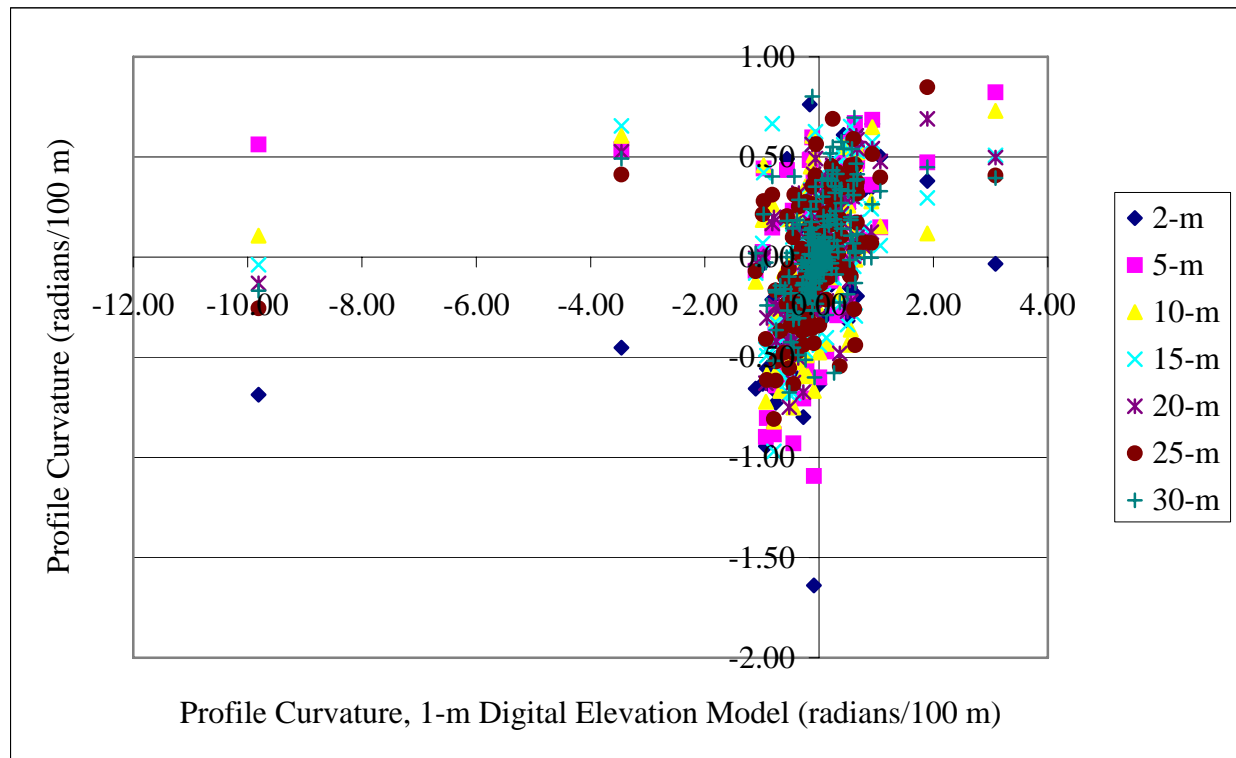


Figure 2.17. Graph of 1-m digital elevation model profile curvature data for 184 core locations *versus* increasing raster cell sizes.

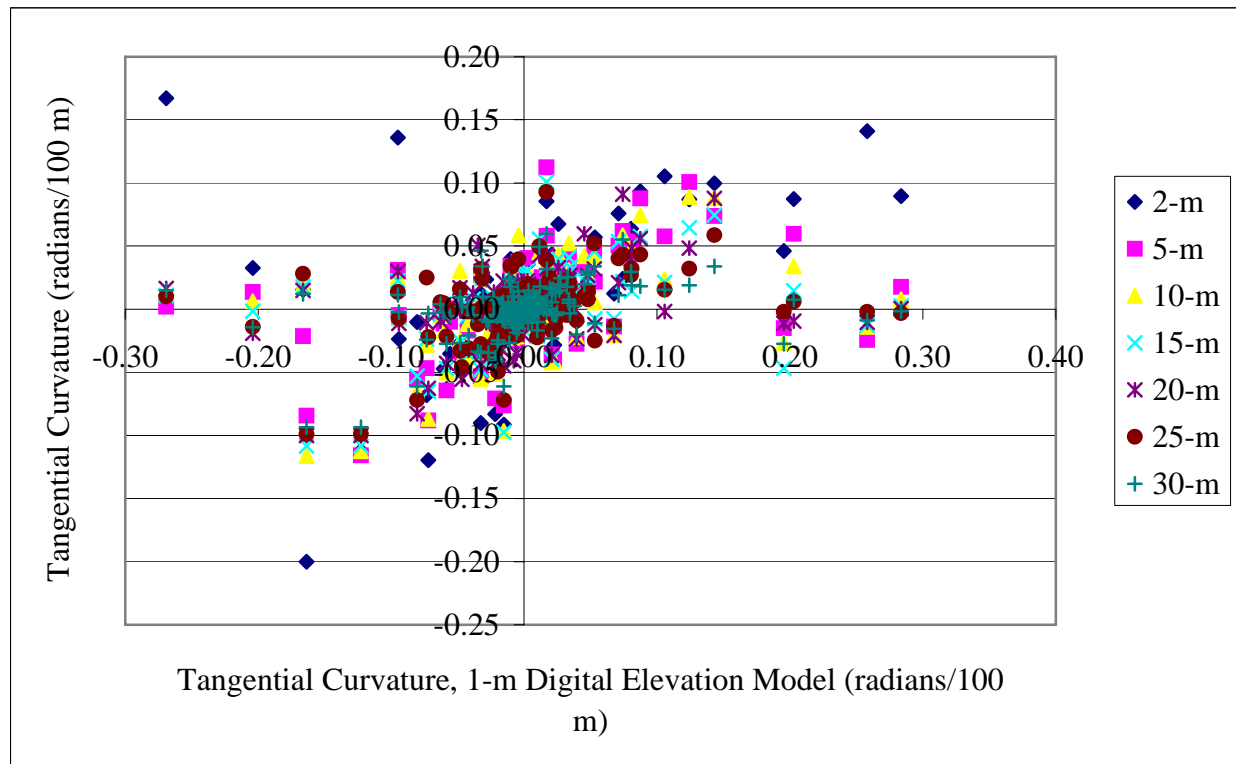


Figure 2.18. Graph of 1-m digital elevation model tangential curvature data for 184 core locations *versus* increasing raster cell sizes.

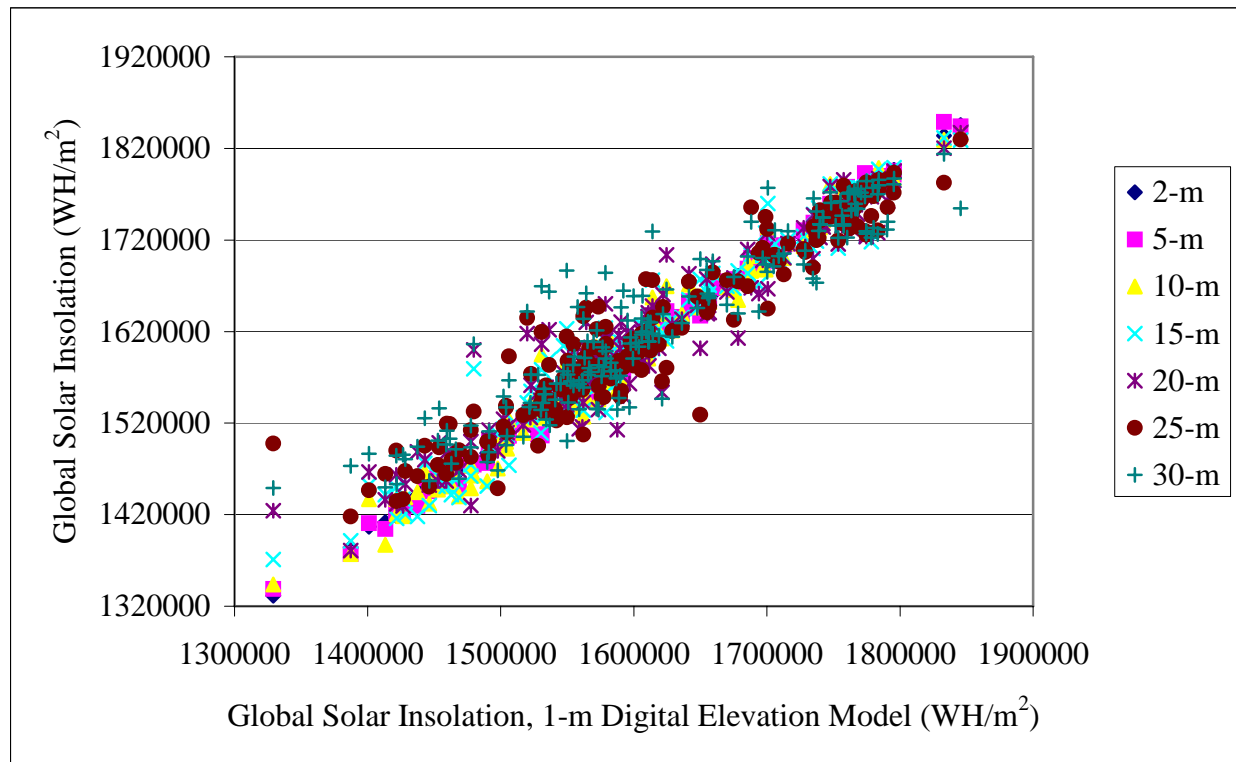


Figure 2.19. Graph of 1-m digital elevation model global solar insolation data for 184 core locations *versus* increasing raster cell sizes.

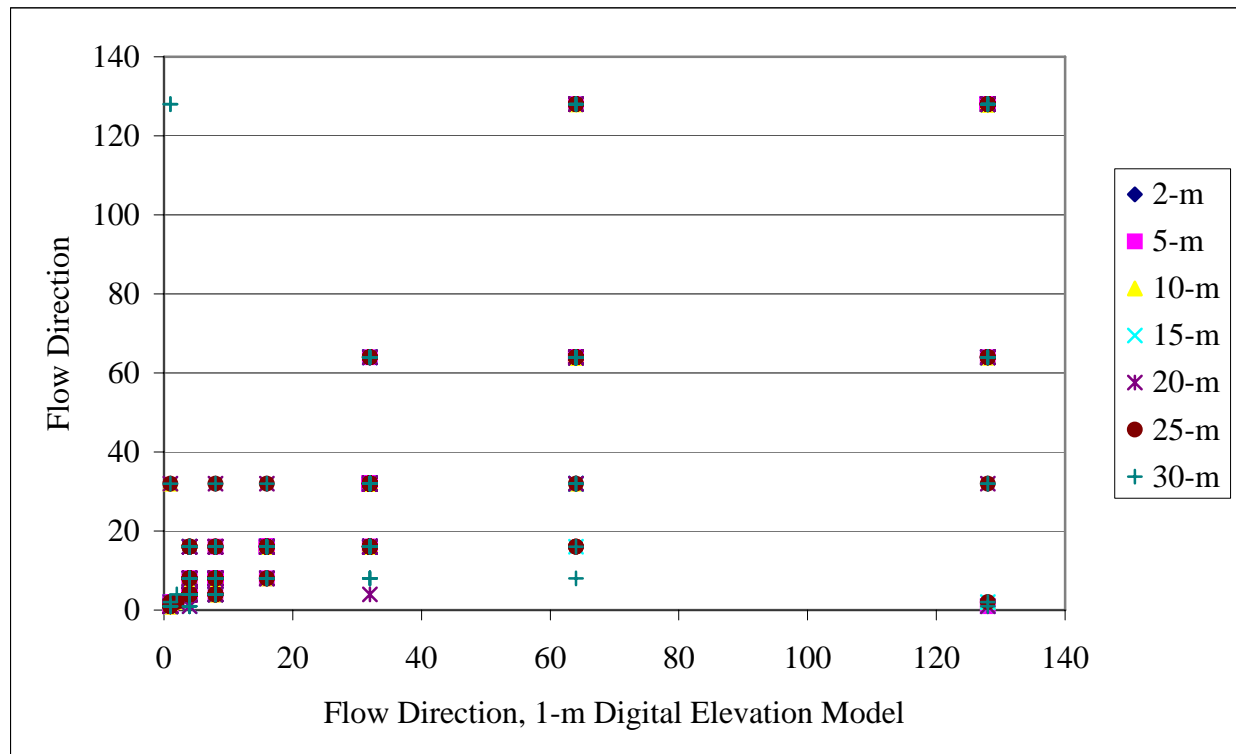


Figure 2.20. Graph of 1-m digital elevation model flow direction data for 184 core locations versus increasing raster cell sizes.

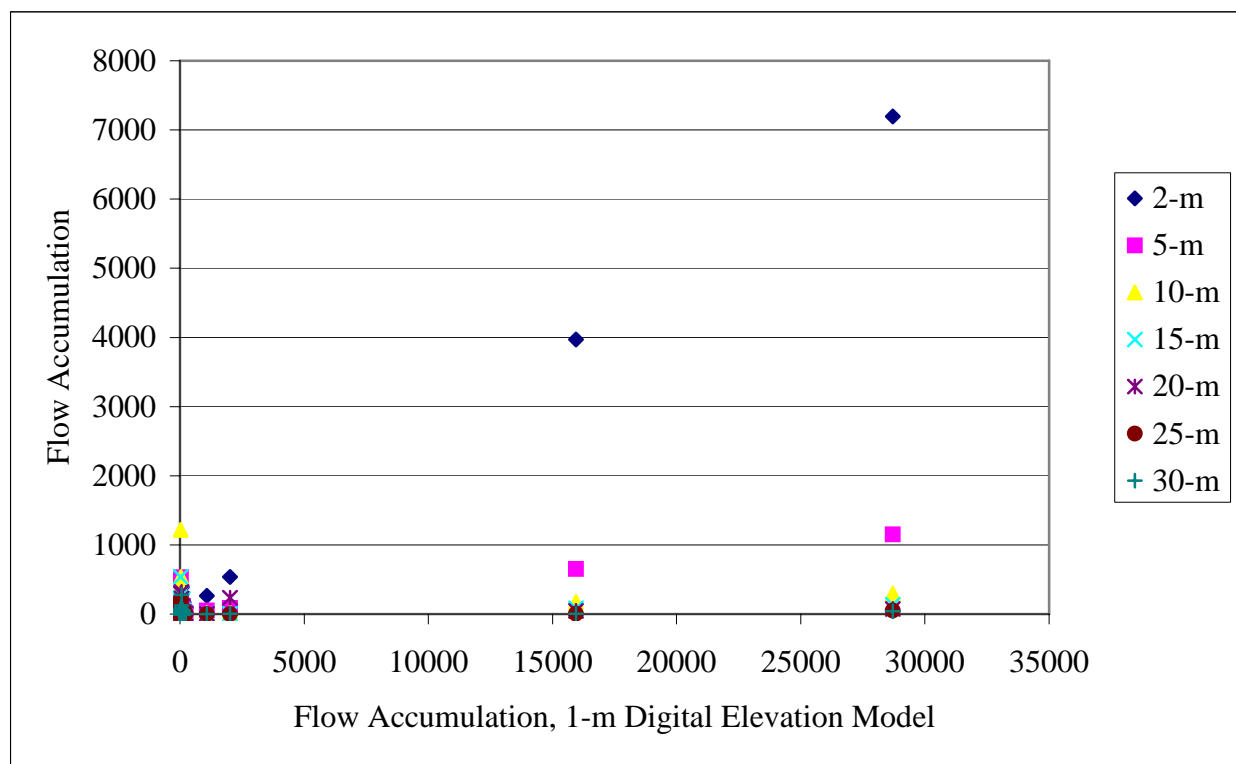


Figure 2.21. Graph of 1-m digital elevation model flow accumulation data for 184 core locations versus increasing raster cell sizes.

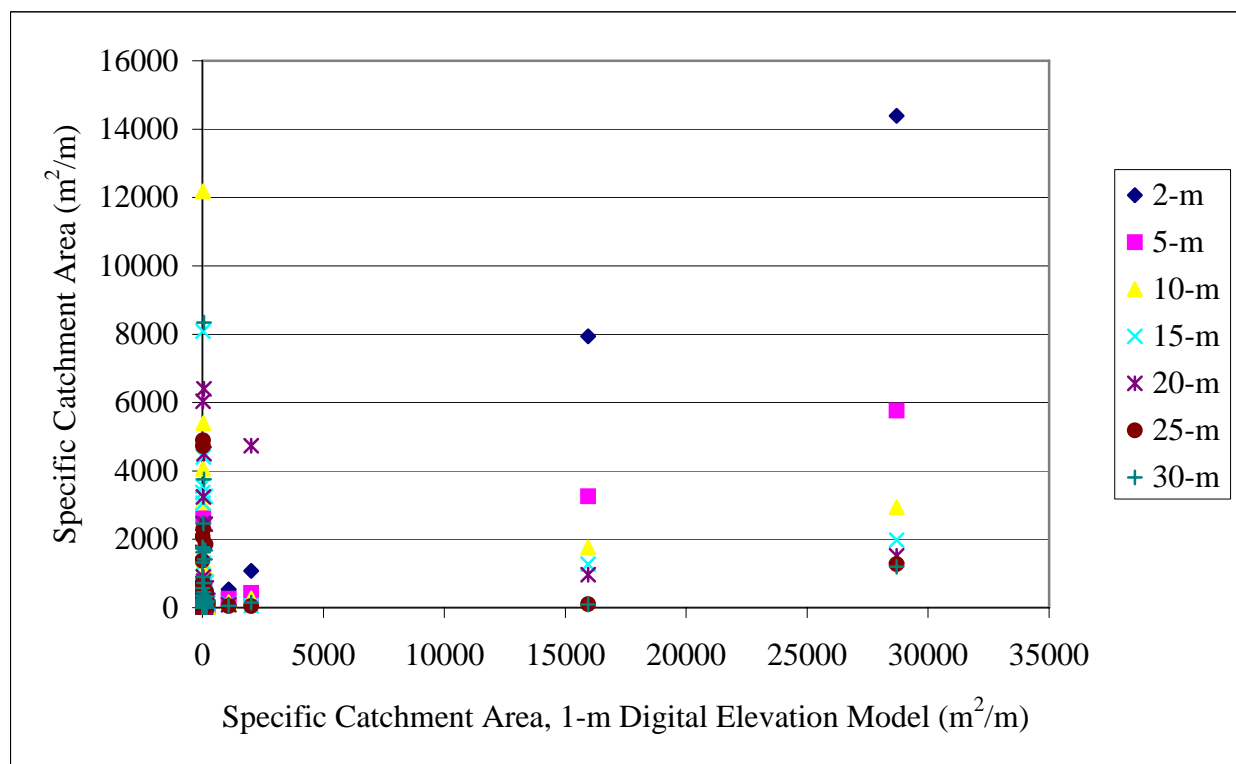


Figure 2.22. Graph of 1-m digital elevation model specific catchment area data for 184 core locations *versus* increasing raster cell sizes.

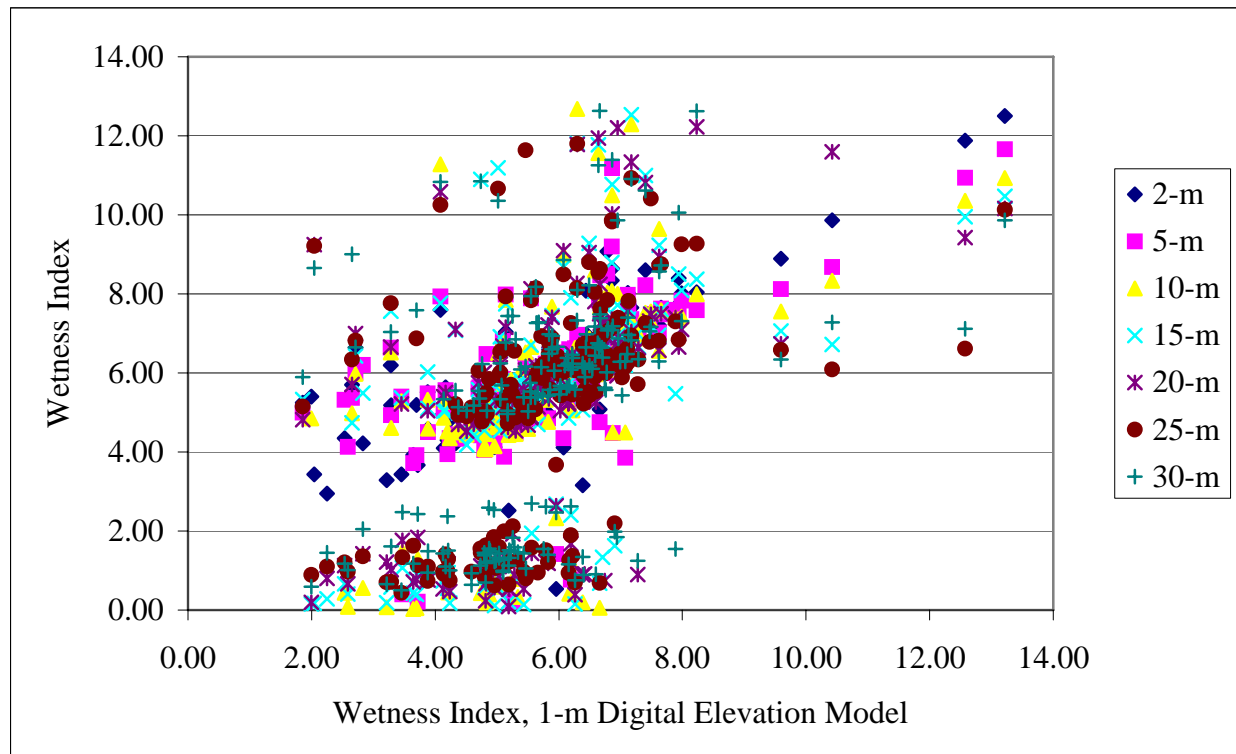


Figure 2.23. Graph of 1-m digital elevation model wetness index data for 184 core locations
versus increasing raster cell sizes.

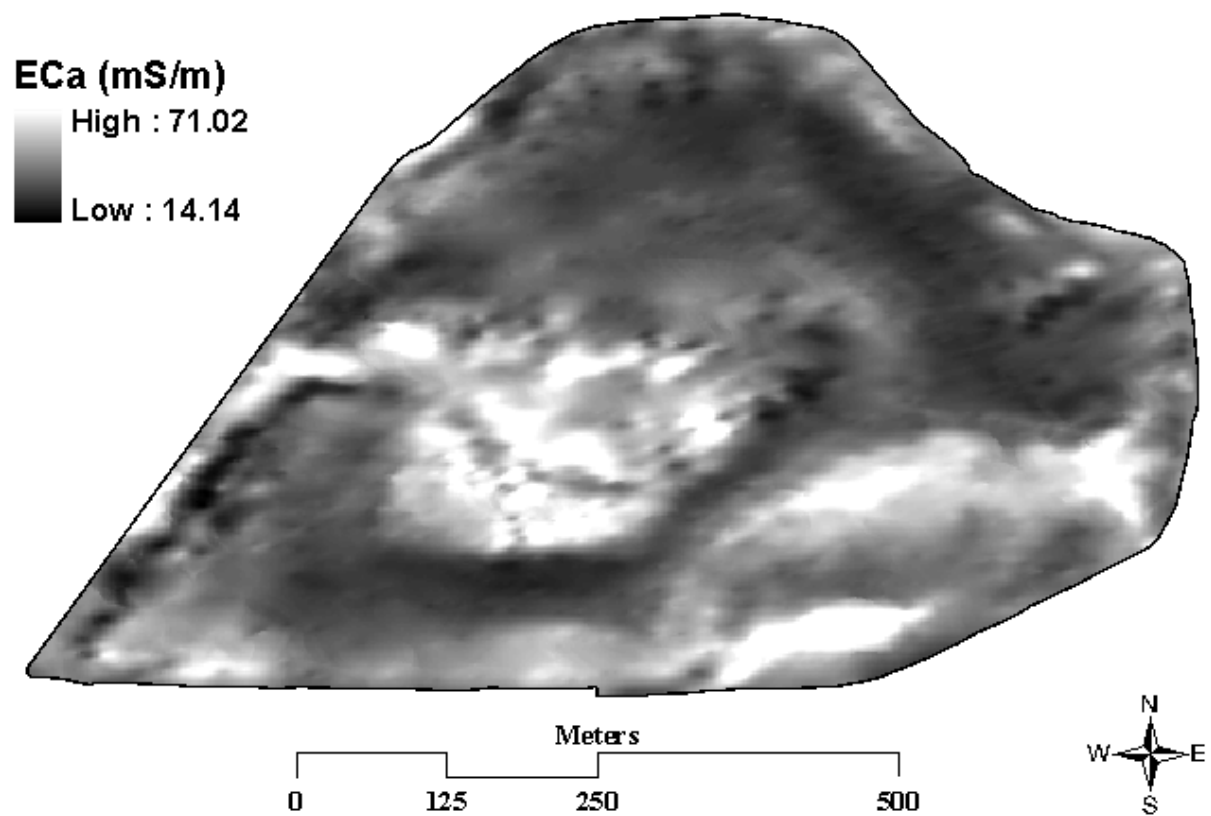


Figure 2.24. Raster of 2-m apparent electrical conductivity (EC_a) for spring of 2000.

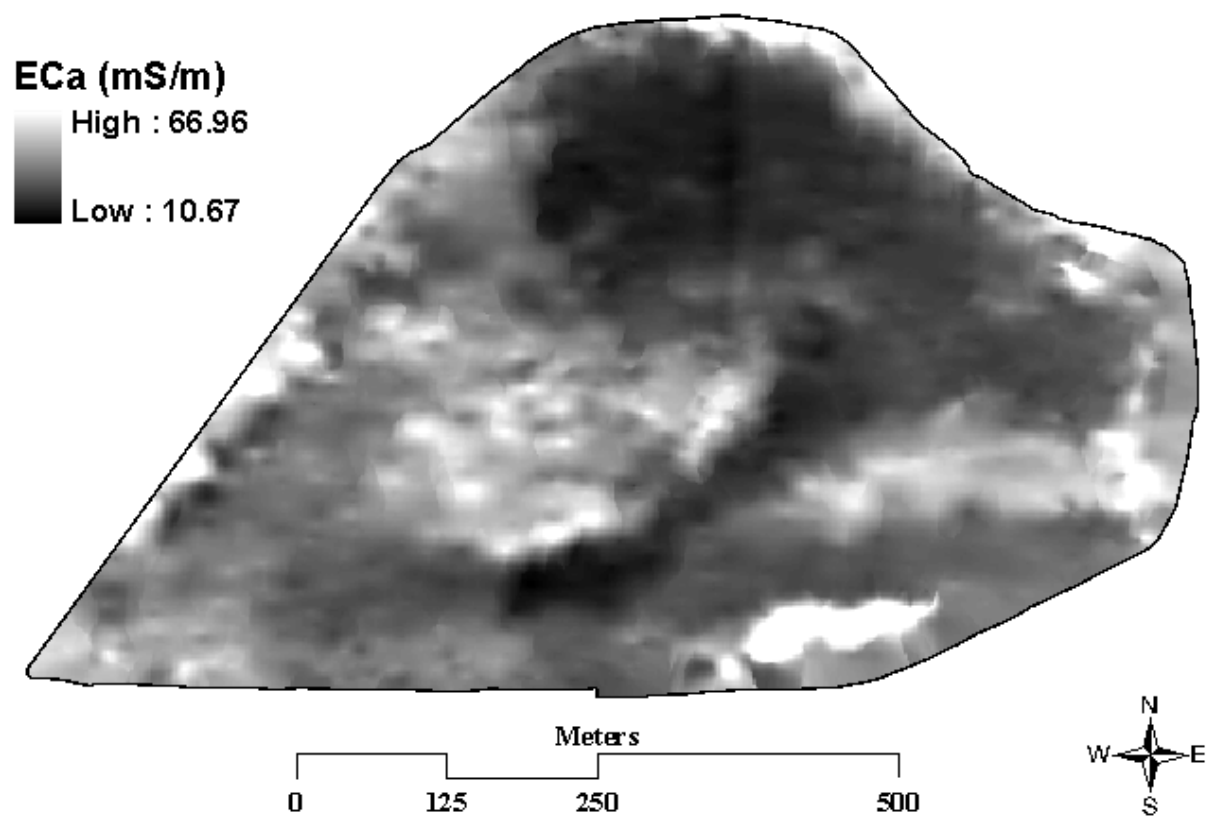


Figure 2.25. Raster of 2-m apparent electrical conductivity (EC_a) for fall of 2000.

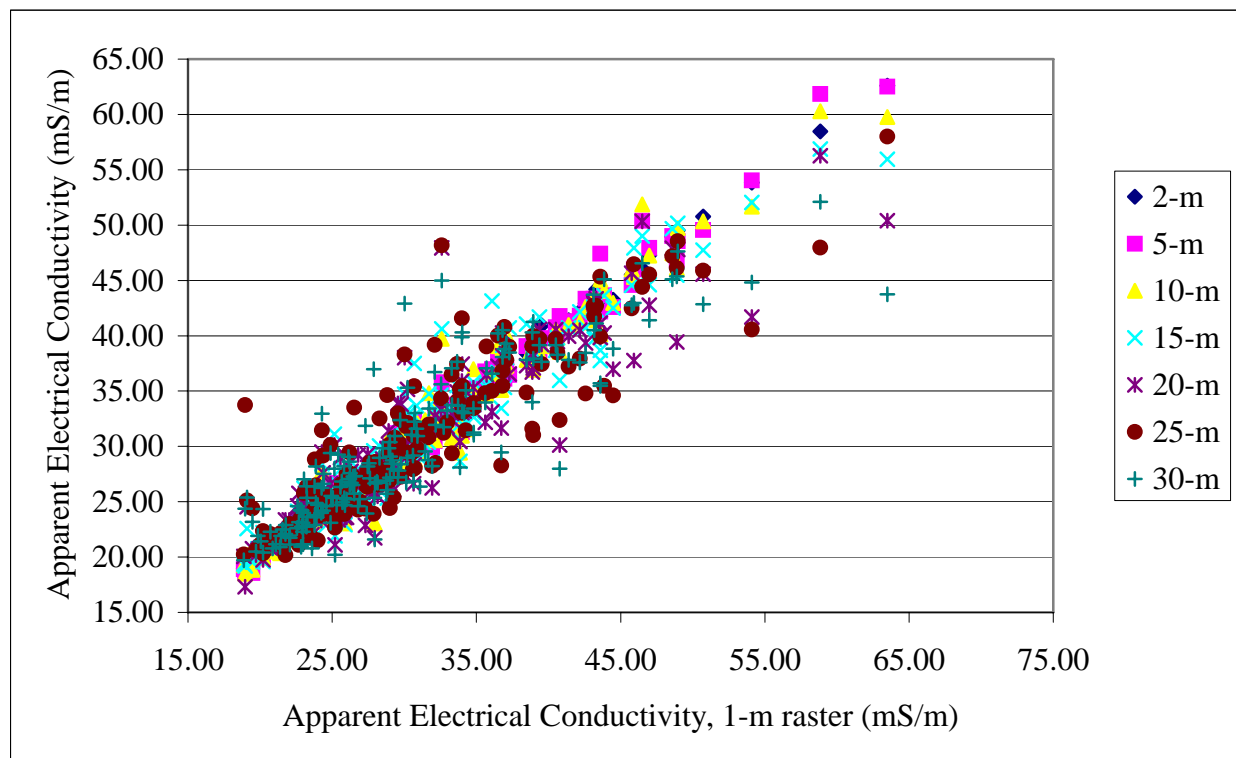


Figure 2.26. Graph of 1-m raster apparent electrical conductivity data for 184 core locations versus increasing raster cell sizes for spring of 2000.

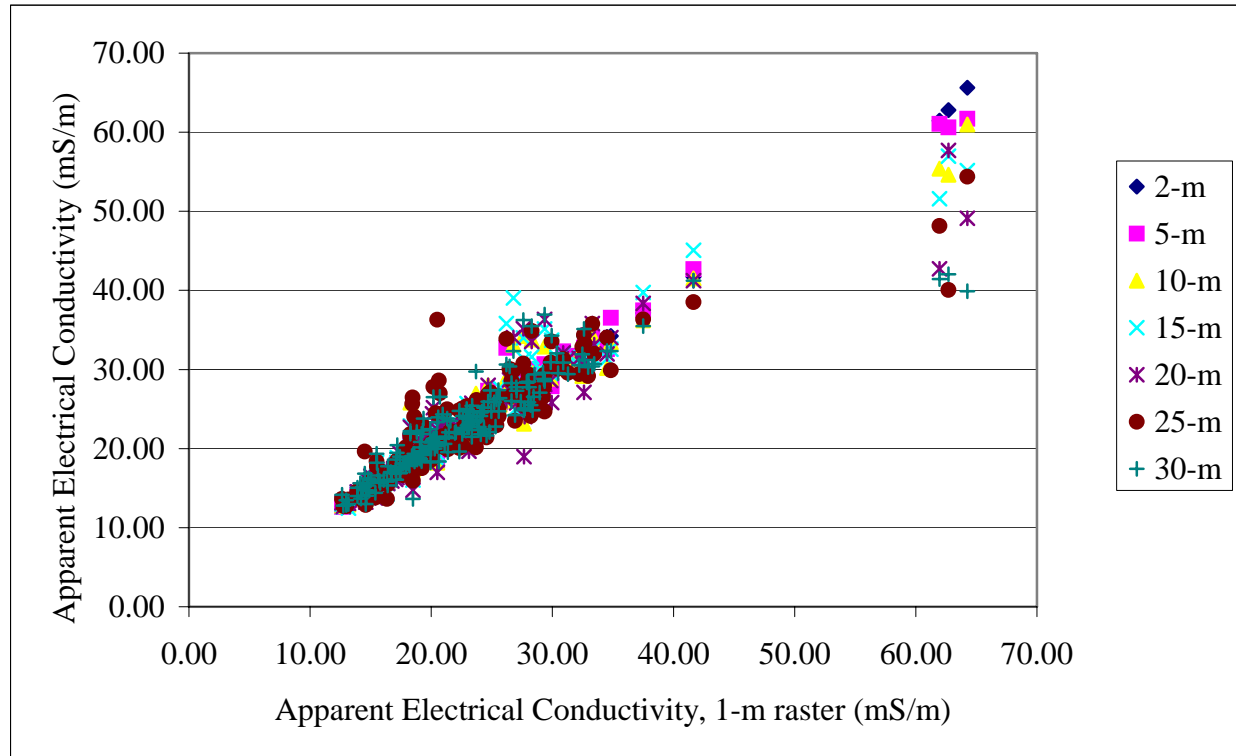
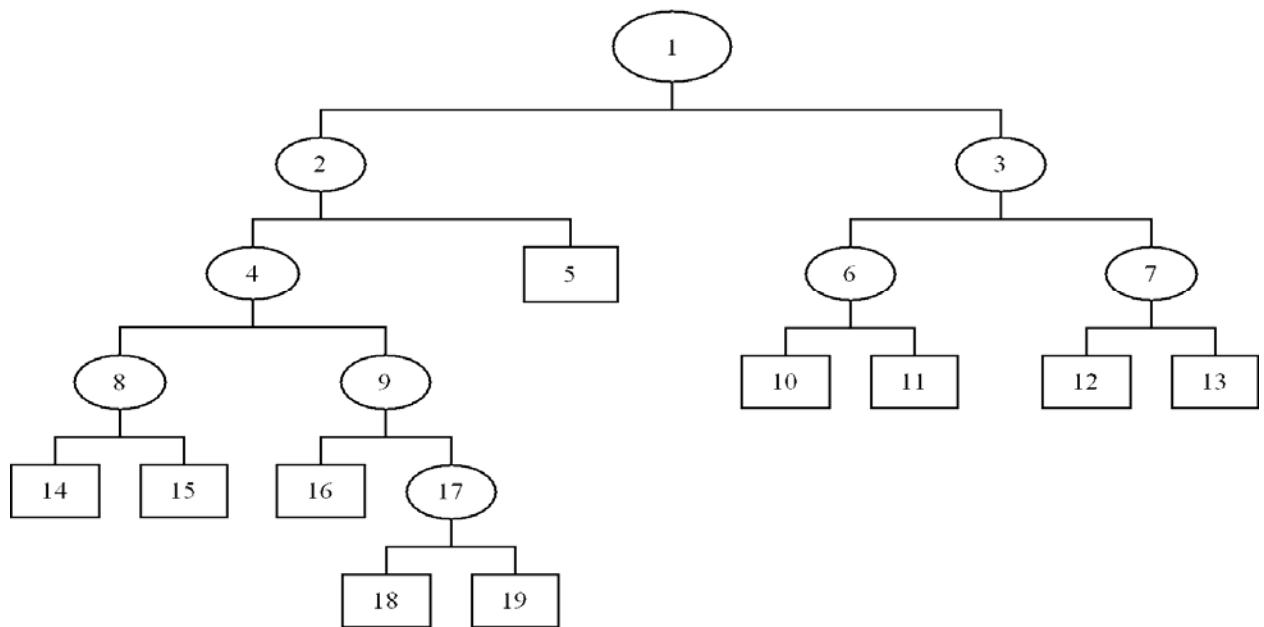


Figure 2.27. Graph of 1-m raster apparent electrical conductivity data for 184 core locations versus increasing raster cell sizes for fall of 2000.



<u>Node</u>	<u>Cores -no.-</u>	<u>Cores with Bt Horizon ---no---</u>	<u>Cores with Bt Horizon ----%----</u>	<u>Total of Bt Cores Present -----%</u>	<u>Splitting Attribute</u>	<u>Raster Cell Size --m--</u>	<u>Splitting Value</u>
1	147	68	46	100	Spring EC _a (mS/m)	5	30.48
2	88	22	25	32	Wetness Index	5	7.36
3	59	46	78	68	Global Insolation (WH/m ²)	30	1676464
4	79	15	19	22	Aspect (degrees)	10	291
5	9	7	78	10	-	-	-
6	30	29	97	43	Global Insolation (WH/m ²)	1	1551404
7	29	17	59	25	Global Insolation (WH/m ²)	25	1745418
8	44	3	7	4	Wetness Index	5	6.205
9	35	12	34	18	Plan Curvature (radians/100 m)	30	0.045
10	9	8	89	12	-	-	-
11	21	21	100	31	-	-	-
12	12	3	25	4	-	-	-
13	17	14	82	21	-	-	-
14	28	0	0	0	-	-	-
15	16	3	19	4	-	-	-
16	16	9	56	13	-	-	-
17	19	3	16	4	Plan Curvature (radians/100 m)	30	0.165
18	10	0	0	0	-	-	-
19	9	3	33	4	-	-	-

Figure 2.28. Classification and Regression Tree analysis output for Bt horizon presence using terrain attributes and EC_a data.

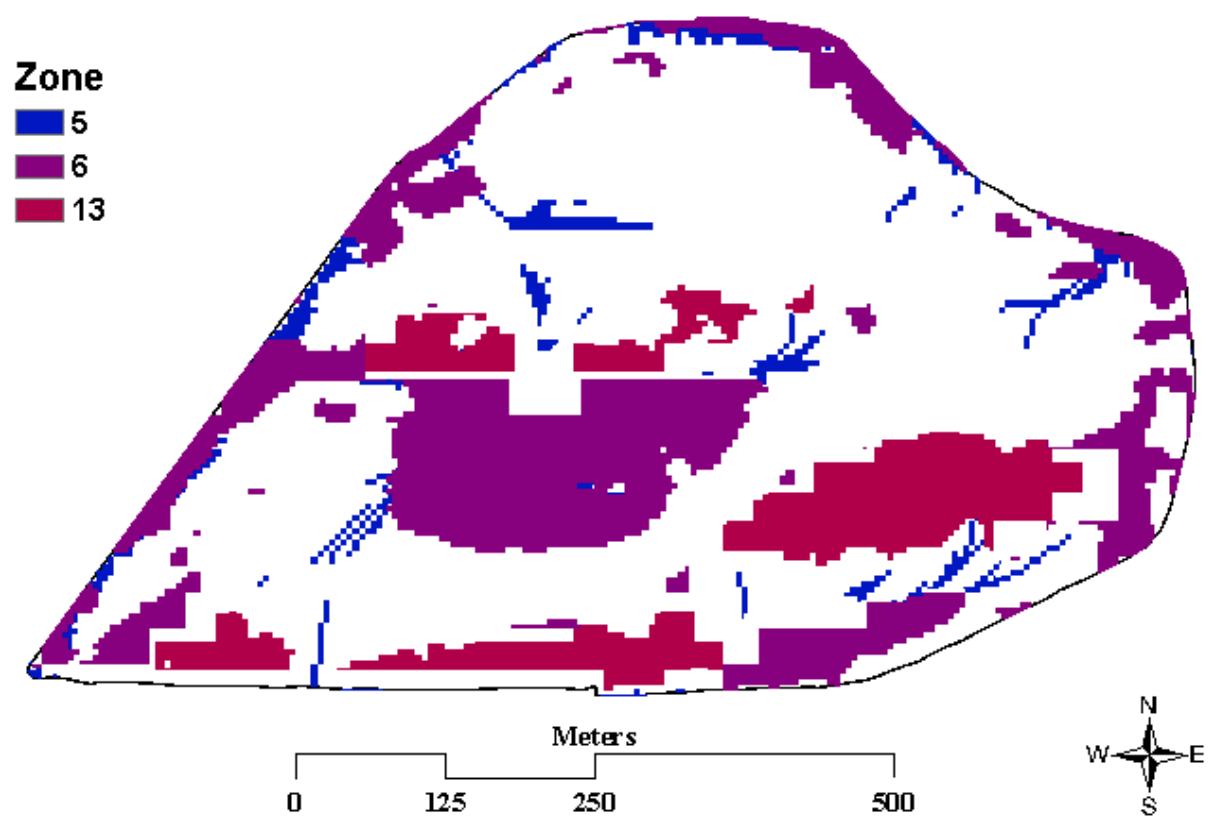
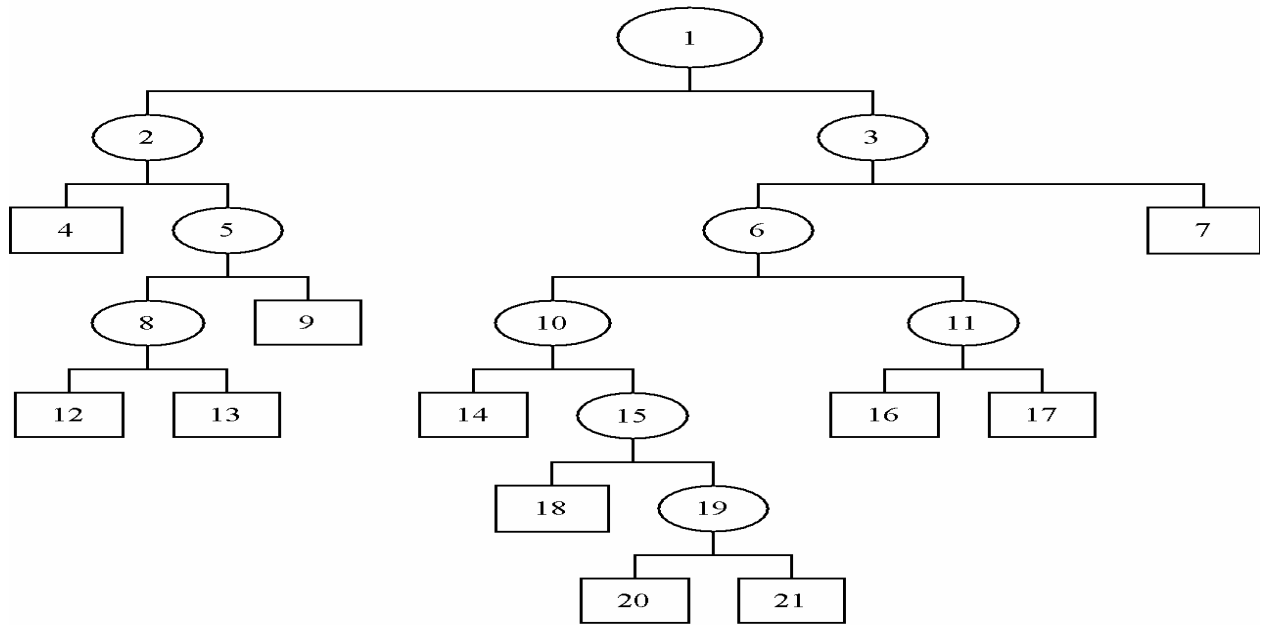


Figure 2.29. Map of zones five, six, and 13 from Classification and Regression Tree analysis using terrain attributes and apparent electrical conductivity data (EC_a).



<u>Node</u>	<u>Cores -no.-</u>	<u>Cores with Bt Horizon</u>	<u>Cores with Bt Horizon</u>	<u>Total of Bt Cores Present</u>	<u>Splitting Attribute</u>	<u>Raster Cell Size --m--</u>	<u>Splitting Value</u>
1	147	68	46	100	Profile Curvature (radians/100 m)	30	-0.025
2	65	16	25	24	Plan Curvature (radians/100 m)	1	0.25
3	82	52	63	76	Wetness Index	10	7.27
4	12	8	67	12	-	-	-
5	53	8	15	12	Elevation (m)	30	804.52
6	64	34	54	50	Wetness Index	25	6.73
7	18	18	100	26	-	-	-
8	44	3	7	4	Plan Curvature (radians/100 m)	25	0.02
9	9	5	56	7	-	-	-
10	46	30	65	44	Plan Curvature (radians/100 m)	15	-0.125
11	18	4	22	6	Profile Curvature (radians/100 m)	2	0.13
12	13	3	23	4	-	-	-
13	31	0	0	0	-	-	-
14	9	9	100	13	-	-	-
15	37	21	57	31	Plan Curvature (radians/100 m)	10	0.025
16	9	4	44	6	-	-	-
17	9	0	0	0	-	-	-
18	11	3	27	4	-	-	-
19	26	18	69	26	Tangential Curvature (radians/100 m)	15	0.015
20	13	12	92	18	-	-	-
21	13	6	46	9	-	-	-

Figure 2.30. Classification and Regression Tree analysis output for Bt horizon presence predicted with terrain attributes.

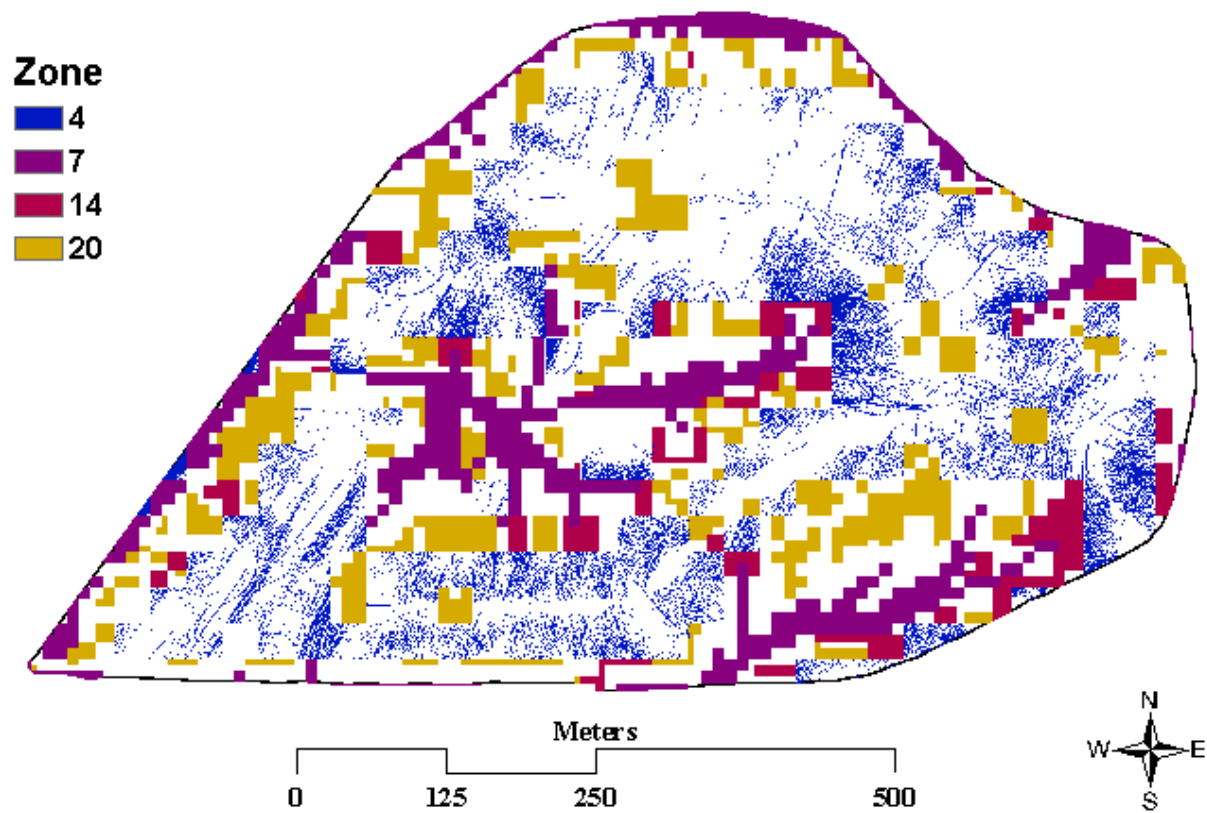


Figure 2.31. Map of zones four, seven, 14, 20 created from Classification and Regression Tree analysis using terrain attributes.

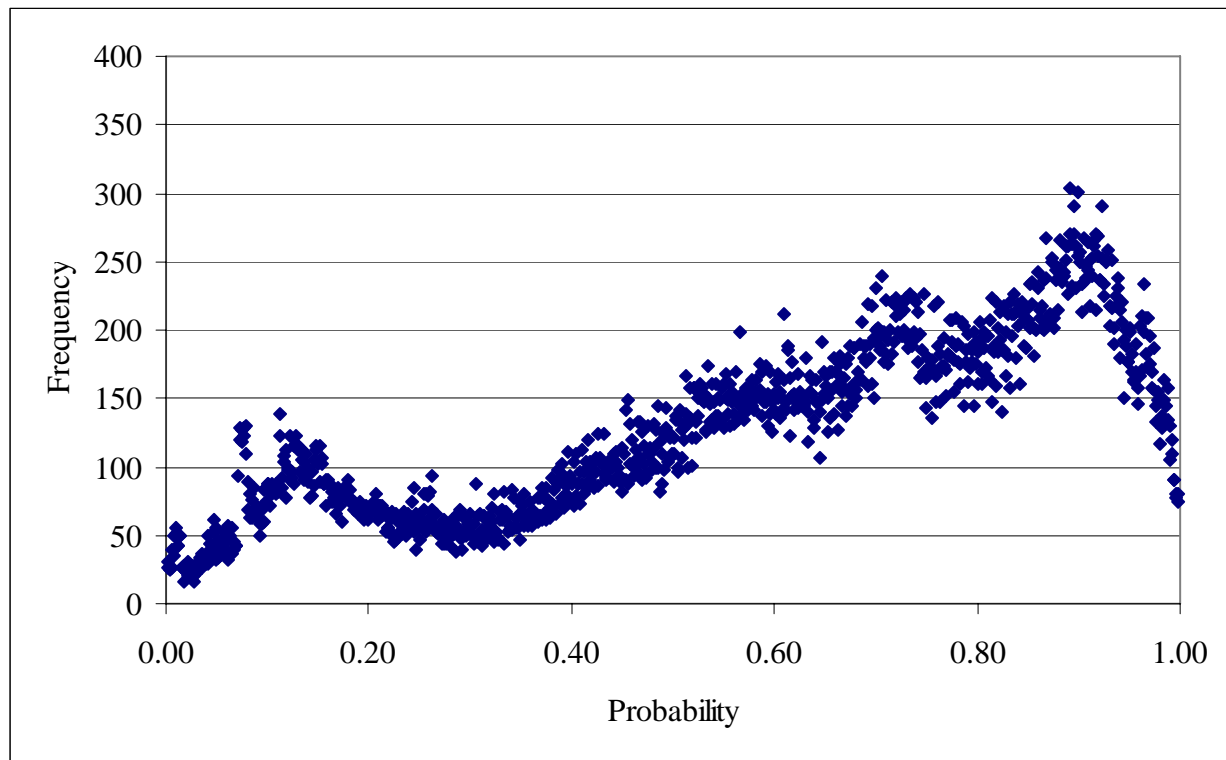


Figure 2.32. Histogram of indicator kriged values for zones five, six, and 13 from classification and regression tree analysis using terrain attributes and apparent electric conductivity (EC_a) data.

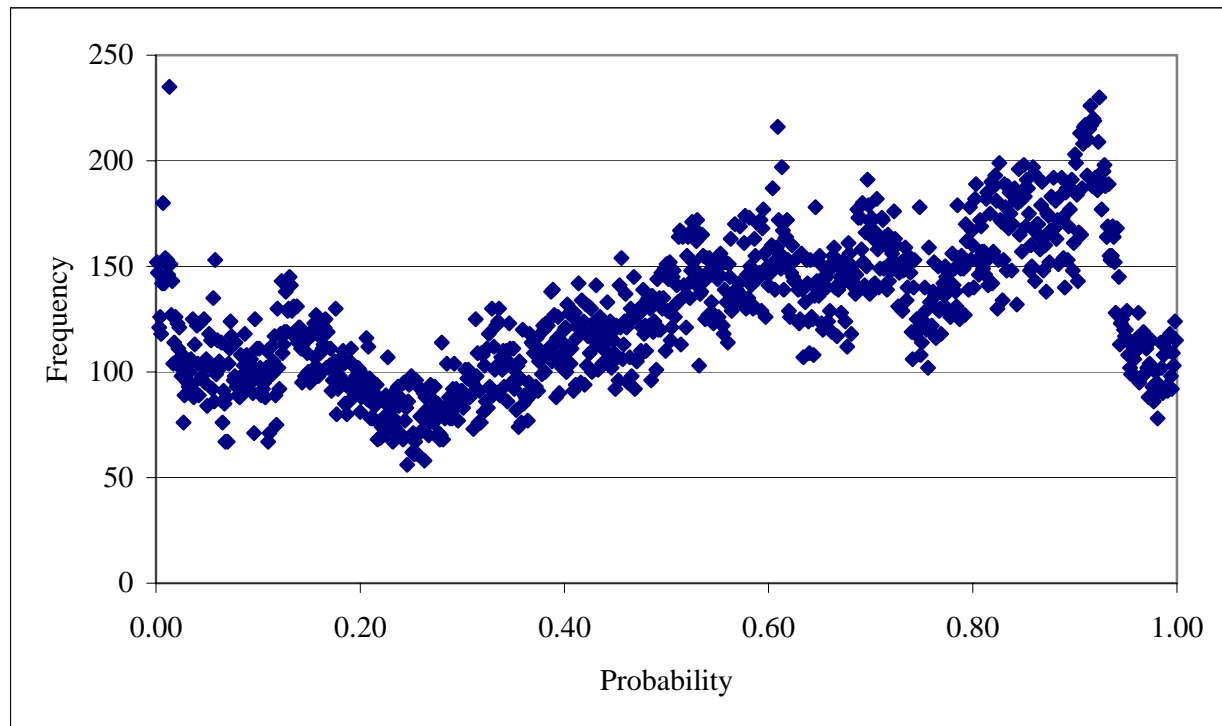


Figure 2.33. Histogram of indicator kriged values for zones four, seven, 14, and 20 from classification and regression tree analysis using terrain attributes.

2.7 References

- Bell, J.C., Cunningham, R.L., Havens, M.W. 1992. Calibration and validation of a soil-landscape model for predicting soil drainage class. *Soil Sci. Soc. Am. J.* 56: 1869-1866.
- Boer, M., Barrio, G.D., Puigdefabregas, J. 1996. Mapping soil depth classes in dry Mediterranean areas using terrain attributes derived from a digital elevation model. *Geoderma* 72: 99-118.
- Brieman, L., Friedman, J.H., Olshen, R.A., Stone, C.J. 1984. Classification and Regression Trees. Wadsworth Publishing,
- Busacca, A.J., McCool, D.K., Papendick, R.I., Young, D.L. 1985. Dynamic impacts or erosion processes on productivity of soils in the Palouse. In *Erosion and Soil Productivity*: 152-169, Proc. Natl. Symposium on Erosion and Soil Productivity, New Orleans, LA. December 10-11, 1984.
- Chaplot, V., Walter, C. 2003. Subsurface topography to enhance the prediction of the spatial distribution of soil wetness. *Hydrological Processes* 17: 2567-2580.
- Chaplot, V., Walter, C., Curmi, P. 2000. Improving soil hydromorphy prediction according to DEM resolution and available pedological data. *Geoderma* 97: 405-422.
- Cook, S.E., Corner, R.J., Greathouse, G., Gessler, P.E., Chatres, C.J. 1996. A rule-based system to map soil properties. *Soil Science Society of America Journal* 60: 1893-1900.
- Friedman J.H. 1984. A variable span smoother. Department of Statistics, Stanford University, Technical Report LCS5.

- Geonics Limited. 2004. Product Update for EM38 Owners. Geonics Limited: March 8, 2004.
- Girgin, B.N., Frazier, B. E. 2004. Landscape position and surface curvature effects on soils developed in the Palouse area, WA [Online]. Available at
<http://remotesens.css.wsu.edu/research/spi.htm> (verified January 13, 2004.)
- Isaaks, E.H., Srivastava, R.M. 1989. Applied Geostatistics. Oxford University Press Inc.
- James, I.T., Waine, T.W., Bradley, R.I., Taylor, J.C., Godwin, R.J. 2003 Determination of Soil Type Boundaries using Electromagnetic Induction Scanning Techniques. Biosystems Engineering 86: 421-430.
- McDonald, E.V., Busacca, A.J. 1992. Late quaternary stratigraphy of loess in the channeled scabland and Palouse regions of Washington state. Quaternary Research 38: 141-156.
- McNeill, J.D. 1992. Rapid, accurate mapping of soil salinity by electromagnetic ground conductivity meters. Advances in Measurement of Soil Physical Properties: Bringing Theory Into Practis. Spec. Publ. 20, SSSA, Madison, WI, 209-229.
- Mertens, M., Inga, N., Huwe, B. 2002. GIS-based regionalization of soil profiles with Classification and Regression Trees (CART). Journal of Plant Nutrition Soil Science 165: 39-43.
- Moore, I.D., Gessler, P.E., Nielsen, G.A., Peterson, G.A. 1993. Soil attribute prediction using terrain analysis. Journal of Soil Science Society of America 57: 443-452.
- Mueller, T.G., Pierce, F.J. 2003. Soil Carbon Maps: Enhancing Spatial Estimates with Simple Terrain Attributes at Multiple Scales. Journal of Soil Science Society of America 67: 258-267.
- National Resource Conservation Service, 1998. Field Book for Describing and Sampling Soils Version 1.1. NRCS, Salt Lake City, UT.

- Odeh, I.O.A., McBratney, A.B., Chittleborough, D.J. 1995. Further results on prediction of soil properties from terrain attributes: heterotopic cokriging and regression-kriging. *Geoderma* 67: 215-226.
- Pan, W.L., Hopkins, A.G. 1991. Plant development, and N and P use of winter barley. *Plant and Soil* 135: 9-19.
- Park, S.J., McSweeney, K., Lowery, B. 2001. Identification of the spatial distribution of soils using a process-based terrain characterization. *Geoderma* 103: 249-272.
- Pennock, D.J. 2003. Terrain attributes, landform segmentation, and soil redistribution. *Soil and Tillage Research* 69: 15-26.
- Schoorl, J.M., Sonneveld, M.P., Veldkamp, A. 2000. Three-Dimensional Landscape Process Modelling: The Effect of DEM Resolution. *Earth Surface Processes and Landforms* 25: 1025-1034.
- Sherlock, M.D., McDonnell, J.J. 2003. A new tool for hillslope hydrologists: spatially distributed groundwater level and soil water content measured using electromagnetic induction. *Hydrological Processes* 17: 1965-1977.
- Soil Conservation Service. 1980. Soil Survey of Whitman County, Washington. USDA Soil Conservation Service.
- Sudduth, K.A., Drummond, S.T., Birrell, S.J., Kitchen, S.J., Kitchen, N.R. 1996. Analysis of spatial factors influencing crop yield. In: Robert, P.C., Rust, R.H., Larson, W.E. (Eds.), Proc 3rd Intl. Conf. On Precision Agriculture, Minneapolis, MN, June 23-26 1996. ASA-CSSA-SSSA, Madison, WI, 129-140.

Sudduth, K.A., Drummond, S.T., Kitchen, N.R. 2000. Measuring and interpreting soil electrical conductivity for precision agriculture. In: Proc 2nd International Geospatial Information in Agriculture and Forestry Conference, Lake Buena Vista, Fl.

Sudduth, K.A., Drummond, S.T., Kitchen, N.R. 2001. Accuracy issues in electromagnetic induction sensing of soil electrical conductivity for precision agriculture. Computers and Electronics in Agriculture 31: 239-264.

Sudduth, K.A., Kitchen, N.R., Bollero, G.A., Bullock, D.G., Wiebold, W.J. 2003. Comparison of Electromagnetic Induction and Direct Sensing of Soil Electrical Conductivity. Agronomy Journal 95: 472-482.

Thompson, J.A., Bell, J.C., Butler, C.A. 2001. Digital elevation model resolution: effects on terrain attribute calculation and quantitative soil-landscape modeling. Geoderma 100: 67-89.

Wilson, J.P., Gallant, J.C. 2000. Terrain Analysis Principles and Application. John Wiley & Sons Inc.